AN ABSTRACT OF THE THESIS OF

Mohammed H. Hassan for the degree of Doctor of Philosophy in Chemical Engineering presented on August 18, 1994.

Title: An Experimental and Simulation Investigation of Gas Transport in a Microporous Silica Membrane

Abstract approved: _____

Dr. James Douglas Way

The permeances of gases with kinetic diameters ranging from 2.6 to 3.9 Å were measured through silica hollow fiber membranes over a temperature range of 298 K to 473 K at a feed gas pressure of 20 atm. Permeances at 298 K range from 10 to 2.3 • 10^5 Barrer/cm and were inversely proportional to the kinetic diameter of the penetrant. The silica hollow fibers are microporous with a mean pore size estimated to be between 6 and 9 Å. Mass transfer through the silica hollow fiber membranes is an activated process. The apparent activation energies ranged from 4.61 to 14.0 kcal/mol and correlate well with the kinetic diameter of the penetrants. The experimental activation energies fall between literature values for zeolites 3A and 4A.

High selectivities were obtained for O_2/N_2 and CO_2/CH_4 mixtures. The O_2/N_2 mixed gas selectivities decreased from 11.3 at 298 K to 4.8 at 423 K and were up to 20% larger than the values calculated from pure gases at temperatures below 373 K. The mixture selectivity for CO_2/CH_4 decreased from 186 to 22.3 over the same temperature range. The differences between the mixture and ideal separation factors is attributed to a competitive

adsorption effect in which the more strongly interacting gases saturate the surface and block the transport of the weakly interacting gases. Similar differences in the separation factors were observed for CO_2/CH_4 mixtures after the membrane had been heated to at least 398 K and then cooled in an inert gas flow. Based on FT-IR results, this unusual behavior is attributed to the removal of physically adsorbed water from the membrane surface.

The interaction energy and the heat of adsorption of CO and CO_2 were higher than those of N_2 and CH_4 respectively using H_3SiOH as the model for silica surface with MP2/6-31+G** level of theory. Experimental observation of the heat of adsorption on silica membranes showed the same behavior.

Several simple models (H_3SiOH, $Si(OH)_4$, and H_2AlOH) were used to describe the silica surface for simulations of interaction with N_2. The heat of adsorption of a nitrogen molecule on $Si(OH)_4$ agreed well with the experimental observation, thus, it was concluded that $Si(OH)_4$ best represent the silica surface of the membrane. Experimental heat of adsorption of nitrogen on silica surface was found to be about twice as much as the values obtained using H_3SiOH or H_2AlOH as the surface model.

An Experimental and Simulation Investigation of Gas Transport in a Microporous Silica Membrane

by
Mohammed H. Hassan

A THESIS
submitted to
Oregon State University

in partial fulfillment of
the requirements for the
degree of

Doctor of Philosophy

Completed August 18, 1994
Commencement June 1995

APPROVED:

Redacted for Privacy

Professor of Chemical Engineering in charge of major

Redacted for Privacy

Head of department of Chemical Engineering

Redacted for Privacy

Dean of Graduate School

Date thesis is presented August 18, 1994

Typed by Mohammed H. Hassan

Acknowledgments

This research project was accomplished with the assistance of many people. I would like to express my appreciation to Dr. J. Doug Way, my major advisor, for his guidance during the project. This project could not have been completed without his technical advise, patience, and moral support. I am grateful to the members of my graduate committee, Dr. S. Kimura, Dr. M. Penner, Dr. A. Sleight, and Dr. C. Wicks. I would like to thank Dr. John Nicholas for his technical support for quantum mechanics calculations, Dr. John Loeser for his help in quantum chemistry, Dr. Paul Thoen for his help in obtaining adsorption data, and Adam King for assembling the experimental apparatus. I would also like to thank Dr. Goran Jovanovic for all his help during last two years.

I am deeply indebted to my parents. Without their continuous encouragement and support in all aspects, I would not be able to achieve what I have today. I wish to thank my wife, Saghar, my little beautiful daughter, Raha, and my brothers, Ali and Ahmed, for their assistance, patience and sacrifice during the period of my study.

This research was supported by the U. S. Department of Energy, Office of Basic Energy Sciences, Division of Chemical Sciences, by grant # DE-FG03-93ER14363. The membranes used in this project were donated by PPG Industries. I am very grateful for these sources of support.

Mohammed H. Hassan

Table of Contents

Table of Contents (Continued)

Table of Contents (Continued)

List of Figures

List of Figures (Continued)

List of Tables

Nomenclature

Symbols List

c	Speed of light
C_i	Concentration of species i
C_t	Total amount adsorbed
C_i^o	Specific amount of i adsorbed at P_i^o
D_i	Diffusion coefficient of species i
D_{io}	Initial diffusion coefficient of species i
$\bar{D}_i$	Effective diffusion coefficient of species i
d_A	Diameter of the adsorbate
d_E	Diameter of the adsorbent
d_o	Arithmetic mean of the adsorbate and adsorbent diameters
E	Energy of the particle
E_i	Energy of species i
E_{MM}	Microporous membrane enhancement factor
E^{act}	Activation energy
$E(r)$	Potential function in r direction (for cylindrical model)
$E(Z)$	Potential function in Z direction (for flat plate model)
f_i	mass flux through the tube wall at the inside radius
g	Geometric factor
g_s	Gaussian function for s orbitals
g_y	Gaussian function for y orbitals
$g_{d_{xy}}$	Gaussian function for d_{xy} orbitals
H	Hamiltonian
H_c	Hook's law constant

h	Plank's constant
J_i	Flux of species i
L	Distance between the plates
L_f	Total length of the Fiber
M_i	Molecular weight of species i
m	Order of repulsion
N	Total number of species
N_A	Density of the adsorbate
N_{av}	Avogadro's number
N_E	Density of the adsorbent
N_i	Flux of species i (flow rate of i per unit area of the membrane)
n	Order of dispersion
P	Pressure of an adsorbate gas (in the Kelvin, H-K, and S-F models)
P_c	Critical pressure
P_i	partial pressure of species i
P_{in}	Pressure inside the fiber
P_{out}	Pressure outside the fiber
P_o	Saturation pressure
P_i^o	Vapor pressure of adsorbate in standard state
P_T	Total pressure
P_1	Pressure at the membrane outlet
Q_i	Permeability of species i
Q_i^*	Volumetric flow rate of species i
Q^{**}	Permeance (normalized flux)
Q_o^{**}	Initial permeance
R	Gas constant
Re	Reynolds number

r	Radial distance
r_i	Inside radius of the fiber
r_o	Outside radius of the fiber
r_p	Pore radius
T	Temperature
T_c	Critical temperature
T_r	Reduced temperature
t	time
$\bar{u}_i$	Average velocity of species i
V	Potential field
V_m	Molar volume of adsorbate
v_z	Gas velocity in Z direction
W	Mass flow rate
X_i	Mole fraction of species i inside lumen at permeate exit
x_i	mole faction of i in adsorbed phase
XP_i	Mole fraction of species i in the permeate flow stream
XR_i	Mole fraction of species i in the residue stream
y_i	Mole fraction of species in gas phase
Z	Distance along the flat plates and the tubes
z_c	Compressibility factor

Greek Symbols

α	A constant in Gaussian functions
α_A	Polarizability of adsorbate
α_E	Polarizability of adsorbent
α_{ij}	Selectivity of species i over j

β	Distance between adjacent sites
δ_{ij}	Kronnicker Delta
γ	Surface tension
λ	Friction factor
ρ	Gas density
θ	Angle of contact between adsorbate and adsorbent
ν_e	Effective vibrational frequency of the molecule
Ψ	Wavefunction
ψ^o	Related to spreading pressure at standard state
ϕ	One-electron wavefunction
κ	A constant used in ab initio theory
χA	Magnetic susceptibility of the adsorbate
χE	Magnetic susceptibility of the adsorbent
ε	Void fraction
μ	Viscosity
τ	Tortuosity
τ_w	Shear stress
$\bar{\varepsilon}_i$	Minimum potential energy of species i
$\bar{\varepsilon}_{o2}$	Minimum potential energy of oxygen atom
σ_i	"Hard sphere" kinetic diameter of species i
σ_{o2}	"Hard sphere" kinetic diameter of oxygen atom

Subscripts and Superscripts

K	Knudsen diffusion
S	Surface diffusion
MS	Molecular sieving

AN EXPERIMENTAL AND SIMULATION INVESTIGATION OF GAS TRANSPORT IN A MICROPOROUS SILICA MEMBRANE

Chapter 1

Introduction

Membrane separations are important in chemical and related industries for product purification and the removal of toxins prior to the release of waste streams into the environment. A membrane is a barrier between two phases, and can be used to separate gas and liquid mixtures if one component of the mixture moves through the membrane faster than the others. Membrane processes have several advantages over other conventional separation technologies (Spillman, 1989) including:

- low capital investment
- ease of operation
- low energy consumption
- cost effectiveness even at low gas volumes
- good weight and space efficiency

Membrane technology has been practiced in the industry for many years for the separation of liquid-liquid and liquid-solid streams (e.g.. reverse osmosis, ultrafiltration, microfiltration, and other membrane-based processes). The technology for gas separation has been practiced since late seventies or early eighties. Several of the applications in industrial gas separations include removal of sulfur and nitrogen oxides from combustion gases, removal of acid gases from natural gas, production of nitrogen from air, and hydrogen recovery in petrochemical production.

According to a recent DOE study (DOE/NBM-80027730), there is an opportunity for annual energy savings of about 40% using membrane technology for gas/liquid separations, and subsequent reduction in demand for imported petroleum, if membrane systems gain wider acceptance. A comprehensive research needs assessment for membrane separations was performed (Baker et al., 1990) for the DOE. Two of the priority topics in gas separations were: the development of a membrane with O_2/N_2 separation factor of 7 to 10 and the improvement of the separation factor for removal of acid gases, CO_2 and H_2S, from fuel gas mixtures to separation factors above 45.

Spillman (1989) identifies three key membrane performance parameters that effect their economic utility for a particular gas separation application. The first is selectivity, which affects the recovery of the process and indirectly impacts membrane area and feed gas flow requirements, of the gases being separated. The second is membrane flux or permeability which simply dictates the required amount of membrane. Life of the membrane is the third parameter which is related to maintenance and replacement costs.

There is an increasing interest to develop membrane technology with the objective of not only getting high permeability and separation factor when using gas separations but also to be able to perform at severe conditions (high temperature, and pressure). Materials such as silica, ceramics, and carbon are potential membrane materials for gas separation because these materials can perform at high temperatures and in aggressive chemical environments (Hsieh, 1988), and they also can exhibit high separation factors.

One of the potential membranes is hollow fiber microporous glass membrane produced by PPG Industries (Way and Roberts, 1992). The objective of this research project is the investigation of the gas transport mechanism(s) through the microporous silica hollow fiber membrane. A

schematic diagram of the gas transport through a microporous silica membrane is shown in Figure 1.1. The hollow fiber membrane system consists of a shell and tube type configuration similar to a shell and tube heat exchanger. Gas enters the shell side, diffuses through the pores of the membrane into the tube side. The pressure driving force required for gas permeation is obtained by operating the shell side at a higher pressure than the tube side.

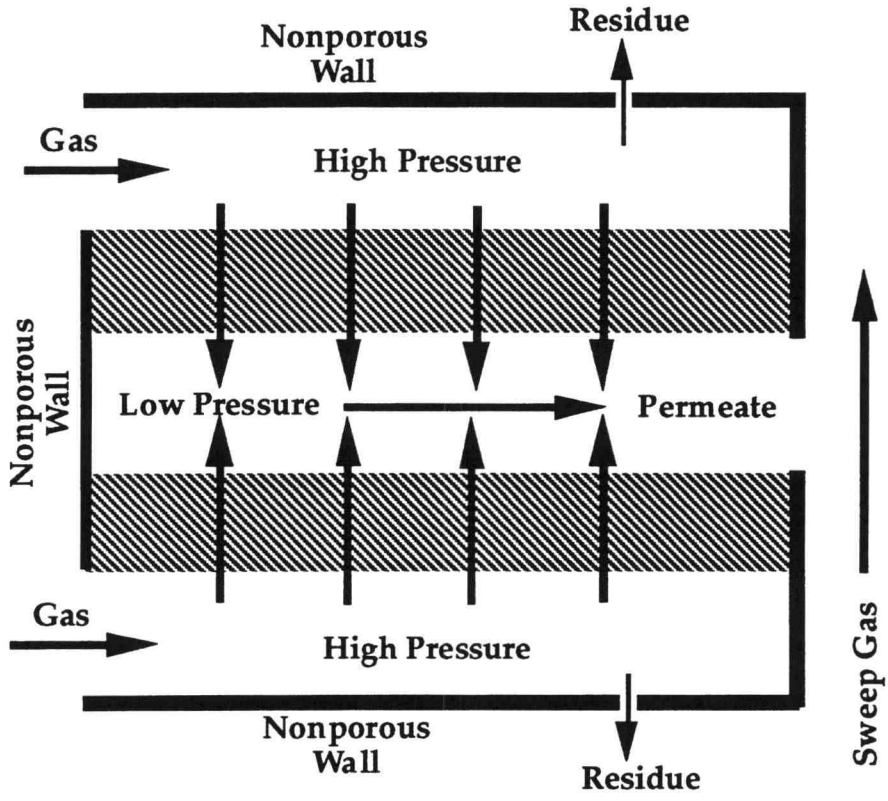

Figure 1.1 Cross-section of a microporous silica hollow fiber membrane.

The objectives of this research project were as follows:

i) To investigate the influence of membrane microstructure on separation performance by measuring pore size distribution

ii) To measure the pure gas permeabilities (He, H_2, O_2, N_2, Ar, CO, CO_2, CH_4, and C_2H_4)

iii) To measure the binary gas mixture permeabilities (CO_2/CH_4, O_2/N_2, N_2/CO), and compare them with pure component permeabilities

iv) To use quantum mechanics for calculation of interaction energies of gaseous species (N_2, CH_4, CO_2, and CO) on silica surface

Chapter 2

Background and Literature Survey

2.1 Transport Mechanisms in Microporous Silica

Transport of gases through microporous materials consists of four different mechanisms as shown in Figure 2.1 (Fleming, 1986). These mechanisms are: 1) Knudsen diffusion, 2) capillary condensation, 3) surface diffusion, and 4) molecular sieving or activated diffusion.

2.1.1 Knudsen Diffusion

Knudsen diffusion, a well understood mechanism, is the result of free molecular motion and occurs in small pores or at low pressures. It is assumed that the molecules of a gas collide more frequently with the wall than with each other. In other words, the mean-free path of the diffusing molecule, λ , is much larger than the size of the pores. A diffusing molecule exchanges energy with the atoms or molecules of the surface after collision with the wall and then it is reflected in a random direction. There is no relation between the velocity of the molecule leaving the surface and the velocity of the incident molecule. In a cylindrical pore, transport can occur due to concentration or pressure difference between outside and inside of the pore. Thus, the diffusive flux of species i in radial direction can be expressed using the Fick's law of diffusion which is:

$$J_i^K = D_i^K \frac{dC_i}{dr} \qquad (2\text{-}1)$$

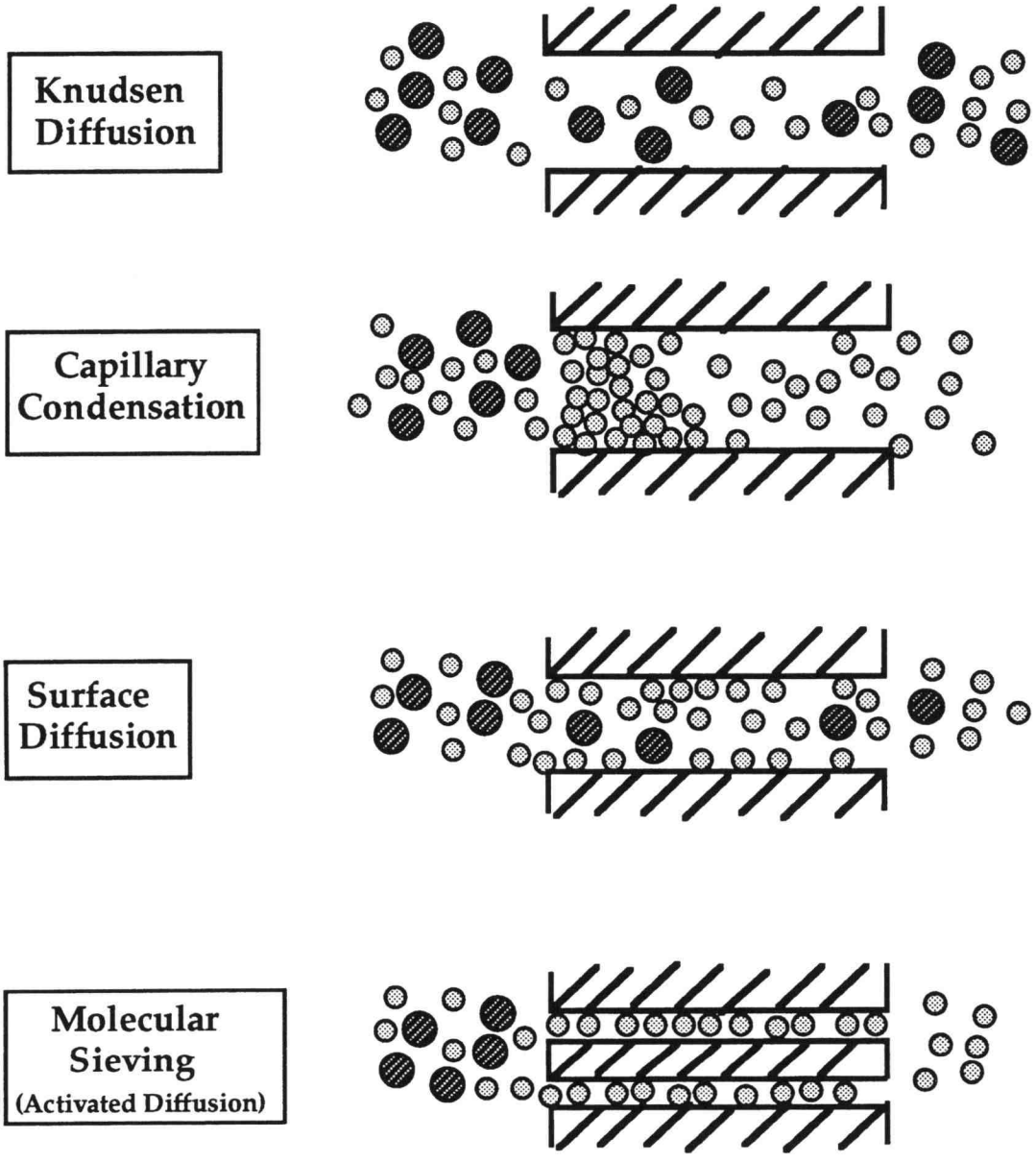

Figure 2.1 Mechanisms of mass transfer through microporous membranes.

where D_i^K, the Knudsen diffusion coefficient of species i, can be obtained from kinetic theory of gases and is given by:

$$D_i^K = \left(\frac{8r_p}{3}\right)\sqrt{\frac{RT}{2\pi M_i}} \qquad (2\text{-}2)$$

From equation 2-2, the Knudsen diffusion coefficient is directly proportional to the pore radius, the square root of temperature, and inversely proportional to the square root of molecular weight. Knudsen diffusion is independent of pressure.

Assuming all factors are equal, the ratio of the flow of species i to that of species j is given by the square root of the inverse of the ratio of their molecular weights. Thus, selectivity, α_{ij}, which is the ratio of the flows, is defined as:

$$\alpha_{ij} = \sqrt{\frac{M_j}{M_i}} \qquad (2\text{-}3)$$

According to equation 2-3, selectivities for gaseous species based on Knudsen diffusion are small since the difference in molecular weight of gaseous species is small. For example, in the Knudsen regime, the selectivity between CO_2 and CH_4, and O_2 and N_2 are 1.7 and 1.1 respectively.

2.1.2 Capillary Condensation

Capillary condensation arises from the effect of surface tension. As a result of the lowering of the equilibrium vapor pressure, condensation occurs in a pore at a vapor pressure below the saturation vapor pressure for the free

liquid (Karger and Ruthven, 1992). The Kelvin equation which is based on thermomechanical equilibrium across the hemispherical meniscus of a capillary condensate within a cylindrical pore, can be used to calculate the reduction in the pressure of an adsorbate gas, P, and it is given as:

$$\ln\frac{P}{P_o} = \frac{-2\gamma V_m}{RTr_p}\cos\theta \qquad (2\text{-}4)$$

where γ and V_m are the surface tension and molar volume of adsorbate respectively. In equation 2-4, θ is the angle of contact between the adsorbate and adsorbent and r_p is the capillary condensate radius.

After the pore fills with condensate, the vapor flux through a cylindrical pore is cut off. Under the effects of pressure gradient and surface tension forces, the condensing sorbate flows through the capillary in a viscous flow (Karger and Ruthven, 1992).

2.1.3 Surface Diffusion

Surface diffusion mechanism can be explained as the ability of molecules to reside on the surface and hop from point to point "along" the surface, with no apparent residence time in the bulk gas phase above the surface. Surface chemistry plays a key role in this mechanism which can be thought of as occurring when the energy state of the diffusing species is dominated by the interaction with the surface. When the interaction with the surface is strong, the diffusing molecules lose their gaseous entity (Xiao and Wei, 1992). This strong interaction causes the diffusing molecules to adsorb to the surface. There is an activated state required for an adsorbed molecule before it is able to jump from one adsorbed site to the next (Karger

and Ruthven, 1992; Gilliland et al., 1974) and this is obtained by means of vibration with the surface atoms (Xiao and Wei, 1992). Pressure or temperature gradient creates a net transport rate of the adsorbed molecules. Thus, the flux of the surface diffusion of species i is given as:

$$J_i^S = \overline{D}_i^S \frac{dC_i^S}{dr} \tag{2-5}$$

Equation 2-5 can also be written as:

$$J_i^S = \overline{D}_i^S \sum_{j=1}^{N} \frac{\partial C_i^S}{\partial P_j} \frac{dP_j}{dr} \tag{2-6}$$

For a pure component, $\frac{\partial C_i^S}{\partial P_j}$ is the slope of the isotherm which can be determined experimentally. For a multicomponent mixture, the term, $\frac{\partial C_i^S}{\partial P_j}$, can be calculated from the pure component isotherm data using the ideal adsorbed solution (IAS) theory (Myers and Prausnitz, 1965), see Appendix A.

The effective surface diffusion, $\overline{D}_i^S$, is given in terms of the distance between adjacent sites, β (usually $\beta = 2r_p$), geometric factor, g (often $g = 1/3$), effective vibrational frequency of the molecule, ν_e, and surface activation energy, E_i^s (Xiao and Wei, 1992) as given:

$$\overline{D}_i^S = g\beta^2 \nu_e e^{-\left(\frac{E_i^S}{RT}\right)} \tag{2-7}$$

where ν_e is proportional to the square root of the Hooke's law constant, H_c, and is defined as:

$$\nu_e = \frac{\sqrt{\frac{H_c}{M}}}{\pi} \qquad (2\text{-}8)$$

From equation 2-7, it can be concluded that:

(1) surface diffusion is an activated process.

(2) the more strongly adsorbed molecules are less mobile.

2.1.4 Molecular Sieving (Activated Diffusion)

Molecular sieving mechanism occurs when the pore size of a membrane approaches the diameter of a diffusing molecule. The diffusion process in molecular sieving is an activated process (Karger and Ruthven, 1992, Xiao and Wei, 1992) with the activation energy depending on the size and shape of the diffusing molecules and the structure of the porous media. This mechanism is strongly and clearly exhibited by zeolite (Barrer, 1978). In the molecular sieving mechanism, the diffusing molecule is in close and regular contact with both sides of the pore wall (in contrast to surface diffusion, where the diffusing species interact with only one surface at a time). Even though the movement of the diffusing molecules from one site to the next becomes restricted and has to overcome the energy barrier, it is assumed that the diffusing molecules retain their gaseous characteristics (Xiao and Wei, 1992) unlike the surface diffusion, where the diffusing molecules lose their gaseous entity due to the strong interaction with the surface.

Molecular sieving materials are endowed with the unique property of discriminating very sharply between molecules of similar width (Koresh and Sofer, 1986 and 1989). Only 0.2-0.3 Å difference in molecular width may cause transport rates to vary by several orders of magnitude.

According to Fick's law of diffusion, the net diffusive flux of species i, J_i^{MS}, in a radial direction is related to the gradient of the concentration of species i and is given as:

$$J_i^{MS} = D_i^{MS} \frac{dC_i}{dr} \tag{2-9}$$

In most cases, D_i^{MS}, the molecular sieving diffusion coefficient is assumed to follow an Arrhenius-type behavior described by an Eyring equation (Way and Roberts, 1992; Karger and Ruthven, 1992; Shelekhin et al., 1992) given as:

$$D_i^{MS} = D_{io}^{MS} e^{-\left(\frac{E_i^{MS}}{RT}\right)} \tag{2-10}$$

The pre-exponential term, D_{io}^{MS}, is related to a jumping frequency and the lattice constant (Barrer, 1941; Riekert, 1970).

A more rigorous treatment of the molecular sieving diffusion coefficient is given by Xiao and Wei (1992). Assuming that the diffusion process is an activated process, the authors calculate the molecular sieving diffusion coefficient of species i, using a modified Eyring equation given as:

$$D_i^{MS} = g\beta\bar{u}_i e^{-\left(\frac{E_i^{MS}}{RT}\right)} \tag{2-11}$$

where g is a geometrical factor (g = 1/3), β is the average length between jumps ($\beta = 2r_p$), $\bar{u}_i$ is the average velocity of species i and can be calculated from the Maxwell distribution:

$$\bar{u}_i = \sqrt{\frac{8RT}{\pi M_i}} \tag{2-12}$$

Combining 2-11 and 2-12, the diffusion coefficient of species i in molecular sieving is given as:

$$D_i^{MS} = g\beta\sqrt{\frac{8RT}{\pi M_i}}e^{-\left(\frac{E_i^{MS}}{RT}\right)} \tag{2-13}$$

The activation energy approaches zero when pore size becomes much larger than the molecular size. In this case, the molecule-zeolite interaction diminishes as in the case of Knudsen diffusion. Thus, equation 2-13 reduces to Knudsen diffusion coefficient (equation 2-2) if $E_i^{MS} = 0$, $\beta=2r_p$, and $g = \frac{1}{3}$.

2.2 Permeability and Selectivity

Separation of gases in inorganic porous membranes has been extensively reviewed (Hwang and Kammermeyer, 1984). They found that the gas transport is controlled by Knudsen diffusion. They also reported higher selectivities for condensable gases than those predicted by the Knudsen diffusion theory. The increase in selectivity is attributed to adsorption and subsequent surface diffusion on inorganic materials such as porous silica

glasses. Transport of H_2, N_2, and CO_2 through γ-alumina membranes at ambient pressure and temperature was studied (Van Vuren et al., 1987). The authors found that the permeabilities of H_2 and N_2 were consistent with the Knudsen diffusion theory, whereas the permeability of CO_2 was found to be 30% higher than predicted on the basis of molecular weight difference. This difference is attributed to surface diffusion of weakly adsorbed CO_2.

Several approaches were directed toward the development of materials with microporous properties in an attempt to increase the separation factors. Some researches (Okubo et al., 1988 and 1989) used chemical vapor deposition techniques to modify microporous Vycor-type glass membranes. The chemical modification improved the mixture separation factor for O_2 and He from the Knudsen value of 3 to 6. A vapor phase alkoxysilane was decomposed and the products reacted with the silica surface to reduce the pore size of the glass membrane. The smaller pore size changed the mass transfer mechanism from Knudsen diffusion to either surface diffusion or molecular sieving. Lin and Burggraf (1992) used a CVD process to deposit ZrO_2 in order to decrease the pore size of an alumina ultrafilter.

To increase the separation factor further, some researchers (Koresh and Sofer, 1983,1986) have studied molecular sieve carbon (MSC) membranes prepared by pyrolysis of polymer films. The authors reported separation factors much higher than those predicted for Knudsen diffusion (e.g., H_2O/O_2 and O_2/N_2 selectivities of 20 and 8, respectively). The high selectivity was attributed to molecular sieving or size discrimination effect. An O_2 permeability of 110 Barrer (1 Barrer = $10^{-10}\frac{cm^3(STP)}{cm\ sec\ cmHg}$) was reported, which is very large compared to typical polymer values (Koresh and Sofer, 1986)

The fabrication of microporous carbon membranes by the pyrolysis of poly(vinylidene chloride) that will selectively permeate alkanes over

hydrogen was reported (Rao and Sircar, 1992, 1993). In contrast to the approach of Koresh and Sofer (1986) described above, Rao and Sircar (1992, 1993) chose to optimize the microstructure of their membranes such that surface diffusion become the controlling mechanism. Although the ideal separation factors from pure gas measurements suggested that the membranes were selective for H_2, in mixed gas transport measurements the membranes were selective for C_2 to C_4 alkanes over hydrogen. At 295 K and a feed pressure of 4.4 atm, the mixture C_4H_{10} separation factor was 94.

Others (Hammel et al., 1989) have reported manufacturing microporous silica hollow fiber gas separation membranes with extremely small pores. According to these reports, hollow glass fibers are leached with acid solutions, removing the alkali metal oxides and producing a network of micropores with a diameter less than 20 Å. Some others (Shelekhin et al., 1991) prepared molecular sieve composite membranes by partially pyrolyzing silicon containing polymer films supported on porous Vycor glass tubes. A H_2/SF_6 separation factor 38 times larger than Knudsen diffusion selectivity was reported for their composite membrane (Shelekhin et al., 1991).

Uhlhorn et al. (1989) have deposited SiO_2 sols on γ-Al_2O_3 supports to produce gas separation membranes which demonstrate molecular sieving behavior. A H_2/N_2 separation factor of 2000 was observed at 723 K. However, the microporous SiO_2 layer was unstable and was reported to densify with prolonged contact with ambient air containing water vapor.

Microporous inorganic membranes were prepared by the sol-gel technique (Brinker et al., 1993). Polymeric silicate sols were deposited on commercial alumina ultrafilters and the resulting membranes were extensively characterized. A mean pore size of less than 10 Å for the silica top layer was inferred from reductions in He and N_2 pure gas permeance values

compared to the alumina support. However, the He/N_2 ideal separation factors were less than the calculated Knudsen value.

Pure gas permeabilities of gases as a function of temperature for microporous silica hollow fiber membranes were reported (Way and Roberts, 1992). These developmental hollow fiber membranes were manufactured by PPG Industries (Hammel et al., 1989). The transport mechanism for gas permeation was shown to be non-Knudsen since several heavier gases such as CO_2 permeated faster than lighter gases such as N_2. High ideal selectivities of 163 and 62.4 were observed at 343 K for H_2/N_2 and H_2/CO, respectively, which compare favorably with polymeric gas separation membranes. It was proposed that the controlling transport mechanisms were surface diffusion and molecular sieving.

Ma and coworkers (1992) have studied gas adsorption and permeability characteristic as a function of temperature using a different sample of the PPG silica hollow fiber membrane. Equilibrium adsorption isotherms for CO_2, H_2O, C_2H_2, CH_4, C_2H_2OH, and CH_2Cl_2 were measured at high pressure and temperatures of 303 and 343 K (Bhankarkar et al., 1992). The Dubinin-Radushevich isotherm was found to give the best fit of the data. No multilayer adsorption or capillary condensation was observed at the experimental conditions. An Arrhenius type relationship between pure gas permeability and temperature for He, CO_2, O_2, N_2, and CH_4 was observed (Shelekhin et al., 1992). The pure gas permeabilities were inversely proportional to the kinetic diameter of the penetrants. High ideal separation factors were observed. It was concluded that adsorption plays a minor role in mass transport in the silica hollow fiber membranes. Shelekhin et al. (1993) used percolation theory to describe the microstructure of the silica hollow fiber membranes. Monte-Carlo methods were used to estimate the

membranes tortuosity factor, porosity, and surface area. The tortuosity was found to be dependent on the total porosity of the membrane and the surface area was inversely proportional to the pore diameter. The pore diameter was estimated to be between 5 and 20 Å.

2.3 Surface Chemistry of Porous Silica

Because of the practical importance of porous silica, the surface properties of this material have been extensively studied. The interaction of silica with several molecules has been studied, mainly by means of vibrational spectroscopy (Knozinger, 1976). The surface chemistry and adsorption behavior of silica can be studied by a series of spectroscopic techniques with varying degrees of success (Garofalini, 1990). Techniques such as IR and Raman spectroscopies have been used to study silica surfaces.

One of the important properties of porous silica is its affinity for moisture (Unger, 1979). Several researches have tried to determine the number of OH^- groups on silica surface. It has been determined that there are 4.5-5 of OH^- groups per square nanometer of the surface by the use of spectroscopic methods such as Proton Nuclear Magnetic Resonance (PMR), and chemical reaction such as esterification or chlorination (Iler, 1979).

The surface chemistry of silica is shown in Figure 2.2 (Iler, 1979). According to the author, the hydroxyl groups start to condense and evolve water extensively above 443 K, and the internal water and hydroxyl groups can be removed starting at 473 K. The smaller the pores, the harder it is to remove water because the surface hydroxyls are hydrogen bonded to each other. There are two kinds of adsorbed water on hydroxylated silica, one that is desorbed during drying at 298-378 K called "physically adsorbed" which

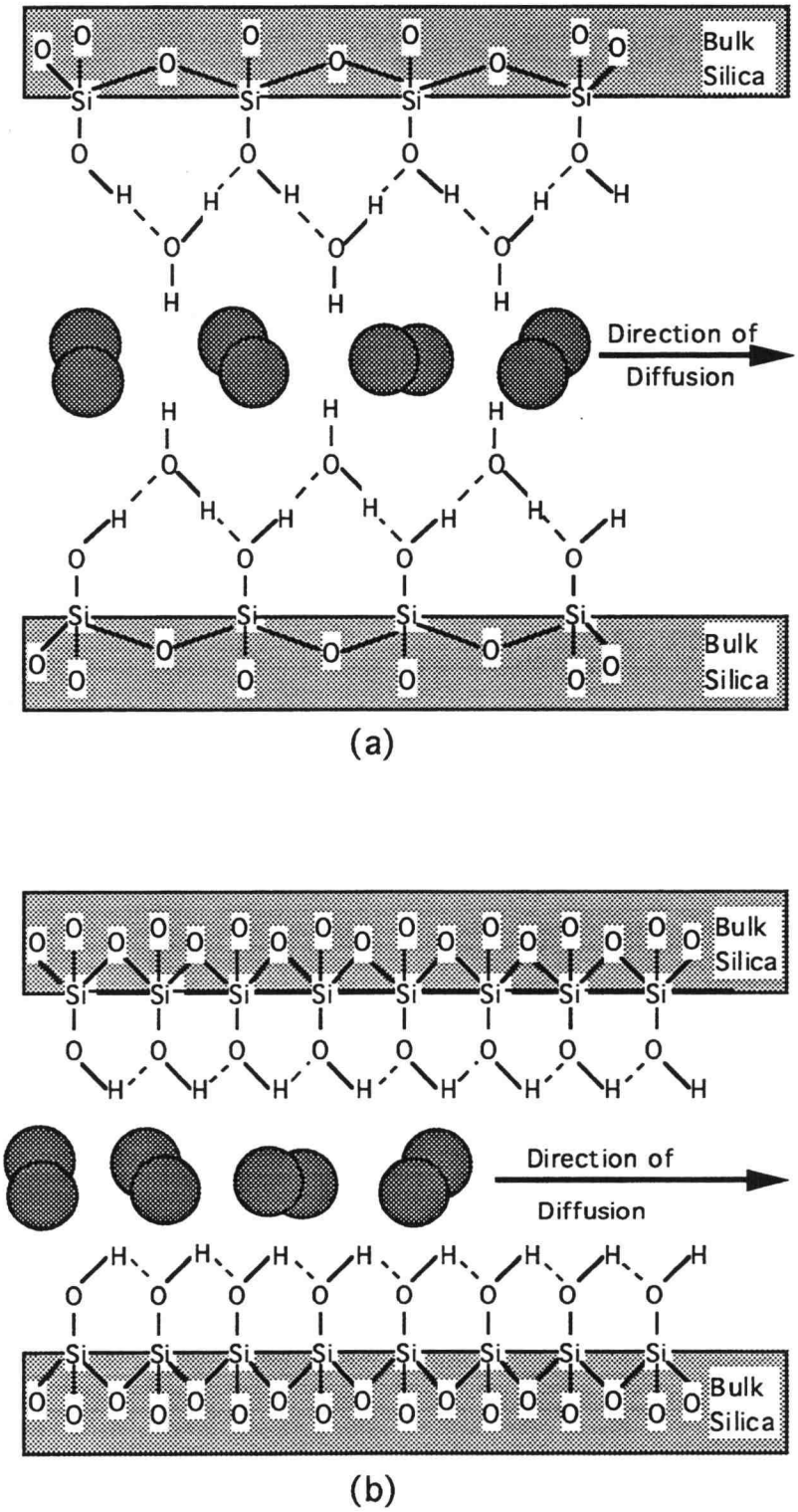

Figure 2.2 Surface chemistry of silica (a) at 298 K and (b) at 448 K.

requires an activation energy of 6.6-8.2 kcal/mole for removal. Water evolved at 378-453 K is called "hydrogen bonded" which requires an activation energy of 10 kcal/mole for removal (Iler, 1979).

2.3.1 Ab Initio Theory for Calculation of Surface Properties

Ab initio theory, which is a nonparametrized molecular orbital treatment, can be used to predict the properties of atomic or molecular systems. This theory is able to evaluate the interatomic forces from the fundamental laws of quantum mechanics, using several constants such as Planck's constant, the electron charge, the speed of the light, the mass of nuclei and electrons, with no empirical or semiempirical constants (Lasaga, 1992). In ab initio theory, Schrodinger equation is used to describe the wavefunction characteristic of a particle as:

$$\left\{-\frac{h^2}{8\pi M}\nabla^2 + V\right\}\Psi(r,t) = \frac{ih}{2\pi}\frac{\partial\Psi(r,t)}{\partial t} \qquad (2\text{-}14)$$

where Ψ is the wavefunction, h is the Plank's constant, V is the potential field in which the particle is moving, and m is the mass of the particle.

Equation 2-14 can be simplified into two equations by using separation of variables: one depends on the position of the particle independent of time and the other is a function of time alone. The time independent Schrodinger equation which is of interest is given as:

$$H\Psi(r) = E\Psi(r) \qquad (2\text{-}15)$$

where E is the energy of the particle and H is the Hamiltonian operator given by:

$$H = -\frac{h^2}{8\pi M}\nabla^2 + V \qquad (2\text{-}16)$$

Equation 2-16 consists of kinetic (first term) and potential (second term) energy terms. The potential energy consists of the summation of all electron-nuclei attractions, all electron-electron, and all nuclear-nuclear repulsions.

Ab initio theory makes use of the Born-Oppenheimer approximation that the nuclei remain fixed on the time scale of electron movement. This simplifies the problem by separating nuclear and electronic motions. As a result, the distribution of electron within a molecular system depends on the position of the nuclei, not their velocities.

In addition, the electrons are approximated as independent particles that interact mainly with the nuclear charges and with an average potential from other electrons. As a result of this approximation, the Schrodinger equation becomes a set of independent one-electron equations. In other words, the exact wavefunction, $\Psi(r)$, can be approximated as a single determinant:

$$\Psi(r) = \phi_1\phi_2\phi_3\phi_4\cdots \qquad (2\text{-}17)$$

Equation 2-17 is known as the Hartree-Fock product which is referred to as Hartree-Fock (HF) approximation. Because the movements of the electrons are assumed to be independent of each other, they are correlated to a certain extent so as to minimize repulsion as much as possible. For example, the Moller-Plesset perturbation theory may be added to the Hartree-Fock

theory to account for electron correlation. In the perturbation theory, Hamiltonian consists of two parts:

$$H = H_{nonperturbed} + \kappa V \qquad (2\text{-}18)$$

The first term is the nonperturbed part and the second term is a part with small perturbation.

The most important part of all ab initio calculations is the choice of atomic orbitals referred to as the basis set (mathematical description of the orbitals). Almost all of the calculations employ Gaussian type orbital basis sets in which each atomic orbital is made up of a number of Gaussian probability functions (see Appendix B). The simplest basis set is STO-3G which is known as a minimal basis set, and with each atomic orbital (STO stands for a hydrogenlike or Slater-type orbital) expanded by three Guassian functions. To obtain a more realistic result, more Gaussians are used to more accurately approximate the orbitals by imposing fewer restrictions on the locations of the electrons in space. The accuracy of the calculations increases as the number of Gaussians increases (large basis set), but more accurate calculations comes only at the expense of greater computational cost.

The most commonly used basis sets are STO-3G, 3-21G, 3-21G*, 3-21G**, 3-21+G**, 4-31G, 4-31G*, 4-31G**, 4-31+G**, 6-31G, 6-31G*, 6-31G**, and 6-31+G**. Nomenclature of the basis sets (except minimal basis set) are as follows: the first number is the number of Gaussian functions used to expand the atomic orbitals in the core of the atom. After a dash, two numbers are usually given for the numbers of Gaussian functions used in expanding the valence atomic orbitals for a split-valence basis sets which allows orbitals to change size. The first and second numbers are the number of Gaussian

functions used to expand the atomic orbitals in the inner and outer orbitals respectively. Polarization effect is usually added for the change of the shape by adding orbitals with angular momentum usually shown by (*). For the systems where electrons are relatively far from the nucleus, a diffuse function shown by (+) is also added. Diffuse functions allow orbitals to occupy a larger region of space (large-size versions of s- and p-type functions).

As an example 6-31+G** basis set uses six Gaussian functions for the core orbitals, three and one Gaussians for the inner and outer valence orbitals respectively, and also adds d (first *) and p (second *) orbitals on all first and second row atoms. In addition, diffuse functions (+) are added to heavy atoms.

2.3.2 Ab Initio Calculations

While there is an abundance of experimental data, there are few theoretical published papers on silica. By means of high-quality ab initio calculations, the interaction of CO (Ugliengo et al., 1989), H_2O (Garofalini, 1990 and Ugliengo et al., 1990), H_2 (De Almeida et al., 1993 and Garrone et al., 1992), and H_2CO (Ugliengo et al., 1990) with silica have been recently studied. In all of these cases, the calculations have been carried out using two simple clusters, Silanol, H_3SiOH, and Orthosilicic acid, $Si(OH)_4$, as molecular models for the isolated surface hydroxyl. The literature shows that the use of either of models to mimic a free hydroxyl group gives interaction energies, geometries, and vibrational modes that satisfactorily agree with experimental results.

In spite of all the reports, the transport mechanism(s) in microporous silica hollow fiber membrane for gas separation is not yet well known. An improved understanding of these mechanism(s) requires the knowledge of pore size distribution and surface chemistry, along with heat of adsorption of the gaseous species at the surface. Studying multicomponent mixtures is another way to increase understanding of the surface effect. Thus, results from pure and multicomponent mixtures, as well as pore size distribution, and heat of adsorption of gaseous species, make it possible to better understand the gas transport mechanism(s) through the microporous silica hollow fiber membrane.

Chapter 3

Pore Size Distribution

3.1 Introduction

One of the steps in better understanding the mechanisms of gas transport through silica membranes is the understanding of the membrane microstructure by measuring pore size distribution. The objective of this chapter is to verify that the average pore size in silica membranes is indeed small (less than 20 Å), so that the possible mechanisms of gas transport through the membranes are the four mechanisms explained in chapter 2. In addition, the pore size distribution gives an indication of the size of the pores. For the activated diffusion mechanism, a smaller pore size results in higher separation factors. Knowing the average pore size, activation energy can also be estimated using Lennard-Jones potential (see Chapter 4).

3.2 Theory

The classification of the pore size adopted by IUPAC is as follows:

- micropores, when pores are less than 20 (Å).
- mesopores, when pores are between 20 - 500 (Å).
- macropores, when pores are greater than 500 (Å).

For calculation of pore size distribution in mesopores the most widely used method is the Kelvin equation (equation 2-4). However, the Kelvin equation has several limitations in the micropore region. One of which is that the concept of forming meniscus by few molecules is meaningless in microporous region.

To be able to calculate the pore size distribution in microporous, two models are used: (1) H-K (slit) model (Horvath and Kawazoe, 1983) and (2) S-F (cylinder) model (Saito and Foley, 1991).

3.2.1 H-K (Slit) Model

Assumptions made in this model are: i) a slab geometry with the slit walls of two infinite planes at a distance of L apart from each other, and ii) adsorption occurs on the two parallel surfaces as shown in Figure 3.1.

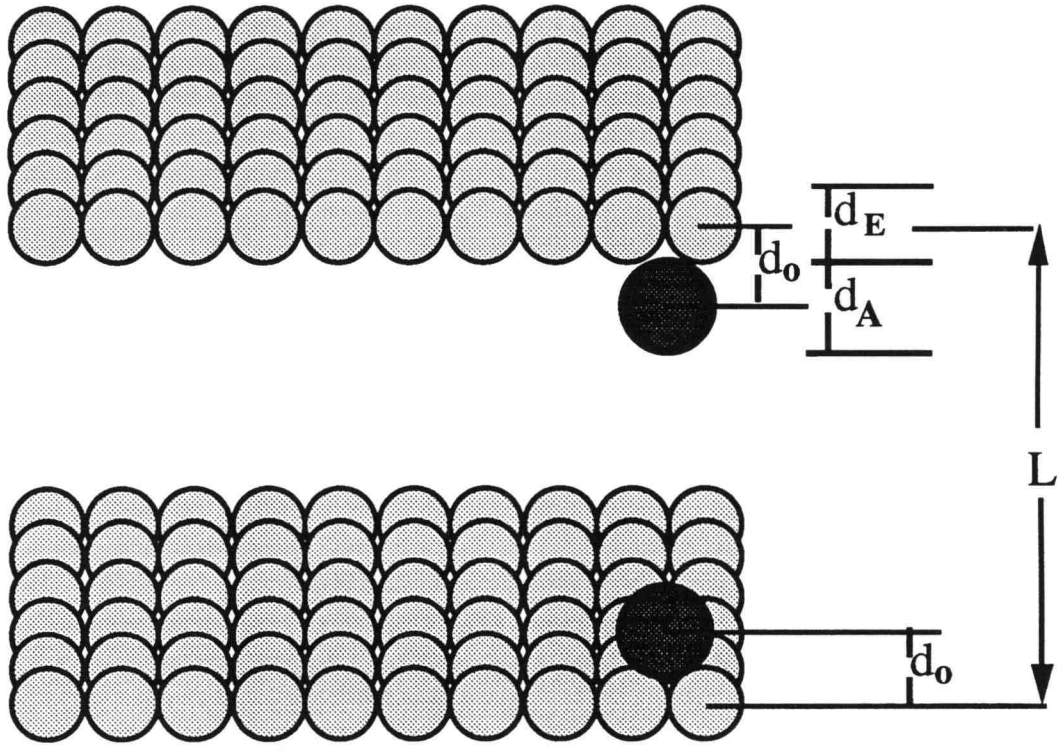

Figure 3.1 H-K (Slit) model representation of the pores.

The energy of interaction, E, between one adsorbate molecule and two layers can be expressed using Lennard-Jones potential and is given as:

$$E(Z) = KE^{*}\left\{-\left(\frac{\sigma}{Z}\right)^{m}+\left(\frac{\sigma}{Z}\right)^{n}-\left(\frac{\sigma}{L-Z}\right)^{m}+\left(\frac{\sigma}{L-Z}\right)^{n}\right\} \tag{3-1}$$

where K and σ are defined as (Everett and Powl, 1976):

$$K = \left(\frac{n}{n-m}\right)\left(\frac{n}{m}\right)^{\frac{m}{n-m}} \tag{3-2}$$

and

$$\sigma = d_o\left(\frac{m}{n}\right)^{\frac{1}{n-m}} \tag{3-3}$$

where n and m are the order of the dispersion and repulsion terms respectively and d_o is the arithmetic mean of the diameters of the adsorbate atoms, d_A, and the adsorbent atoms, d_E. Horvath and Kawazoe (1983) used the values of 10 for n and 4 for m.

In the case of the pore filled with adsorbate molecules, the value of E^{*} is defined as:

$$E^{*} = \frac{3}{10}\left(\frac{N_E A_{EA} + N_A A_{AA}}{d_o^4}\right) \tag{3-4}$$

where the dispersion constants (A_{EA}, A_{AA}) are given using the Kirkwood-Muller equations:

$$A_{EA} = \frac{6Mc^2\alpha_E\alpha_A}{\left(\frac{\alpha_E}{\chi_E} + \frac{\alpha_A}{\chi_A}\right)} \tag{3-5}$$

$$A_{AA} = \frac{3Mc^2\alpha_A\chi_A}{2} \tag{3-6}$$

To calculate the pore size distribution, the net potential energy of interaction between the layers is equated with the free energy of adsorption at equilibrium as follows:

$$RT\ln\left(\frac{P}{P_o}\right) = N_{av}\frac{\int_{d_o}^{L-d_o} E(Z)dZ}{\int_{d_o}^{L-d_o} dZ} \tag{3-7}$$

Combining equations 3-1 through 3-7 results in the Horvath and Kawazoe (1983) for the slit like geometry and it is given as:

$$RT\ln\left(\frac{P}{P_o}\right) = N_{av}\frac{N_A A_{AA} + N_E A_{EA}}{\sigma^4(L-2d_o)}\left(\frac{\sigma^4}{3(L-d_o)^3} - \frac{\sigma^{10}}{9(L-d_o)^9} - \frac{\sigma^4}{3d_o^3} + \frac{\sigma^{10}}{9d_o^9}\right) \tag{3-8}$$

where N_{av}, is Avogadro's number, N_A and N_E are the density of adsorbate and adsorbent per unit area respectively, α_E and α_A are the polarizability of the adsorbent and the adsorbate respectively, χ_E and χ_A are the magnetic susceptibility of the adsorbent and the adsorbate respectively.

3.2.2 S-F (Cylinder) Model

Assumptions made for this model are: i) perfect cylindrical pore with finite radius, r_p, and infinite length, ii) only a single layer of atoms in the inside wall, iii) only inside adsorption, and iv) only adsorbate-adsorbent interaction is allowed as is shown in Figure 3.2.

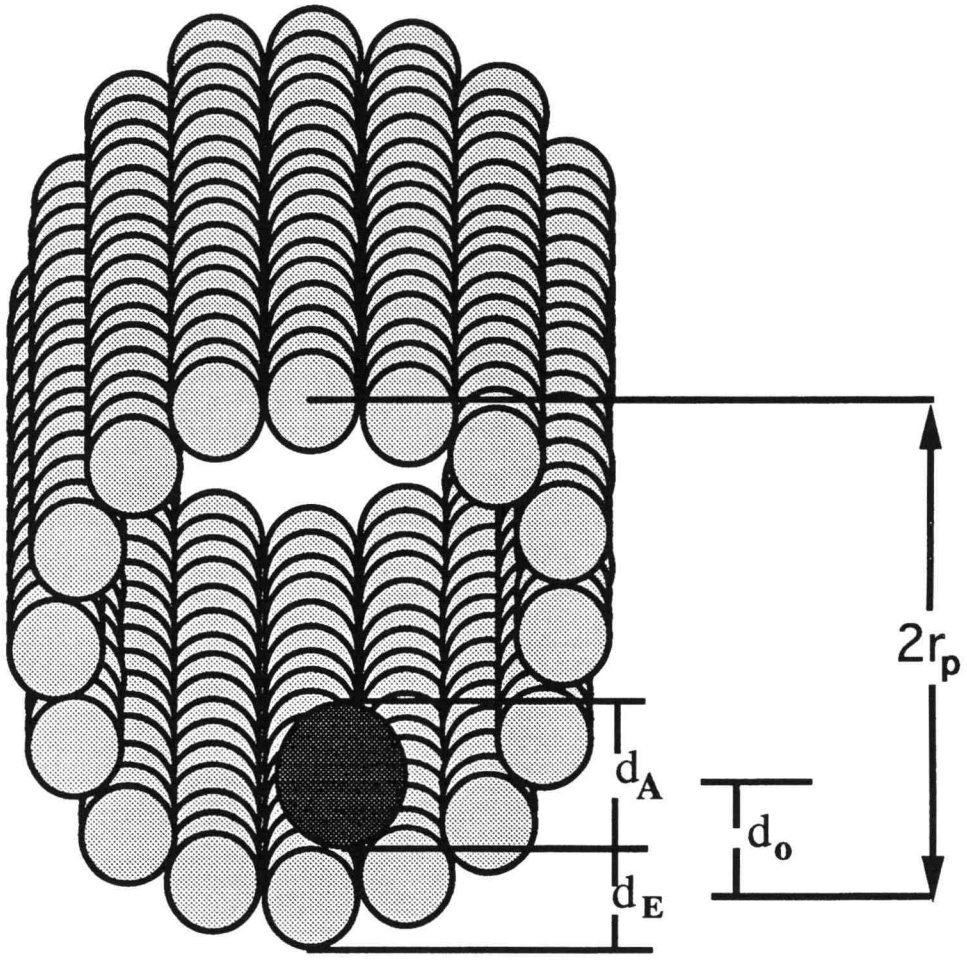

Figure 3.2 S-F (Cylinder) model representation of the pores.

The potential energy of interaction, E(r), between the adsorbate molecules and the inside wall of the cylinder is given as (Everett and Powl, 1976):

$$E(r) = \frac{5}{2}\pi E^* \left\{ \frac{21}{32}\left(\frac{d_o}{r_p}\right)^{10} \sum_{k=0}^{\infty} \alpha_k \left(\frac{r}{r_p}\right)^{2k} - \left(\frac{d_o}{r_p}\right)^{4} \sum_{K=0}^{\infty} \beta_k \left(\frac{r}{r_p}\right)^{2k} \right\} \qquad (3\text{-}9)$$

where constants α_k, and β_k are given by:

$$\sqrt{\alpha_k} = \frac{\Gamma(-4.5)}{\Gamma(-4.5-k)\Gamma(k+1)} \qquad (3\text{-}10)$$

$$\sqrt{\beta_k} = \frac{\Gamma(-1.5)}{\Gamma(-1.5-k)\Gamma(k+1)} \qquad (3\text{-}11)$$

E^* is given in equation 3-4, and the dispersion constants are the same as equations 3-5 and 3-6.

For a cylindrical pore, the area-averaged interaction potential is defined as:

$$\overline{E} = \frac{\int_0^{r_p - d_o} 2\pi r E(r) dr}{\int_0^{r_p - d_o} 2\pi r dr} \qquad (3\text{-}12)$$

Evaluating equation 3-12 by the use of equations, 3-4, 3-5, 3-6, and 3-9, and equating free energy of adsorption with the result of equation 3-12, the resultant equation is given by:

$$RT\ln\left(\frac{P}{P_o}\right)=\frac{3}{4}\pi N_{av}\frac{N_A A_{AA}+N_E A_{EA}}{d_o^4}\sum_{k=0}^{\infty}\left\{\frac{1}{k+1}\left(1-\frac{d_o}{r_p}\right)^{2k}\left[\frac{21}{32}\alpha_k\left(\frac{d_o}{r_p}\right)^{10}-\beta_k\left(\frac{d_o}{r_p}\right)^{4}\right]\right\} \tag{3-13}$$

where α_k and β_k can be approximated as:

$$\alpha_k=\left(\frac{-4.5-k}{k}\right)^2\alpha_{k-1} \tag{3–14}$$

$$\beta_k=\left(\frac{-1.5-k}{k}\right)^2\beta_{k-1} \tag{3–15}$$

with α_o and β_o both equal to one in equations 3-14 and 3-15.

3.3 Adsorption Isotherm and Pore Size Distribution

The next step in calculating the pore size distribution is to obtain an experimental adsorption isotherm (relationship between amount adsorbed and the relative pressure). Argon adsorption isotherm at 87.5 K for hollow fiber silica membranes was obtained using a high resolution pore analyzer (Omnisorp 100, Coulter Electronics, Hialeah, FL). Argon is used as the adsorbate to eliminate errors caused by the interaction of the quadrupole moment of nitrogen with the surface. Since the kinetic diameter of argon is 3.4 Å, smaller pores (if present) can be inaccessible to argon, thus, can not be measured. The silica hollow fiber sample exhibited a Type I isotherm characteristic of microporous materials (Gregg and Sing, 1982) as shown in

Figure 3.3. Figure 3.4 presents a pore size distribution for the silica fiber sample calculated with the data from Figure 3.3 using both the slit model (Horvath-Kawazoe potential function, equation 3-8) and the cylindrical model (Saito and Foley potential function, equation 3-13). The calculated average pore diameters are 6.2 Å for the slit model and 8.9 Å for the cylindrical model. The average pore size using the cylindrical model was higher than the average pore size using the flat plate model because more interactions are taken into account in the cylindrical model. The pore geometry of the silica hollow fibers is tortuous and neither model describes the actual physical situation. However, the pore size of the silica hollow fiber membranes should be between the geometrical extremes of two flat parallel plates and a right cylinder. Table 3.1 gives the values of the physical constants used in the pore size calculations with both of the H-K and S-F models.

To examine the validity of the potential functions, argon physical adsorption measurements were performed using zeolites with a range of known pore sizes including $AlPO_4$, mordenite, and silicalite powder (Thoen et al., 1994). By calculating the average pore diameter for the zeolite with a known structure, it is demonstrated that the actual pore diameter of the zeolite structure falls between the pore diameters predicted by the potential functions except for the case of silicalite powder in which the predicted pore diameter is about 10% lower than the actual pore size when S-F model is used. This might be due to the fact that the pores in silicalite powder are spherical which takes more interactions into account compared to two flat parallel plates (H-K model) and a right cylinder (S-F model). Comparison of the predicted and actual pore diameters for $AlPO_4$, mordenite, and silicalite powder is presented in Table 3.2. The actual pore diameter of a zeolite is

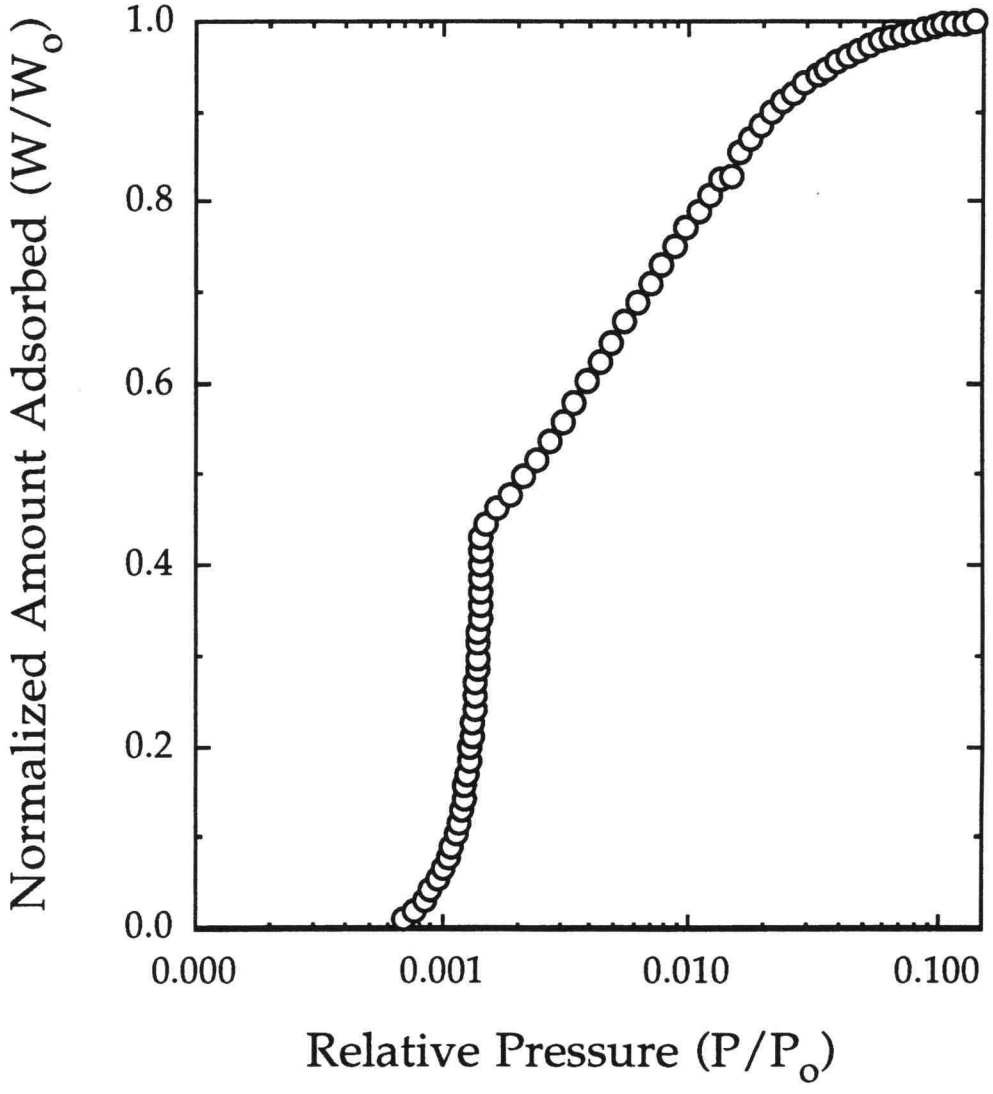

Figure 3.3 Low pressure argon adsorption isotherm at T = 87.5 K.

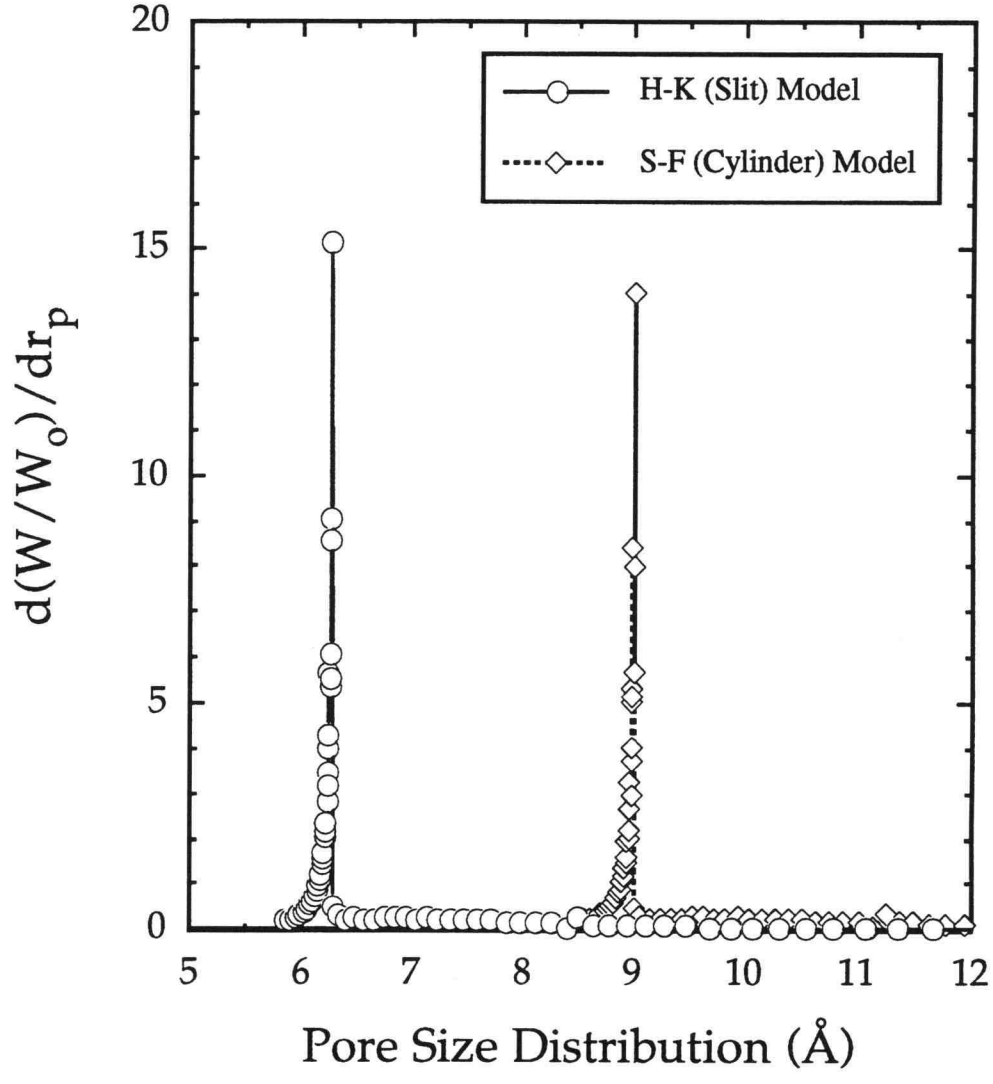

Figure 3.4 The pore size distribution for the silica hollow fiber membrane material calculated from Ar physical adsorption data at 87.5 K using the Horvath-Kawazoe (parallel plate) and Saito-Foley (cylinder) potential functions.

Table 3.1 Parameters for Pore Size Calculations

Parameter	Oxide Ion	Argon
Diameter, d(Å)	3.04[a]	3.40[b]
Polarizability, $\alpha(cm^3)$	0.85×10^{-24}[c]	1.63×10^{-24}[c]
Magnetic Susceptibility, χ (cm^3)	1.94×10^{-29}[c]	3.22×10^{-29}[c]
Density, N (molecules/cm^2)	3.75×10^{15}[d]	7.61×10^{14}[d]

a Micromeritics ASAP 2000 manual
b Kinetic diameter
c Values are derived from data found in Ross and Olivier (1964)
d Values are from liquid densities

Table 3.2 Comparison of the Predicted and Actual Pore Diameter of $AlPO_4$, Mordenite, and Silicalite Powder Using Argon Adsorption Data

Zeolite	Actual (Å)	H-K Model (Å)	S-F Model (Å)
$AlPO_4$	6.0	4.0	7.4
Mordenite	7.5	6.0	8.6
Silicalite Powder	6.0	4.1	5.6

calculated from the structural model of the oxygen rings forming the pore, based on an assumed diameter for the oxygen atom.

3.4 Pore Size Calculation

Equations 3.8 and 3.13 with adsorption data and physical parameters from Table 3.1 are used to obtain pore size distribution. To calculate pore size, a MATLAB computer program was developed to obtain a relationship between pore size, r_p, and relative pressure, P/P_o, [$r_p = f(P/P_o)$]. In addition, a FORTRAN program was developed to read adsorption data and relate the amount adsorbed, W, to the pore size, r_p, [$W = f(r_p)$]. The program also performs numerical differentiation to obtain $d(W/W_o)/dr_p$, where W_o is the amount adsorbed at saturation. The documentation of pore size calculation is presented in Appendix D.

3.5 Conclusions

The results show that the pore size of the microporous silica membrane is 6.2 Å and 8.9 Å using H-K and S-F potential functions respectively. The pore geometry of the silica hollow fibers is tortuous and neither model describes the actual physical situation. However, the pore size of the silica hollow fiber membranes should be between the geometrical extremes of two flat parallel plates and a right cylinder. Also, the distribution of the pores are found to be narrow. The validity of the potential functions and the model parameters in Table 3.1 is examined by performing argon physical adsorption measurements using zeolites with a range of known pore sizes.

Chapter 4

Pure and Binary Gas Mixture Permeation

4.1 Introduction

This chapter is essential in better understanding the mechanisms of gas transport in microporous silica membranes. Temperature and pressure effects on permeance of gaseous species with kinetic diameters between 2.6 to 3.9 Å are studied in this chapter. The kinetic diameter is the hard sphere diameter for the penetrant molecules calculated from a transport property such as viscosity or thermal conductivity (Breck, 1974). Comparison of the permeance values of the gaseous species with different molecular weights and dependency of temperature on permeance are useful in concluding the importance of molecular sieving and Knudsen diffusion mechanisms during gas transport through the microporous silica membranes. The values of activation energy and its dependency on kinetic diameter of gaseous species are also important in better understanding the transport mechanisms through microporous silica membranes.

The effect of membrane surface chemistry on gas transport through the silica membranes can be studied by obtaining permeation experiments with gas mixtures and comparing the results with those obtained using only pure gases.

4.2 Theory

4.2.1 Flux Equation for Diffusion Through Silica Hollow Fiber Membranes

A silica hollow fiber membrane can be considered as a long tube (length to diameter ratio $\rangle 10^3$). One end of the membrane is usually sealed off, and the other end is kept open. The gas diffuses from one side of the fiber where the total pressure, P_T, is higher than the other side of the fiber (lower pressure side).

For steady state, with no chemical reaction, the continuity equation becomes:

$$\nabla N_{i,total} = 0.0 \tag{4-1}$$

Total flux of species i (mole flow rate of species i per unit area of the membrane), $N_{i,total}$, can be defined as the combination of the flux through the pores of the membrane, $N_{i,pore}$, and the flux through the solid lattice of the membrane, $N_{i,lattice}$ given by:

$$N_{i,total} = \varepsilon N_{i,pore} + (1-\varepsilon) N_{i,lattice} \tag{4-2}$$

where ε is the void fraction.

Diffusion through the solid lattice is much slower than that through the pores even for gases with small molecular diameter at high temperatures. This has been verified by calculating the flux of He at high temperatures in nonporous silica. The data for this calculation was obtained from Barrer (1951). Thus, equation 4-2 reduces to:

$$N_{i,total} = \varepsilon N_{i,pore} \tag{4-3}$$

Bhankarkar et al. (1992) studied equilibrium properties of gaseous species on a microporous silica membrane very similar to the membranes used in this study by obtaining high pressure adsorption isotherms for several gases. They observed no hysteresis in the adsorption/desorption cycle. Thus, it was concluded that capillary condensation for gases at the temperatures and pressures of interest does not occur (Bhankarkar et al., 1992). Therefore, the total flux is the flux through the pores and it is the combination of the gas phase (molecular sieving and/or Knudsen) diffusion and the adsorbed phase (surface) diffusion, assuming no capillary condensation.

4.2.2 Relationship Between Diffusion Coefficient and Permeability

The permeability of i, Q_i, is defined as the ratio of the flux of i, J_i, passing through a membrane of straight pores over the pressure gradient, ∇P_i, which is given as:

$$Q_i = -\frac{J_i}{\nabla P_i} \tag{4-4}$$

Assuming $J_i = N_i$ and using Fick's law of diffusion, equation 4-4 reduces to:

$$Q_i = \varepsilon D_i \sum_{j=1}^{N} \frac{\partial C_i}{\partial P_j} \tag{4-5}$$

The term, $\frac{\partial C_i}{\partial P_j}$, in equation 4-5, describes the dependency of permeability on pressure. The permeability equation (equation 4-5) can be reduced for the three different mechanisms:

1) Knudsen diffusion mechanism: the flow is in the gas phase in Knudsen regime. Therefore, assuming ideal gas law, equation 4-5 reduces to:

$$\frac{\partial C_i}{\partial P_j} = \frac{1}{RT} \tag{4-6}$$

and

$$Q_i^K = \varepsilon \frac{D_i^K}{RT} \tag{4-7}$$

Combination of equation 4-7 with equation 2-2 and taking the tortuosity factor, τ, into account, the permeability equation in Knudsen regime reduces to:

$$Q_i^K = \frac{8\varepsilon}{3\tau} r_p \sqrt{\frac{1}{2\pi RTM_i}} \tag{4-8}$$

2) Surface diffusion mechanism: the permeability equation in surface diffusion regime, after accounting for the tortuosity factor, τ, reduces to:

$$Q_i^S = \frac{\varepsilon}{\tau} \overline{D}_i^S \sum_{j=1}^{N} \frac{\partial C_i^S}{\partial P_j} \tag{4-9}$$

Combining equation 4-9 with equation 2-7:

$$Q_i^S = \frac{\varepsilon}{\tau} g\beta^2 \nu_e \left(\sum_{j=1}^{N} \frac{\partial C_i^S}{\partial P_j} \right) e^{-\left(\frac{E_i^S}{RT}\right)} \qquad (4\text{-}10)$$

The pressure dependency term, $\frac{\partial C_i^S}{\partial P_j}$, in equation 4-10 can be obtained from the slope of the adsorption isotherm at pressure P_i for a single component. For the multicomponent mixtures, the pressure dependency term, $\frac{\partial C_i^S}{\partial P_j}$, in equation 4-10, can be calculated by using the ideal adsorbed solution (IAS) theory (see Appendix A).

3) Molecular sieving or activated diffusion mechanism: since the diffusing molecules are assumed to retain their gaseous characteristics, equation 4-6 is valid for this mechanism as well. Thus, from equations 4-5 and 4-6, the permeability equation in molecular sieving regime, after the tortuosity factor, τ, is taken into account, reduces to:

$$Q_i^{MS} = \frac{\varepsilon}{\tau} \frac{D_i^{MS}}{RT} \qquad (4\text{-}11)$$

After combining equations 4-11 with 2-13 and assuming $\beta = 2r_p$ and $g = 1/3$, the resultant equation can be written as:

$$Q_i^{MS} = \frac{8}{3}\left(\frac{\varepsilon}{\tau}\right) r_p \sqrt{\frac{1}{2\pi RTM_i}} e^{-\left(\frac{E_i^{MS}}{RT}\right)} \qquad (4\text{-}12)$$

Thus, the total permeability (by combining the three mechanisms, the transport in Knudsen and molecular sieving regimes are considered to occur in gas phase whereas the transport in surface diffusion regime is considered to occur in the adsorbed phase) can be written as:

$$Q_i^{total} = Q_i^{gas-phase(MS/K)} + Q_i^{adsorbed-phase(Surf.diffusion)} \tag{4-13}$$

Or:

$$Q_i^{total} = \frac{\varepsilon}{\tau}\left(\frac{D_i^{gas}}{RT} + \overline{D}_i^{S}\sum_{j=1}^{N}\frac{\partial C_i^{S}}{\partial P_j}\right) \tag{4-14}$$

where D_i^{gas} is the gas phase diffusion coefficient in molecular sieving and/or Knudsen diffusion.

After rearranging, equation 4-14 can be written as:

$$E_{MM} = 1 + \frac{\overline{D}_i^{S}}{D_i^{gas}}RT\sum_{j=1}^{N}\frac{\partial C_i^{S}}{\partial P_j} \tag{4-15}$$

where the microporous membrane enhancement factor, E_{MM}, is defined as:

$$E_{MM} = \frac{Q_i^{total}}{Q_i^{gas-phase}} = \frac{\tau}{\varepsilon}RT\frac{Q_i^{total}}{D_i^{gas}} \tag{4-16}$$

After combining with the gas phase and surface diffusion coefficients, D_i^{gas}(equation 2-13) and $\overline{D}_i^S$ (equation 2-7) respectively and equation 2-8, equation 4-15 simplifies to:

$$E_{MM} = 1 + r_p \sqrt{\frac{H_c RT}{2\pi N_{av}}} \left(\sum_{j=1}^{N} \frac{\partial C_i^S}{\partial P_j} \right) e^{-\left(\frac{E_i^S - E_i^{gas}}{RT} \right)} \qquad (4\text{-}17)$$

Equation 4-17 is a general equation that accounts for both the temperature and pressure dependencies on permeability for transport of gaseous species through the microporous membranes for pure components as well as multicomponent mixtures. The microporous membrane enhancement factor, E_{MM} can be calculated if r_p, $\frac{\partial C_i^S}{\partial P_j}$, E_i^S, and E_i^{gas} are known. The value of r_p can be estimated from the pore size measurements (Chapter 3), $\frac{\partial C_i^S}{\partial P_j}$ can be obtained from the high pressure adsorption isotherms, E_i^{gas} can be estimated from Lennard-Jones potential (see section 4.2.3) for molecular sieving mechanism and is zero in Knudsen regime, and E_i^S is related to the heat of adsorption of i (Gilliland et al., 1974).

4.2.3 Estimation of Activation Energy

Lennard-Jones potential can be used to estimate the magnitude of the activation energy (Way and Roberts, 1992; Xiao and Wei 1992). To be able to use this potential, only the interaction between diffusing molecules and the surface oxygen atoms are taken into account, ignoring all other interactions, such as the interaction between diffusing molecules with each other and with

silicon atoms at the surface. Assuming eight oxygen atoms at the perimeter of the pore (Xiao and Wei, 1992), the Lennard-Jones potential is given as:

$$E_i = \sum_{\text{Oxygen-atoms}} 4\bar{\varepsilon}_{i-o2}\left\{\left(\frac{\sigma_{i-o2}}{r_p}\right)^{12} - \left(\frac{\sigma_{i-o2}}{r_p}\right)^{6}\right\} \tag{4-18}$$

where:

$$\bar{\varepsilon}_{i-o2} = \sqrt{\bar{\varepsilon}_i \bar{\varepsilon}_{o2}} \tag{4-19}$$

$$\sigma_{i-o2} = \frac{\sigma_i + \sigma_{o2}}{2} \tag{4-20}$$

where σ_i, σ_{o2} are the "hard sphere" kinetic diameter and $\bar{\varepsilon}_i, \bar{\varepsilon}_{o2}$ are the minimum potential energy of species i and the oxygen molecule (o_2) respectively and r_p is the intermolecular distance (or pore radius for molecular sieving).

For the average pore size of 6.4 Å, the activation energy of several gaseous species was calculated using equations 4-18 to 4-20 and the results are shown in Table 4.1. These results were obtained using the interactions of the diffusing molecules with eight oxygen molecules present at the perimeter of the pore (Xiao and Wei, 1992). Although this assumption oversimplifies the phenomena, the model can nevertheless reveal some features of the interaction between the diffusing molecules and the pores of silica membranes.

Table 4.1 Estimation of Activation Energy Using Lennard-Jones Potential with 6.4 Å as the Pore Diameter

Component	$\bar{\varepsilon}_i/k$ (1/K)	$\bar{\varepsilon}_{i-O_2}/k$ (1/K)	$\sigma_{i\text{-}O_2}$ (Å)	E_i (kcal/mole)
He	10.2	34.7	3.01	-0.47
H_2	37.0	66.1	3.19	-0.08
CO_2	195.2	151.8	3.38	5.21
Ar	119.8	118.9	3.43	5.92
O_2	118.0	118.0	3.46	7.17
N_2	95.1	105.9	3.58	12.68
CO	100.2	108.7	3.61	15.12
CH_4	148.2	132.2	3.64	21.24
C_2H_4	243.0	169.3	3.71	37.35

4.3 Experimental

4.3.1 Membrane Materials

PPG Industries provided the microporous hollow fiber membranes used in this work. The fibers were manufactured by melt extrusion of borosilicate glass followed by acid leaching to remove the alkali oxides producing a network of pores less than 20 Å in diameter (Hammel et al., 1989). The inside and outside diameters of the hollow fibers were measured to be 35 μm and 45 μm respectively using scanning electron microscopy as presented in Figure 4.1. The fibers were 14.0 centimeter long.

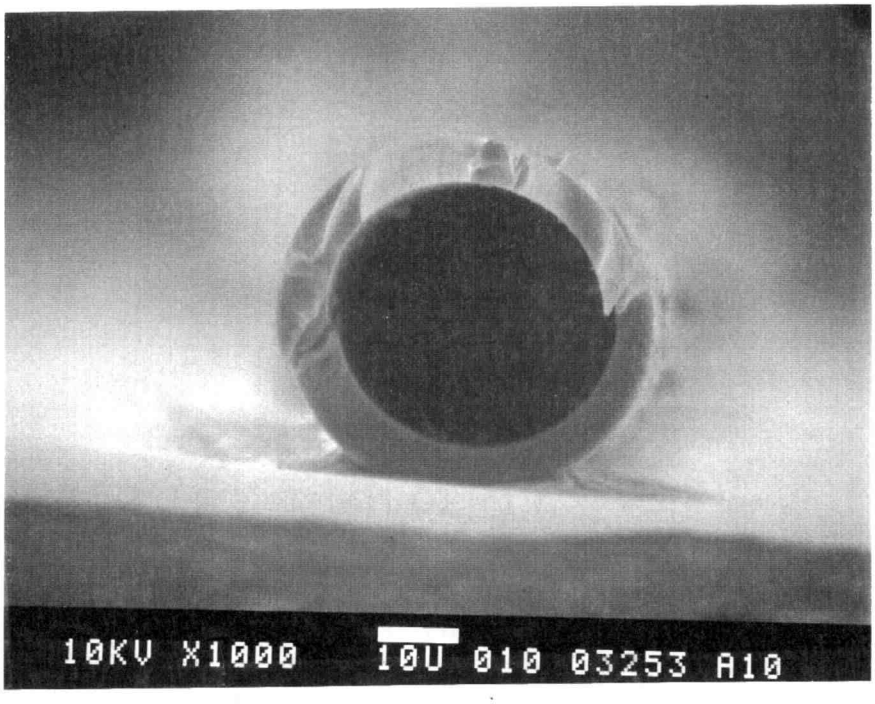

Figure 4.1 SEM photograph of the silica hollow fiber membrane.

4.3.2 Transport Measurements

The schematic diagram of the silica membrane test system is shown in Figure 4.2. The system can be divided into three sections: i) controlling and mixing section, ii) separation section, and iii) analyzing section. In the controlling and mixing section, one is capable of mixing up to three different gases. In this section, three mass flow controllers (Brooks Model 5850E), which were able of providing full scale flows of 20 to 500 standard cubic centimeters per minute (sccm) depending on the size of the internal orifices, were used. To have an indication of the flow rates, the controllers were commanded with a Tylan-General Model RO-28 (Torrance, CA) control box. To control the temperature, an oven capable of temperatures up to 623 K was used in the separation section. The oven could accommodate two test cells each approximately 20 cm long. Silica hollow fiber membranes were placed inside the test cells. One end of the membrane was sealed off using a torch flame, and the other end was kept open. The gas flows over the fiber that was usually kept at 20 atm using a backpressure regulator. Finally, in the analyzing section, the residue and the permeate streams were measured using bubble flow meters. The composition of the residue and permeate streams were measured using gas chromatography (Hewlett-Packard Model 5890, Series II). Data acquisition and injection sequence were handled automatically with the Hewlett-Packard ChemStation computer program.

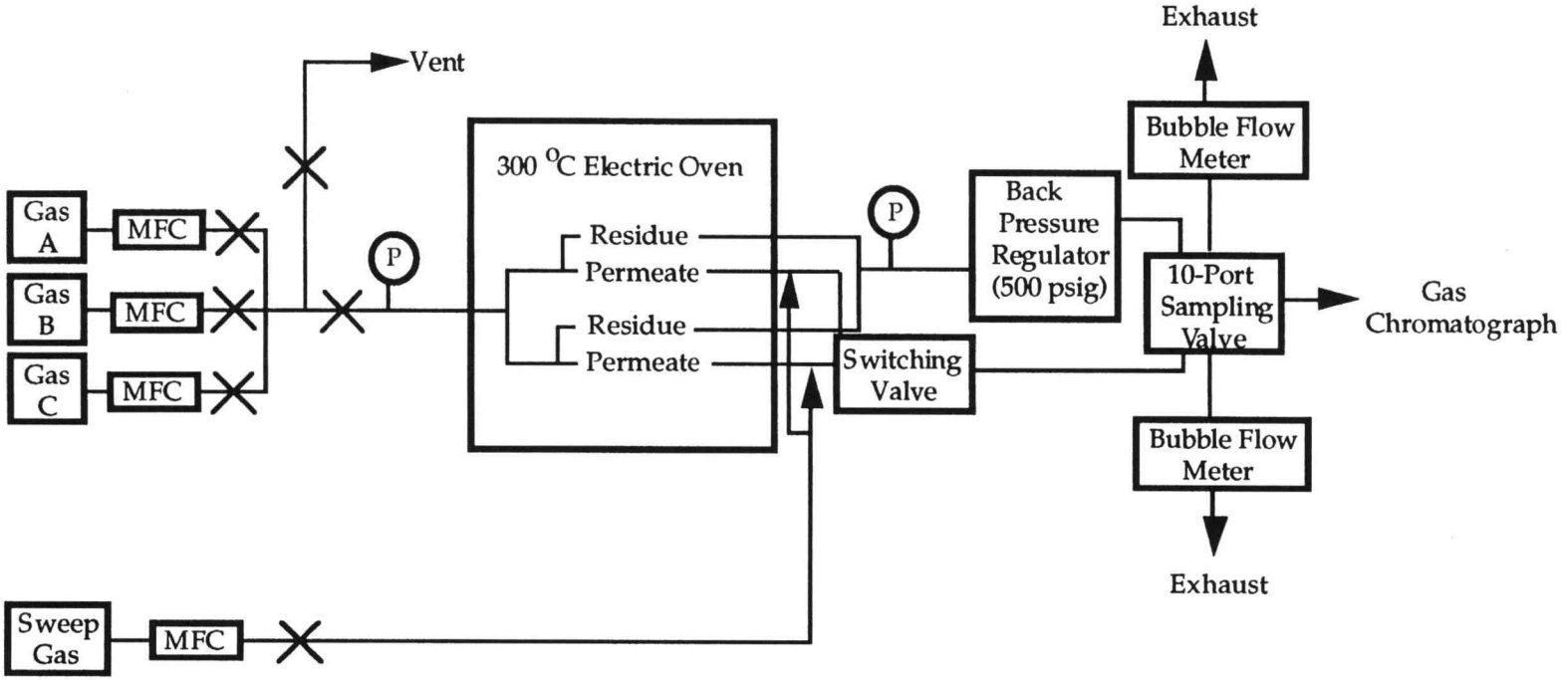

Mixed gases flow into the oven where the membrane cell is located. Feed to the membrane flows over the outside of the fiber; a small portion permeates through the fiber. The nonpermeate, or residue, stream and the permeate stream are analyzed by gas chromatography. Flow of the permeate is determined with a bubble flow meter.

Figure 4.2 Schematic diagram of the inorganic hollow fiber membrane test system. MFC refers to a mass flow controller.

4.4 Data Reduction

To reduce the raw data, two methods were used depending on the permeate flow rate:

i) For low permeate flow rate (constant pressure inside the fiber):

1) Pure gas permeability, Q_i, was calculated from the permeate flow rate (volumetric flow rate, Q_i^*), feed pressure, P_i, and the membranes dimensions (inside radius, r_i, outside radius, r_o, and length, L_f) by using the equation:

$$Q_i = \frac{Q_i^*(STP)\ln\left(\frac{r_o}{r_i}\right)}{2\pi L_f \Delta P_i} \qquad (4\text{-}21)$$

Ideal gas selectivity or separation factor, α_{ij}, is defined as the ratio of pure gas permeabilities (selectivity and separation factor are used interchangeably in the text):

$$\alpha_{ij} = \frac{Q_i}{Q_j} \qquad (4\text{-}22)$$

2) Multicomponent gas mixture permeability can be calculated from the flow rate of each component of the feed gas, the feed gas pressure, the flow rate of the permeate gas, the composition of the permeate gas, the permeation temperature, and the dimensions of the membranes. Since the permeate flow rates were small and no reliable method is known that is capable of measuring the sometimes very small flow rates coming from the membranes, a helium sweep stream, which has

a much higher rate than the permeation rate, was used. For multicomponent gas mixtures, equation 4-21 is still valid, however, the quantity ΔP_i can be calculated from the following equation:

$$\Delta P_i = XR_i P_{out} - P_{in} X_i \tag{4-23}$$

where P_{out} and P_{in} are the total pressure on outside (feed gas) and inside (permeate gas) of the fiber respectively. Also, XR_i and X_i are the mole fractions of species i in the residue stream and inside lumen at permeate exit respectively. In equation 4-18, the pressures, P_{out} and P_{in}, were 20 and 1 atmosphere, respectively. The mole fraction in the residue stream, XR_i, is also known (mixed by mass flow controllers and checked by chromatography). The mole fraction, X_i, (at the exit of the membrane) can be related to the measured permeate mole fractions determined by chromatography is given by:

$$X_i = \frac{XP_i}{\sum_{j=1}^{N} XP_j} \tag{4-24}$$

where XP_i is the mole fraction of species i in the permeate flow stream measured by chromatography. Thus, the permeabilities can be obtained using equations (4-21, 4-23, and 4-24). The selectivity or separation factor of species i to species j, α_{ij}, is given by:

$$\alpha_{ij} = \frac{Q_i}{Q_j} = \left(\frac{XP_i}{XP_j}\right)\left(\frac{\Delta P_j}{\Delta P_i}\right) \tag{4-25}$$

ii) High permeate flow rate (changing pressure inside the fiber):

1) Pure gas permeability can be calculated using the same approach as Ma and coworkers (1992) used to reduce the raw data. The equations derived by Ma and coworkers were modified to account for differences in physical situations (see Appendix C).

2) Binary gas permeabilities can be obtained by using the procedures as given by Pan (1986).

Finally, the permeance or pressure normalized flux, Q^{**}, in all cases, is defined as :

$$Q^{**} = \frac{Q}{r_i \ln\left(\frac{r_o}{r_i}\right)} \qquad (4\text{-}26)$$

where r_i and r_o are the inside and outside radius of the fiber respectively.

4.5 Single Component Experimental Results and Discussion

4.5.1 Reproducibility of Membranes

In some cases, good reproducibility of permeance data was observed for CH_4 as reported in Figure 4.3. Although the behavior is the same in all cases, up to a 20% difference, in some instances, was seen in permeance values for both CH_4 and He between two different membranes. As a result of this difference, each set of experiments was conducted with the same membrane.

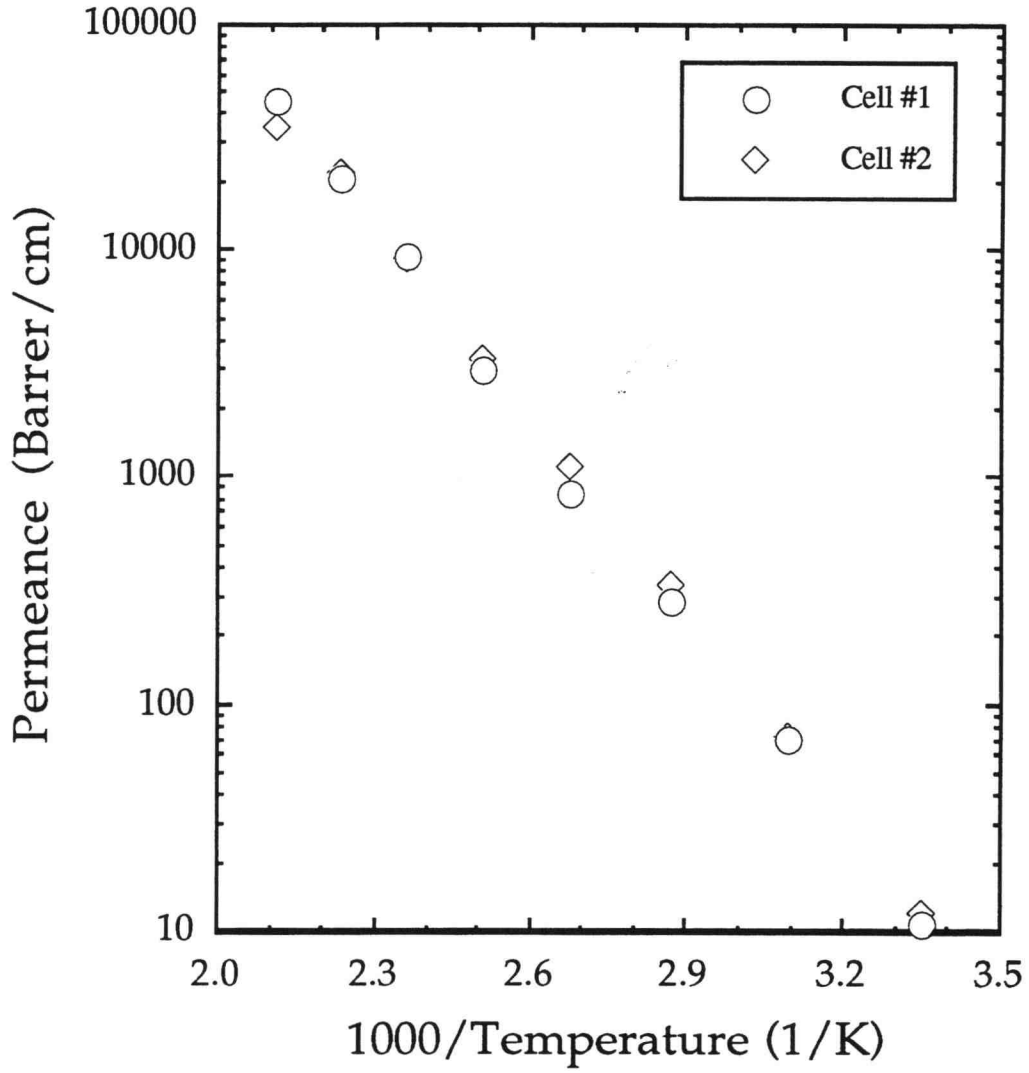

Figure 4.3 Reproducibility of the silica hollow fiber membranes for methane at 20.4 bar.

Conducting the experiment for several different fibers at the same condition and reporting the average values for the final results is an alternative way to overcome the differences among membranes.

4.5.2 Effect of Differential Pressure on Permeance

The effect of differential pressure on permeance values of CO_2, and He is presented in Figure 4.4. At low ΔP (P_{feed}<1.5 bar), the permeance value of CO_2 sharply increased with small increases in ΔP. The change in CO_2 permeance started to decrease as ΔP is increased further (1.5<P_{feed}<5.0). Finally, there was no change in CO_2 permeance with an increase in ΔP. Increasing pressure would increase surface coverage and the surface diffusion flux up to the saturation pressure of the adsorption isotherm at the temperature and pressure corresponding to the permeation measurements. Similar behavior was observed for He molecules, however, it needed higher feed pressure for He to reach the plateau value. The reason might be that high pressure is required to saturate the surface, due to the low interacting nature of He. Similar behavior for He was observed by others (Koresh et al., 1989) for a carbon molecular sieve adsorbent. This behavior is consistent with a conceptual model of permeation through the silica hollow fiber membranes of both surface diffusion and activated diffusion occurring in parallel.

Ash et al. (1973) observed the NH_3 permeability in a microporous carbon membrane increased with increasing differential pressure below 273 K. Xiao and Wei (1992a, 1992b) reported that the diffusivities of benzene and toluene increased sharply with increasing concentration at temperatures of 338 K and below.

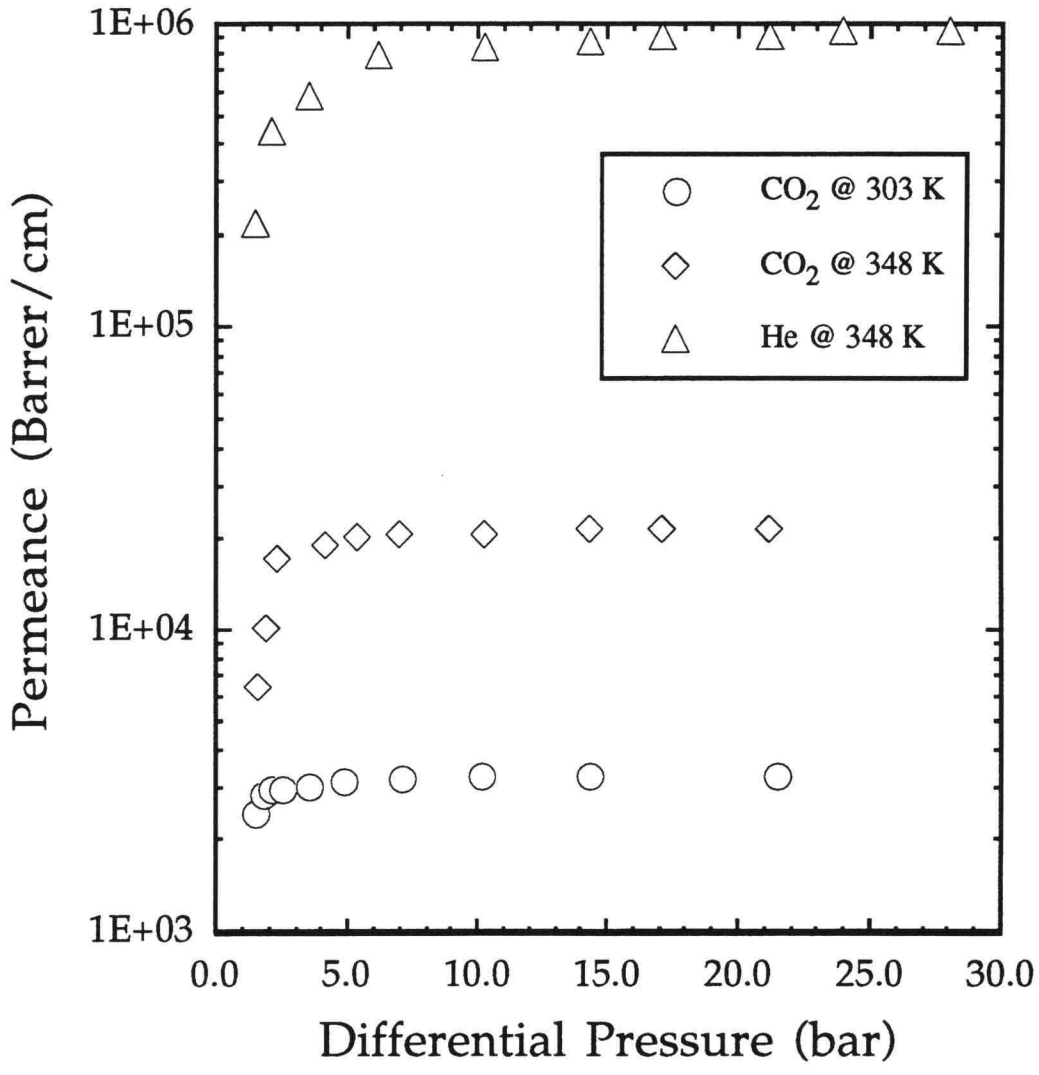

Figure 4.4 The influence of differential pressure on the permeance of helium at 348 K and carbon dioxide at 303 K and 348 K.

This trend of increasing permeability with increasing differential pressure is opposite of what was reported (Koresh and Sofer, 1986) for CO_2, CH_4, and N_2O permeation in molecular sieve carbon membranes. Shelekhin et al. (1992) reported that the CO_2 permeability was constant as the differential pressure decreased to 1 bar.

From Figure 4.4, the permeance value of He was higher than CO_2 at the same temperature. It is easier for He molecules to diffuse through the pores because of the smaller kinetic diameter than CO_2.

4.5.3 Effect of Temperature on Permeance

Permeation data were obtained for pure gases (He, H_2, CO_2, O_2, N_2, Ar, CH_4, CO, and C_2H_4), and binary gas mixtures (CO_2/CH_4, N_2/CO, and O_2/N_2). Arrhenius plots of permeance for pure gases as a function of temperature (298 to 473 K) are presented in Figures 4.5, 4.6 and 4.7. The Figures indicate that the permeability decreases as the size of the diffusing molecules increases. In addition, the results show that permeability increases exponentially with temperature, as observed for molecular sieve adsorbents (carbons, zeolites).

Arrhenius plots for the permeance data were originally prepared using the permeation equation obtained from the classical Eyring equation to model an activated mass transport process:

$$Q^{**} = Q_o^{**} e^{-\left(\frac{E^{act}}{RT}\right)} \qquad (4\text{-}27)$$

where Q^{**} is the permeance, Q_o^{**} is the pre-exponential factor, and E^{act} is the apparent activation energy. Plots of the logarithm of the pure gas

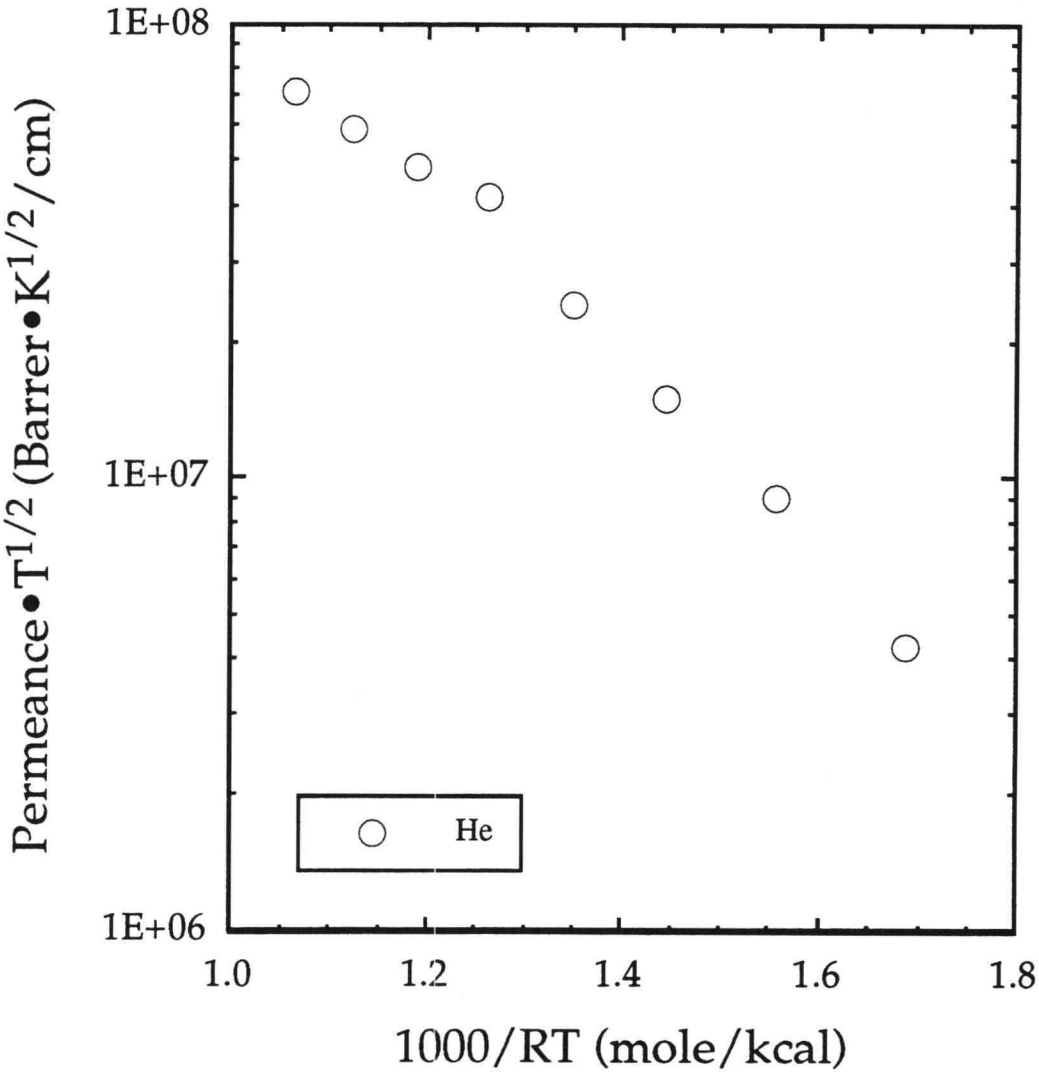

Figure 4.5 Arrhenius plot for pure gas He permeation data at 20.4 bar. A single hollow fiber test cell was used in all of the experiments.

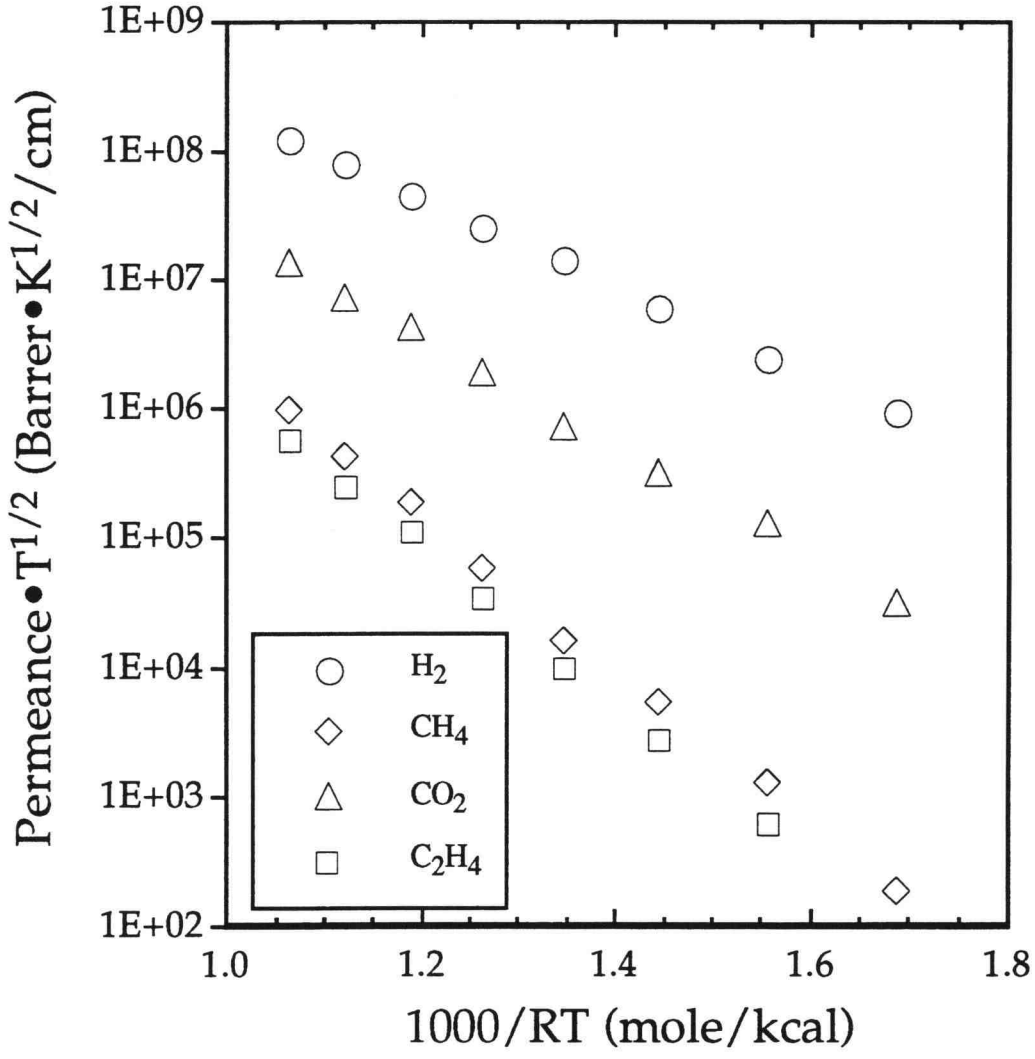

Figure 4.6 Arrhenius plot for pure gas hydrogen, carbon dioxide, methane, and ethylene permeation data at 20.4 bar. A single hollow fiber test cell was used for all of the experiments.

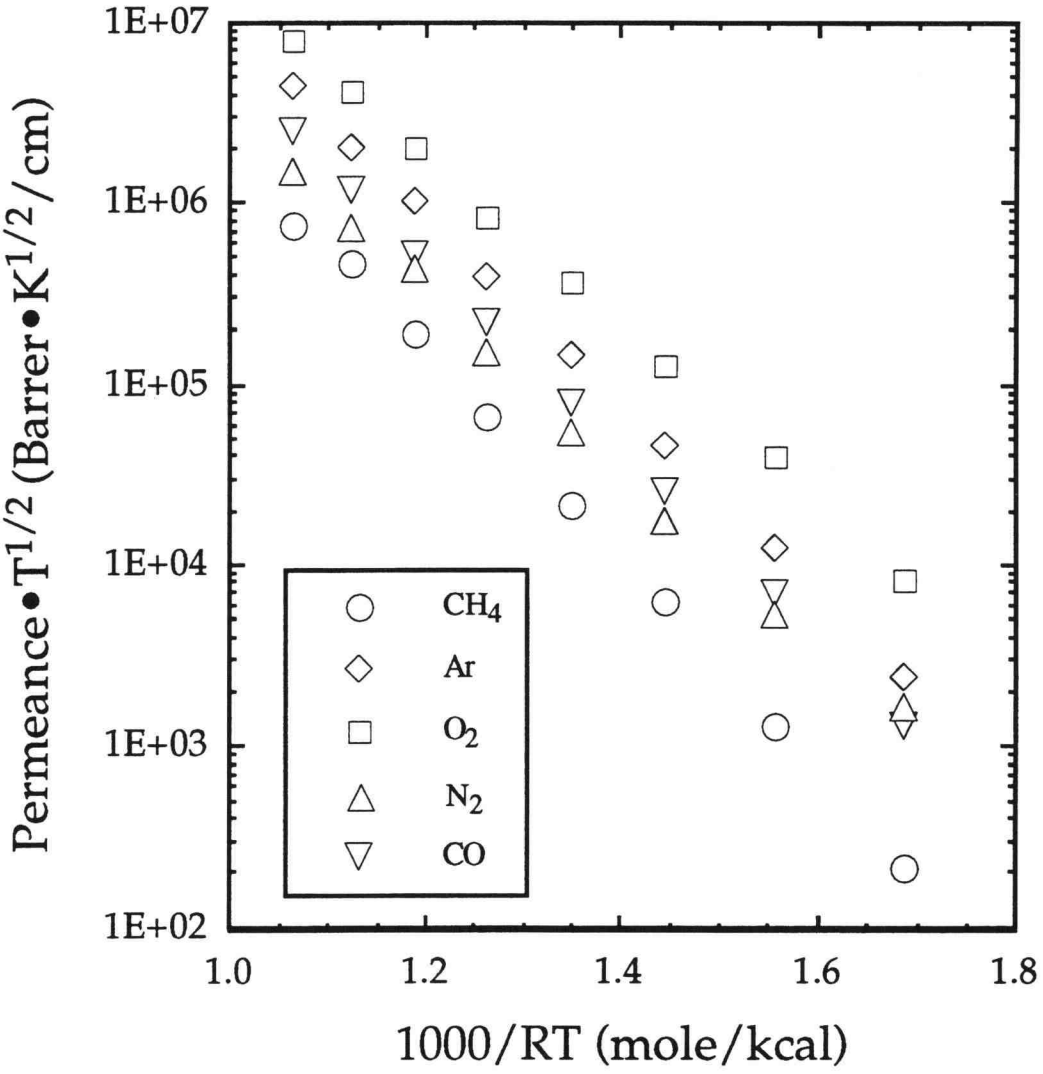

Figure 4.7 Arrhenius plot for pure gas oxygen, argon, carbon monoxide, nitrogen, and methane permeation data at 20.4 bar. A single hollow fiber test cell was used for all of the experiments.

permeance as a function of 1/RT were linear for all of the gases with the exception of He, where the plot flattened out at higher temperatures.

The discussion of the development of a unified theory for activated diffusion of pure alkanes in zeolites is reported (Xiao and Wei, 1992a, 1992b). The Eyring equation is modified to include the temperature dependence of velocity and a factor describing the partitioning of the penetrant into the zeolite pore. The permeance equation obtained from the modified Eyring equation is given as:

$$Q^{**} = \frac{8\varepsilon}{3\tau}\left(\frac{r_p}{r_i \ln\frac{r_o}{r_i}}\right)\left(\sqrt{\frac{1}{2\pi RTM}}\right)e^{-\left(\frac{E^{act}}{RT}\right)} \qquad (4\text{-}28)$$

where Q^{**} is the permeance, ε and τ are porosity and tortuosity respectively, r_p is the pore radius, r_i and r_o are the inside and outside radius of the fiber, and E^{act} is the apparent activation energy.

From equation 4-28, the $\ln\left(Q^{**}\sqrt{T}\right)$ was plotted as a function of 1/RT. Although, this produced a much better linear fit for He permeability data, using equation 4-28 did not affect the linearity of the fit for any other gases compared to equation 4-27. A sensitivity analysis revealed that the effect of temperature is greatest when the activation energy is small, as in the case for He.

Table 4.2 is a comparison of H_2 permeance values and H_2/N_2 ideal separation factors measured in this study with literature values for similar microporous membrane materials and a cellulose ester commercial polymer membrane at or close to 298 K. The silica hollow fiber membrane used in the present work has the lowest H_2 permeance and the largest separation factor.

The H_2 permeance of the silica hollow fiber membrane material is a factor of 40 smaller than the permeance of the cellulose ester polymer membrane.

Table 4.2 Comparison of H_2 Permeance Values and H_2/N_2 Separation Factors for Several Membrane Materials

Membrane Material	Temperature (K)	H_2 Permeance (Barrer/cm)	H_2/N_2 Separation Factor	Reference
PPG silica hollow fiber membrane	298	$5.23 \bullet 10^4$	545.	This work
PPG silica hollow fiber membrane	298	$5.78 \bullet 10^5$	84.	Shelekhin et al. (1992)
Asymmetric cellulose ester polymer membrane	298	$2. \bullet 10^6$	67.	W. R. Grace Gracesep product literature (1985)
Composite microporous carbon membrane	295.1	$5.20 \bullet 10^5$	1.73	Rao and Sircar (1993)
Molecular sieve carbon hollow fiber	298	$2.43 \bullet 10^6$	26.	Koresh and Sofer (1987)

A similar silica hollow fiber membrane also manufactured by PPG Industries used by Shelekhin et al. (1992) had a H_2 permeance that was an order of magnitude larger than the membrane material used in this study. However, the H_2/N_2 ideal separation factor of the membrane used by Shelekhin et al. (1992) was a factor of 6.5 smaller than the value we obtained. The remaining microporous materials in Table 4.2 were molecular sieve

carbon membranes prepared by the pyrolysis of polymer films. The Air Products Selective Surface Flow membrane (Rao and Sircar, 1992 and 1993) was designed to selectively permeate hydrocarbons and had an order of magnitude higher flux, but a very low H_2/N_2 selectivity. Finally, the molecular sieve carbon membrane of Koresh and Sofer (1983, 1986, 1987) had a H_2 permeance larger than the cellulose ester polymer material and a modest separation factor of 26. For the microporous materials in Table 4.2, it appears that the permeance and ideal separation factor are inversely proportional.

Ideal separation factors (ratios of pure gas permeances) corresponding to the permeance data in Figures 4.5, 4.6 and 4.7 are presented in Table 4.3 at three temperatures: 298, 348, and 423 K. All separation factors decrease as the temperature increases which is due to the less permeable penetrant having a larger activation energy. Consequently, the differences in flux are smaller as the temperature increases. The separation factors are generally quite large when compared to polymer membranes that operate via a solution-diffusion mechanism (Zolandz et al., 1992). At 298 K, the ideal separation factors for O_2/N_2, CO_2/CH_4, N_2/CH_4, and He/CH_4 are 9.20, 156, 7.76, and $2.34 \bullet 10^4$, respectively.

However, the ideal separation factors reported here for silica hollow fiber membranes are similar to other microporous materials designed to separate penetrants via activated diffusion. Koresh and Sofer (1983) reported an O_2/N_2 separation factor of 7.1. Shelekhin et al. (1992) reported ideal separation factors at 303 K using similar silica hollow fiber membranes. They observed very large N_2/CH_4 and CO_2/CH_4 selectivities of 50 and 1675, respectively. These values are over a factor of six larger than we observed. However, Shelekhin et al. (1992) measured an O_2/N_2 separation factor of 3 to 4 which is substantially smaller than we observed for pure gases and

mixtures. These differences could be due to a larger mean pore size for Shelekhin's silica fibers compared to the membrane material used in the present work. In any case, the microstructure of the silica hollow fiber samples used by Shelekhin et al. (1992) are significantly different than those used in the present work. Interestingly, the separation factors we obtained for gases possessing large differences in kinetic diameter, such as He/CH_4 and H_2/CH_4, are similar to those reported by Shelekhin.

Table 4.3 Ideal Separation Factors at 20.4 Bar

Temperature (K)	CO_2/CH_4	N_2/CH_4	O_2/N_2	H_2/N_2	H_2/CH_4	He/CH_4
298	156.	7.76	9.20	545.	$4.97 \cdot 10^3$	$2.34 \cdot 10^4$
348	67.0	2.82	7.89	351.	$1.16 \cdot 10^3$	$4.65 \cdot 10^3$
423	20.8	2.31	4.81	103.	$2.35 \cdot 10^2$	$3.10 \cdot 10^2$

The slopes of the Arrhenius plots correspond to the apparent activation energy for diffusion in the silica hollow fiber membranes. Figure 4.8 shows the influence of kinetic diameter (an approximate measure of molecular size) of the penetrant on the activation energy. Since the gas molecules are not spherical, other measures of molecular size could improve the correlation. Values of the apparent activation energies range from 4.61 (He) to 14.0 (C_2H_4) kcal/mole and were directly proportional to the kinetic diameters of the penetrant molecules as shown in Figure 4.8.

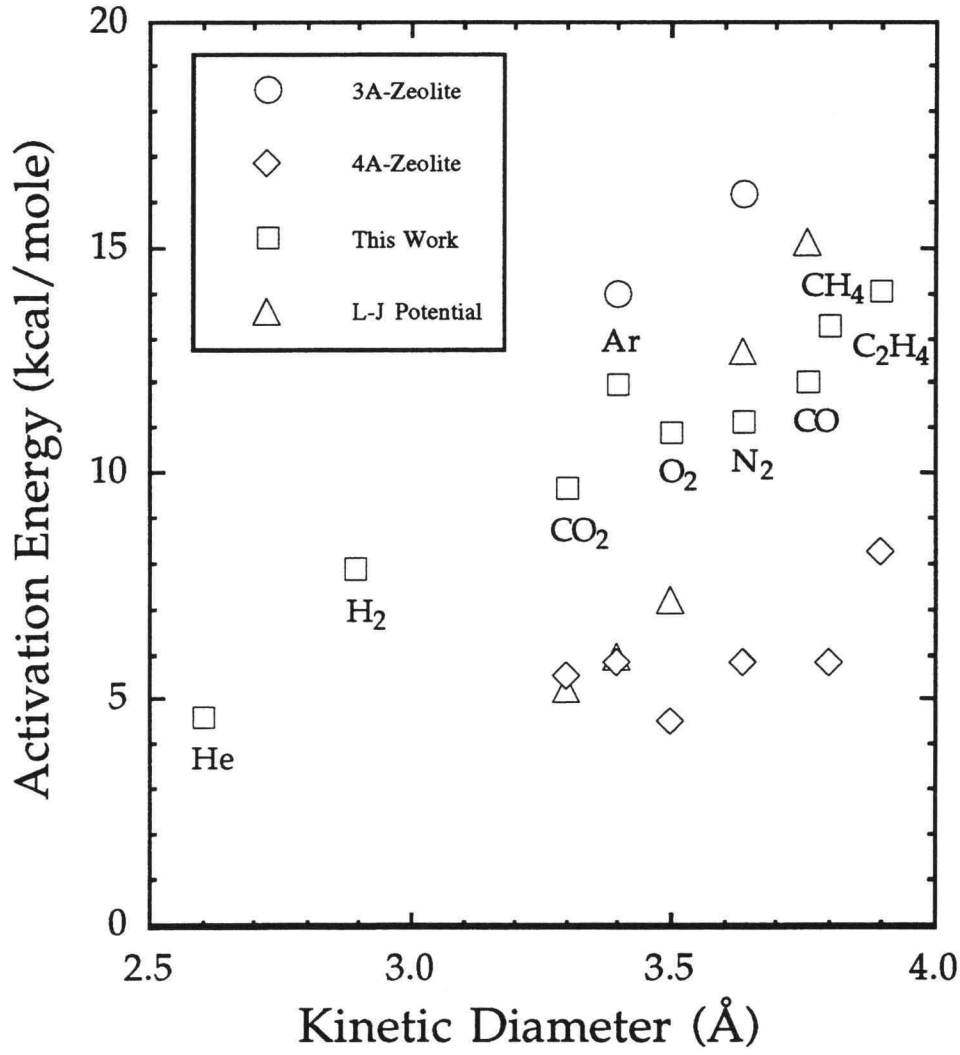

Figure 4.8 The influence of kinetic diameter on the apparent activation energy for diffusion in silica hollow membranes.

The activation energies calculated from Lennard-Jones potential and the average pore size of 6.4 Å agreed reasonably well with the experimental values. The apparent activation energies for the silica hollow fiber membranes are between the activation energies reported for 3 A zeolite (Rabo, 1976) and 4 A zeolite (Karger and Ruthven, 1992) as shown in Figure 4.8. The apparent activation energies obtained in the present are a factor of 2 to 11 times larger than those previously reported by Ma and coworkers (Shelekhin et al., 1992) for a different sample of PPG silica hollow fiber membranes. The lower activation energy values reported by Shelekhin et al. correspond to much higher permeability values than those measured in this research.

Effect of the kinetic diameter on permeance at three different temperatures is presented in Figure 4.9. The permeance values are inversely proportional to the kinetic diameter of the penetrant molecules. The reason is that the larger the molecule, the harder it is to pass through the micropores in the silica membranes, resulting in lower permeance value.

4.6 Binary Gas Mixture Experimental Results and Discussion

Additional information about the mass transfer mechanisms in the PPG silica hollow fiber membranes was obtained by performing permeation experiments with gas mixtures and comparing the results with those obtained using only pure gases. The comparison experiments were performed using the same single hollow fiber for both pure gases and gas mixtures.

It is common in the polymer membrane literature that the ideal or pure gas separation factors are larger than the mixed gas values (Zolandz et al., 1992). For both O_2/N_2 and CO_2/CH_4 mixtures, we have observed the

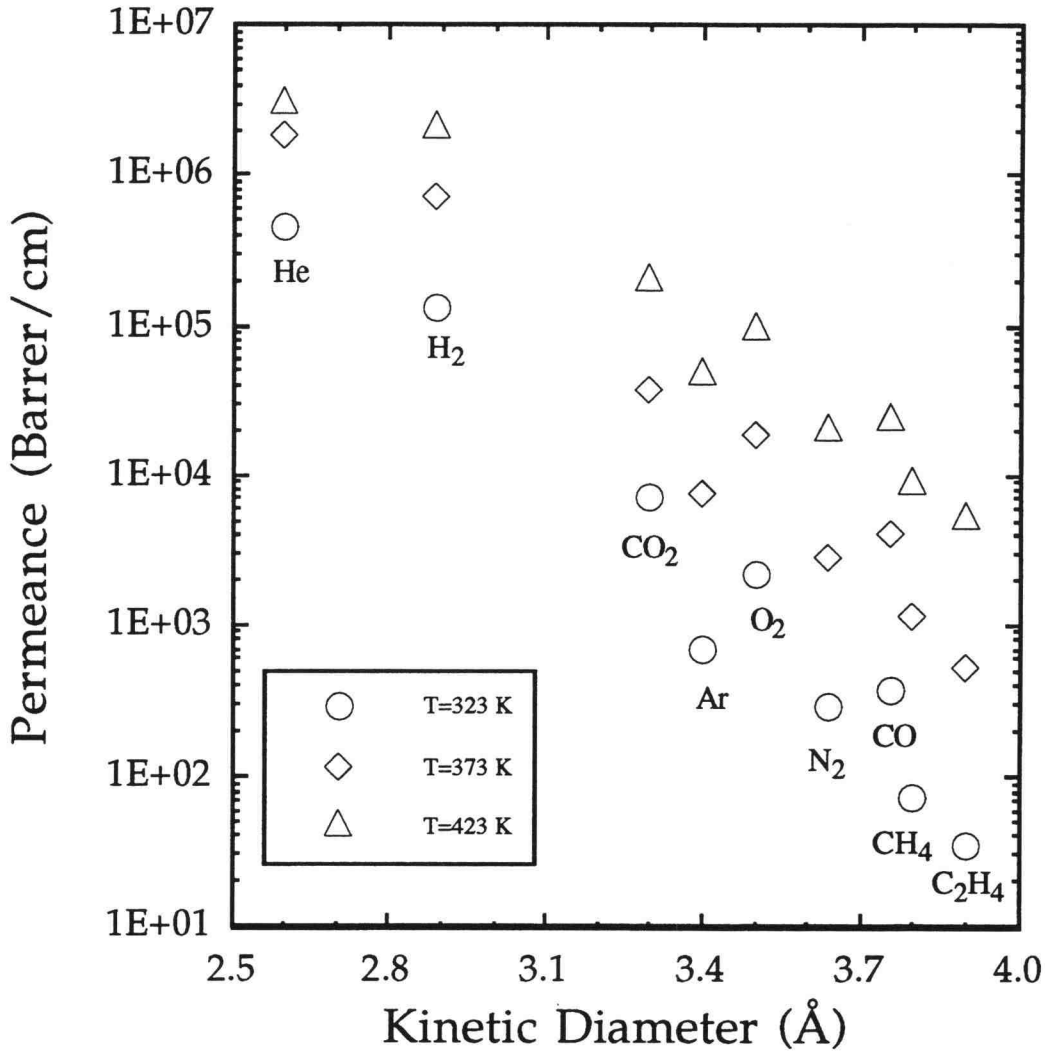

Figure 4.9 The influence of kinetic diameter on permeance for diffusion in silica hollow membranes at 20.4 bar and 323 K, 373 K, and 423 K.

unusual behavior of the mixture separation factors being larger than the ideal separation factors obtained with pure gas permeability data. Figure 4.10 presents O_2/N_2 separation factor data for both mixture and pure gas experiments that nicely illustrates this unusual behavior for the silica hollow fiber membranes. At temperatures from 298 K to 373 K, the mixed gas O_2/N_2 separation factors are up to 20% larger than the pure gas values. Above 373 K the pure gas and mixed gas separation factors coincide.

Separation factor values of 10 to 12 for O_2 over N_2 are large and they compare very favorably to separation factors reported for polymer membranes. An O_2/N_2 separation factor of 11.3 is over 50% higher than the most selective commercial polymer membrane material in the literature (Muruganandam et al., 1987).

Rao and Sircar (1993) have described a microporous carbon membrane where the mixture separation factors exceed the ideal gas values for the separation of light hydrocarbons from hydrogen. The greatest difference was seen for butane, the penetrant with the highest affinity for the carbon membrane surface. The mixed gas separation factor for C_4H_{10} over H_2 was 94 compared to an ideal value of 1.2. The authors attribute the large difference in separation factors to competitive adsorption, where the hydrocarbons preferentially occupy adsorption sites over hydrogen. Competitive adsorption reduces the surface diffusion flux of hydrogen compared to the pure gas experiments.

As shown in Table 4.4, the mixed gas O_2 permeance values were larger than those measured for pure O_2 at all temperatures. However, the percent difference between the mixed gas for pure gas O_2 permeance values decreased

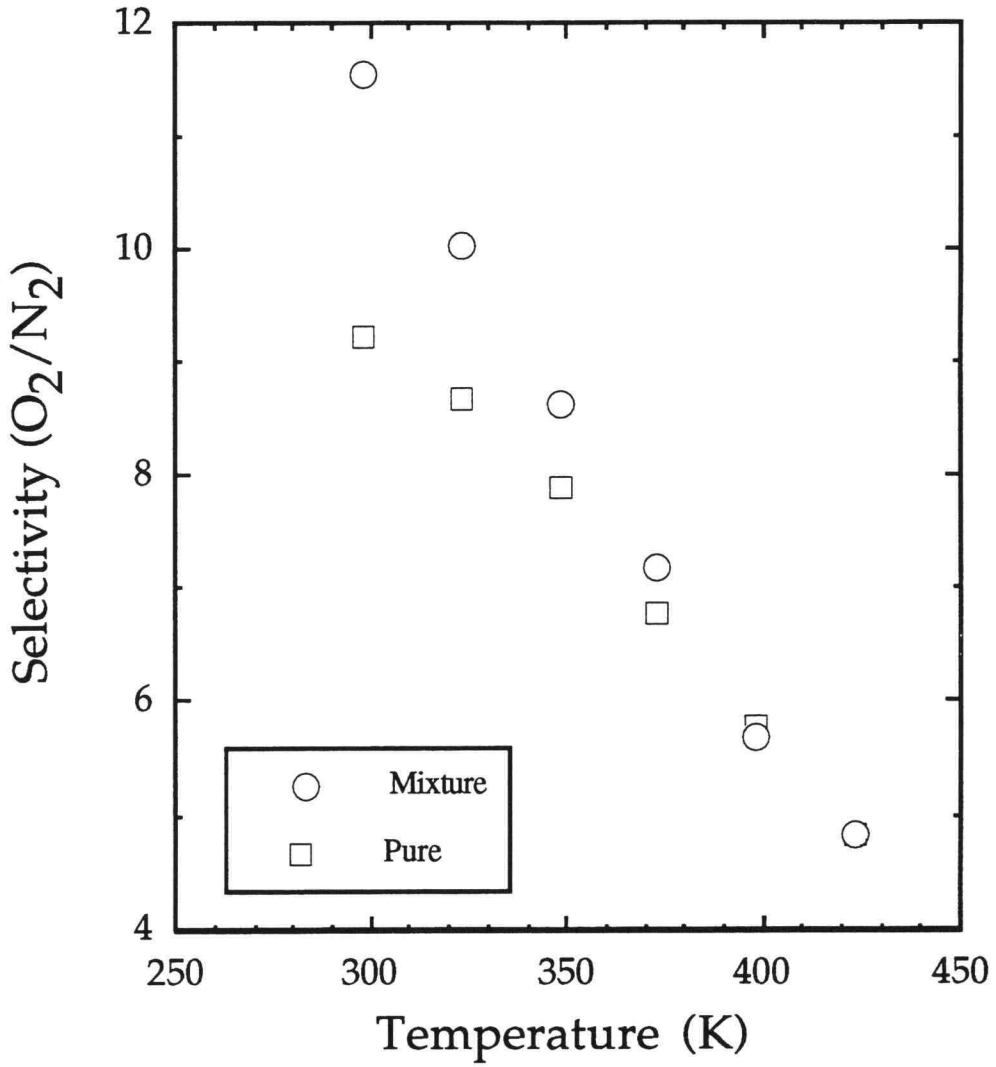

Figure 4.10 Comparison of the mixed gas and pure gas oxygen/nitrogen separation factors at 20.4 bar for a single silica hollow fiber membrane test cell. The mixed gas separation factors are larger for temperatures up to 375 K.

as the temperature increased. The opposite trend was observed for N_2. At 298 K, there was a small difference between the mixed gas and pure gas permeance N_2 values. As the temperature increased, the mixed gas N_2 permeance increased faster than the pure gas values and the difference between them increased to about 15%. Therefore, the activation energy for diffusion was slightly larger for N_2 in the binary mixture than pure N_2.

Table 4.4 Comparison of Pure and Mixed Gas Permeances for the O_2/N_2 Separation at 20.4 Bar

Temperature (K)	Pure Gas N_2 Permeance (Barrer/cm)	Mixed Gas N_2 Permeance (Barrer/cm)	Pure Gas O_2 Permeance (Barrer/cm)	Mixed Gas O_2 Permeance (Barrer/cm)
298	4.46E+01	4.67E+01	4.17E+02	5.29E+02
323	1.93E+02	2.13E+02	1.69E+03	2.10E+03
348	6.53E+02	7.54E+02	5.19E+03	6.39E+03
373	2.13E+03	2.50E+03	1.45E+04	1.77E+04
398	5.87E+03	6.95E+03	3.40E+04	3.89E+04
423	1.43E+04	1.68E+04	6.89E+04	8.00E+04

Rao and Sircar (1992) have also observed situations where the mixed gas permeability is larger than the pure gas value. In their experiments with

microporous carbon membranes at 295 K, they measured a mixed gas butane permeability of 230 Barrer compared to the pure gas butane permeability of 190 Barrer.

A similar comparison of pure and mixed gas permeation was performed for the CO_2/CH_4 separation. As shown in Figure 4.11, the difference between the mixture separation factors and the pure gas values is much smaller than we observed for the air separation factors on a percentage basis. The experiments were performed by starting at 298 K and increasing the temperature up to 423 K. At that point, the hollow fiber membrane cell was cooled to 289 K in high purity He. Then the experiments were repeated at 298 K and 323 K. Surprisingly, the CO_2/CH_4 separation factors increased. After cooling, the mixture separation factor at 298 K was 10% larger than the pure gas value. The mixed gas CO_2/CH_4 separation factor at 298 K increased by 40% after cooling.

Very similar results were obtained in an experiment where the hollow fiber membrane was heated to 398 K in He, and then cooled to 298 K where pure and mixed gas permeation experiments were performed. Subsequently, both pure and mixed gas permeation experiments were performed over a temperature range of 298 to 423 K. At 298 K, the mixed gas separation factor was 21% larger than the pure gas permeance ratio. Comparing the activation energies of diffusion for these experiments to prior pure and mixed gas permeation studies, the activation energies for CO_2 and CH_4 diffusion decreased by 10 to 17%.

In the CO_2/CH_4 experiments, the pure gas permeances were always 10 to 20% larger than the mixed gas values at all experimental conditions as shown in Figure 4.12. The difference between pure gas and mixed gas permeance values was largest for CH_4, which is less interacting than CO_2

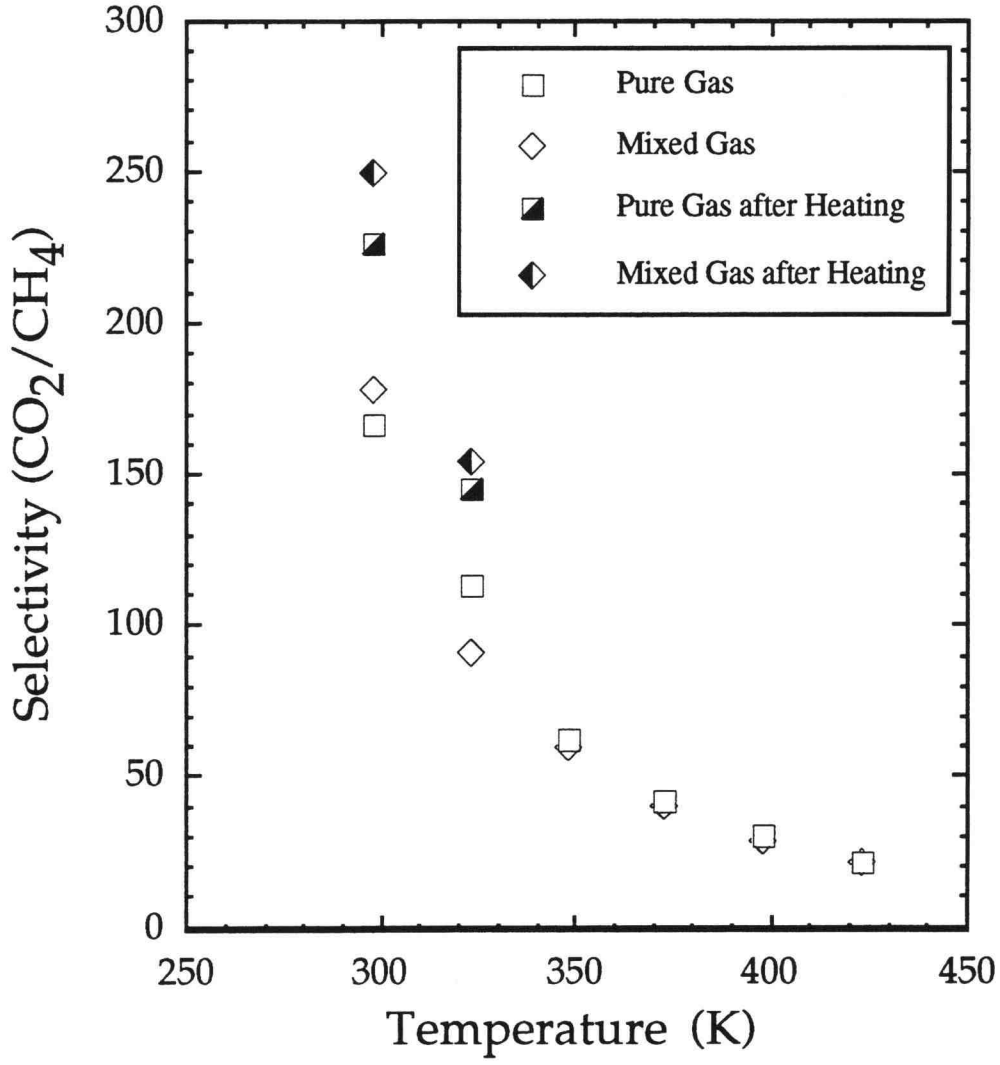

Figure 4.11 Comparison of the mixed gas and pure gas carbon dioxide/methane separation factors at 20.4 bar for a single silica hollow fiber membrane test cell. The open symbols represent the measurements that were done first. After the experiment at 423 K, the silica hollow fiber test cell was cooled in He, and the experiments were repeated.

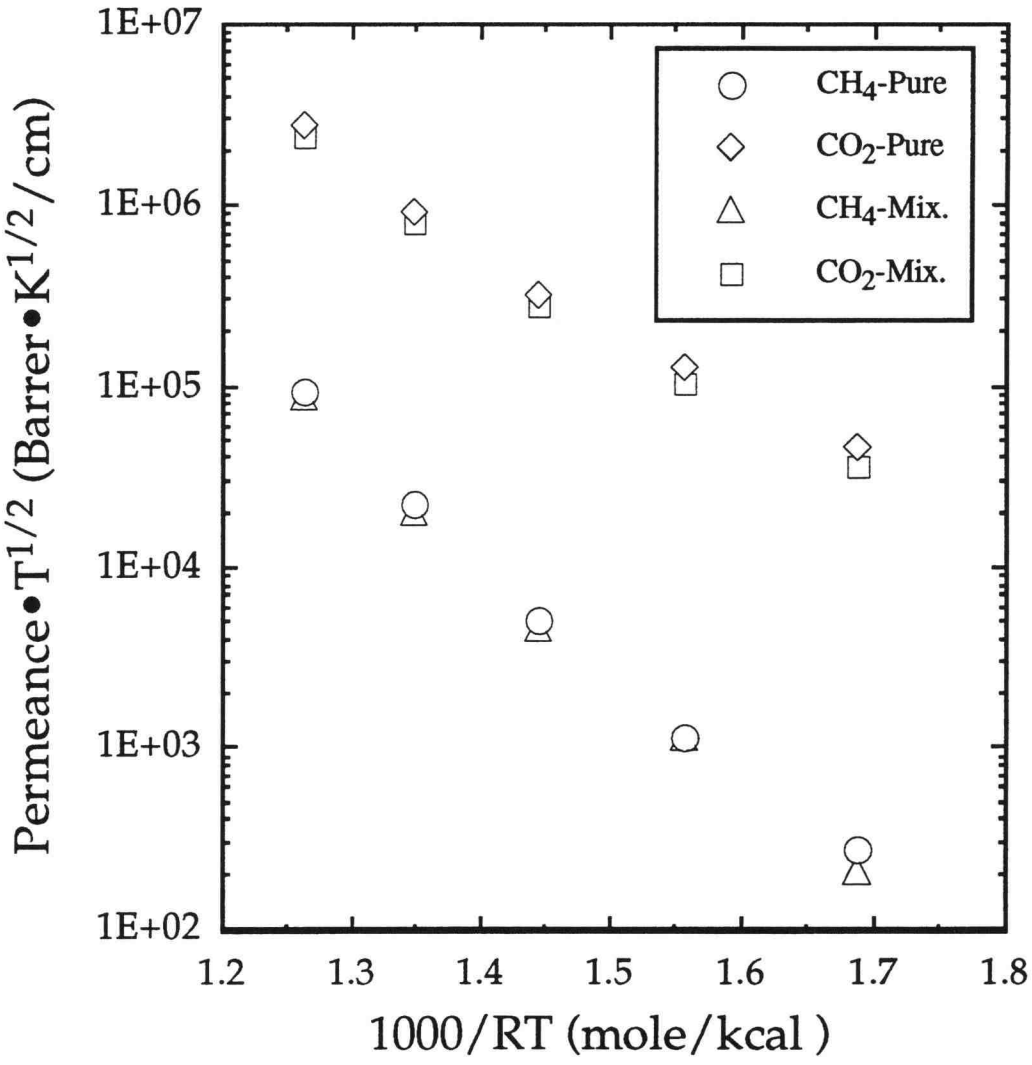

Figure 4.12 Comparison of the mixed gas and pure gas carbon dioxide/methane permeance values at 20.4 bar for a single silica hollow fiber membrane test cell.

based on adsorption data for silica hollow fiber membranes (Bhankarkar et al., 1992). The difference between the pure and mixed gas permeances was largest at 298 K. However, after heating to 423 K, all the pure and mixed gas CO_2 and CH_4 permeance values increased by up to a factor of two. The 40% increase in the CO_2/CH_4 separation factor at 298 K after heating and cooling was primarily due to the fact that the mixed gas CO_2 permeance increased by 158% compared to 84% for the CH_4 permeance.

The differences in permeability and selectivity due to heating the hollow fiber membrane may be due to the removal of physically adsorbed water from the membrane surface. The water may have been "screening" the penetrant molecules from the polar SiO_2 surface. Removal of the water would increase the interaction between the CO_2 and membrane surface which could possibly increase surface diffusion contribution of the total flux.

Fourier transform infrared (FT-IR) spectroscopy was used to investigate the interaction of water with the silica membrane surface (Hassan et al., 1994). The results showed that the hydroxylated membrane surface was covered by physically adsorbed water at ambient conditions. The physisorbed water could be removed by heating the silica membrane to 450 K or exposure to pressures below $1 \bullet 10^{-4}$ torr (Hassan et al., 1994).

An analogous situation occurs for zeolites used for a pressure swing adsorption separation (Frankiewicz et al., 1983). The zeolites are ion exchanged to leave a multivalent cation in the zeolite cavity such as Ca^{++}. The Ca zeolites are then activated by heating in a high purity inert gas to remove water from the adsorption sites. Removal of the water increases the interaction between the exchanged cation and the adsorbate, improving the selectivity of the adsorption separation.

Our proposed explanation for the higher separation factors is that during the surface diffusion of mixtures, competitive adsorption takes place on the surface of the membrane. The more strongly adsorbed gas would preferentially occupy the adsorption sites on the pore surface, impeding adsorption and surface diffusion of the more weakly adsorbed gas. From the extensive literature on adsorption in microporous zeolites, carbons, and ceramics, it is well established that gas adsorption in porous solids decreases drastically as the temperature increases (Breck et al., 1974, Gregg et al., 1982). Our pure and mixed gas data for the O_2/N_2 and CO_2/CH_4 separations with silica hollow fiber membranes are also consistent with this observation. The mixed gas separation factors and the pure gas permeance ratios approach each other as temperature is increased.

The effect of temperature on separation factors and permeance for both pure and binary mixture (N_2/CO) are presented in Figures 4.13 and 4.14 respectively. The selectivities of N_2/CO were less than unity for temperatures greater than 25 ^oC, meaning that the permeance of the larger gas (CO) was higher than the smaller gas (N_2) which might be due to the surface effect as explained above. The selectivity of the binary mixture was higher than the pure components at low temperatures; however, this difference was small at higher temperatures suggesting that the effect of surface interactions diminished as the temperature was increased.

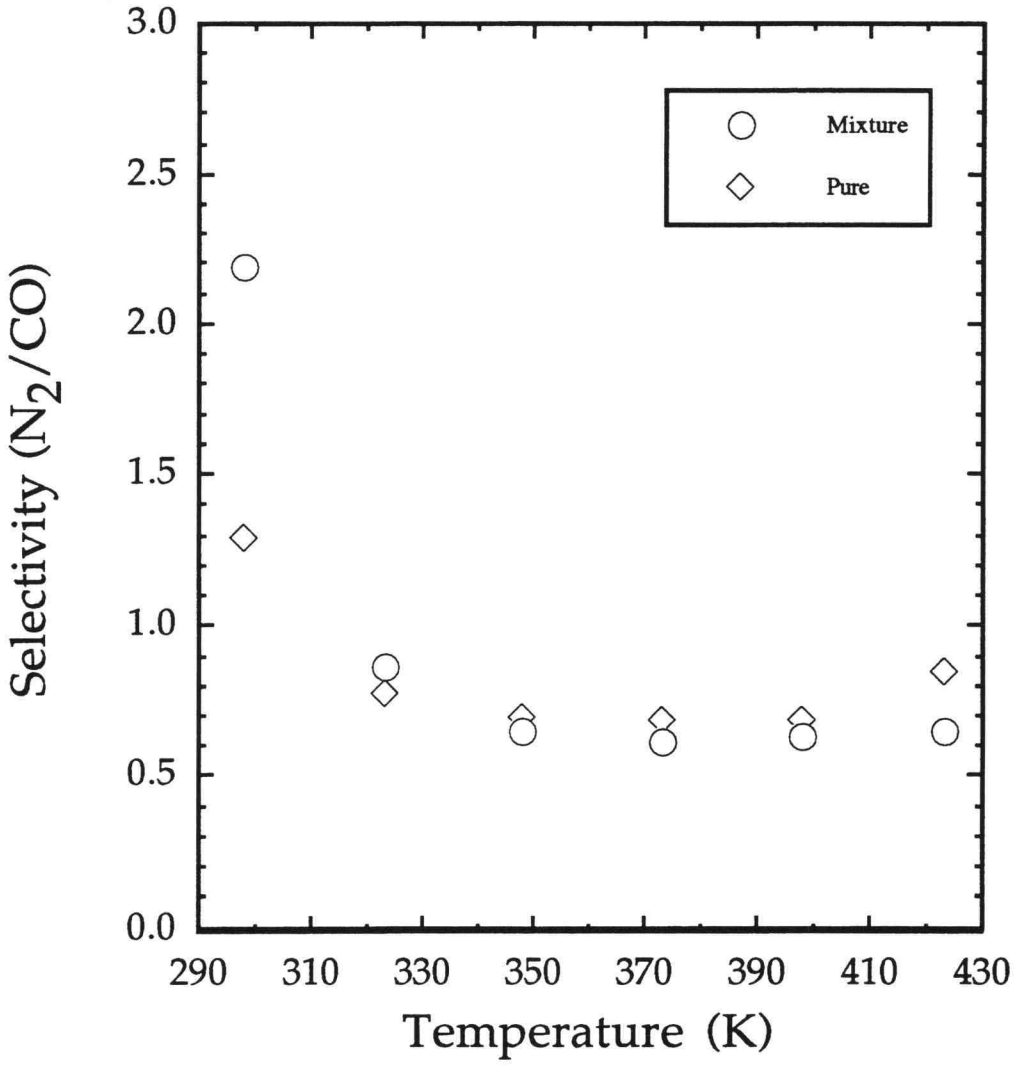

Figure 4.13 Comparison of the mixed gas and pure gas carbon monoxide/nitrogen separation factors at 20.4 bar for a single silica hollow fiber membrane test cell.

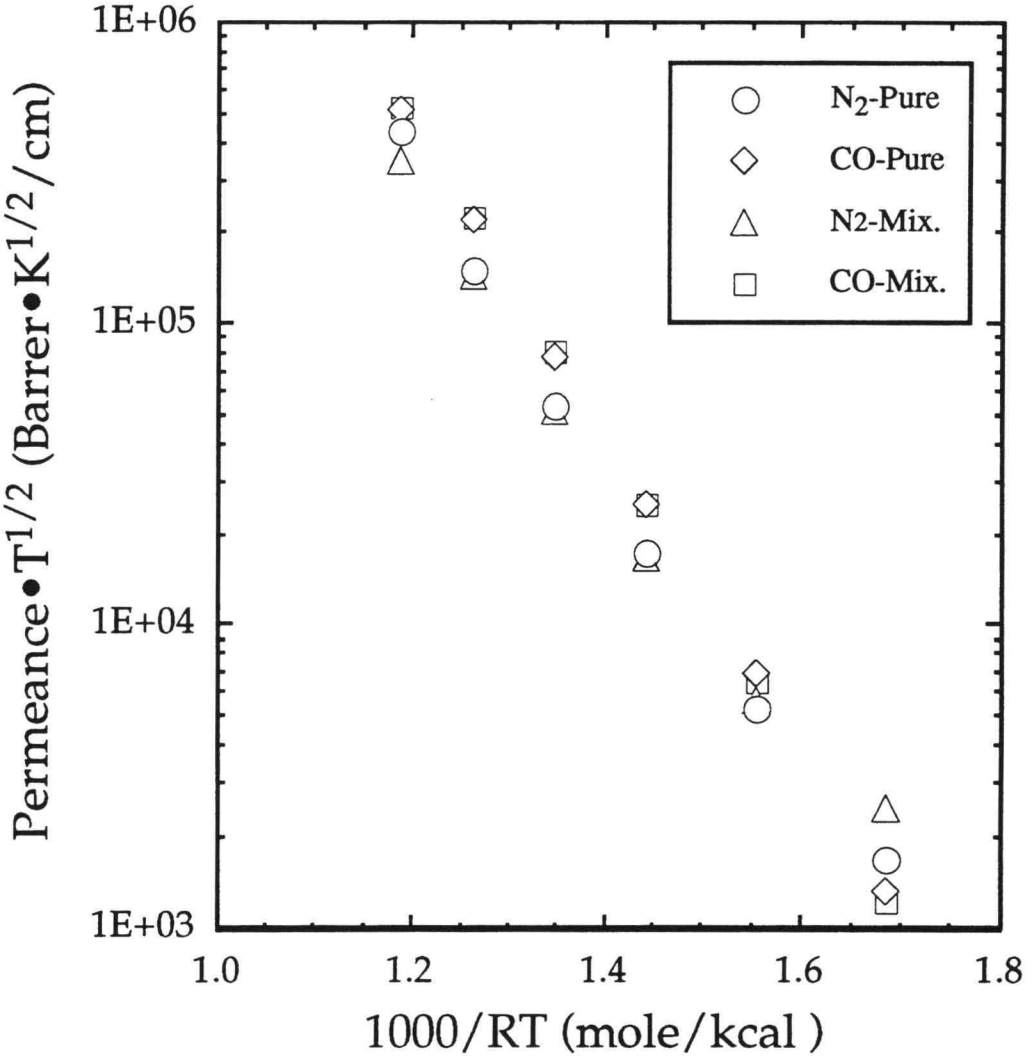

Figure 4.14 Comparison of the mixed gas and pure gas carbon monoxide/nitrogen permeance values at 20.4 bar for a single silica hollow fiber membrane test cell.

4.7 Conclusions

4.7.1 Pure Gas Permeation

The permeances of gases with kinetic diameters ranging from 2.6 to 3.9 Å were measured through silica hollow fiber membranes over a temperature range of 298 K to 473 K at a feed pressure of 20 atm. Permeances at 298 K range from 10 to 2.3 • 10^5 Barrer/cm for CH_4 and He, respectively, and were inversely proportional to the kinetic diameter of the penetrant. Mass transfer through the silica hollow fiber membranes is an activated process. Activation energies for diffusion through the membranes were calculated from the slopes of Arrhenius plots of the permeation data. The energies of activation ranged from 4.61 to 14.0 kcal/mole and correlate well with the kinetic diameter of the penetrants. The experimental activation energies, which was between literature values for zeolite 3 A and 4 A, agreed reasonably well with the theoretical values calculated from Lennard-Jones potential.

4.7.2 Binary Mixture Permeation

High selectivities were obtained for O_2/N_2 and CO_2/CH_4 mixtures. The O_2/N_2 mixed gas selectivities decreased from 11.3 at 298 K to 4.8 at 423 K and were up to 20% larger than the values calculated from pure gas permeances at temperatures below 373 K. At temperatures above 373 K, the mixture and pure gas separation factors were equal. The mixture separation factor for CO_2/CH_4 decreased from 186 to 22.3 over the same temperature range. The differences between the mixture and ideal separation factors is attributed to a competitive adsorption effect in which the more strongly

interacting gases saturate the surface and impede the transport of the weakly interacting gases. The more strongly adsorbed gas would preferentially occupy the adsorption sites on the pore surface, preventing adsorption and surface diffusion of the more weakly adsorbed gas. Similar differences in the separation factors were observed for CO_2/CH_4 mixture after the membrane had been heated to above 398 K and then cooled in flowing He to 298 K. At 298 K after annealing, the CO_2/CH_4 separation factor increased by 40% and the CO_2 permeance more than doubled. The increase in CO_2 and CH_4 permeances corresponded to a 10 to 17% decrease in the activation energy for transport after heating to 423 K and then cooled in He. Based on the FT-IR results (Hassan et al., 1994), this unusual behavior is attributed to the removal of physically adsorbed water from the membrane surface.

Chapter 5

Calculation of Interaction Energy Using Quantum Mechanics

5.1 Introduction

In order to investigate the fundamental interactions that influence mass transport in the micropores of the silica fiber membranes, quantum mechanics calculations were performed to estimate the strength and nature of the interactions of penetrant gases with a model silica surface. Ab initio theory was used to obtain the interaction energy of several gaseous species (N_2, CH_4, CO_2, and CO) with the silica surface. The gas that has highest interaction energy with the surface is expected to adsorb more to the surface, thus, has higher surface diffusion.

The surface structure of an amorphous silica hollow fiber membrane is complex. However, two simple clusters silanol, H_3SiOH, and orthosilicic acid, $Si(OH)_4$ have been used (De Almeida et al., 1993, Garrone et al., 1992, Ugliengo et al., 1990, 1989, and Wagner et al., 1992) to mimic the surface of porous silica.

In this chapter, the interaction energies and the heat of adsorption values of several gaseous species (N_2, CO, CO_2, and CH_4) on silica surface using silanol, H_3SiOH, as the surface model are calculated. The influence of the interaction energy of a nitrogen molecule on a silica surface using three different surface models (H_3SiOH, $Si(OH)_4$, and H_2AlOH) is also studied. Then, the heat of adsorption of a nitrogen molecule on all three surface models are calculated and compared with the experimental value.

5.2 Theoretical Methods

A variety of molecules to model the surface of the silica membrane were used. To study the nature of terminal hydroxyls, silanol, H_3SiOH, and orthosilicic acids, $Si(OH)_4$ were used. Orthosilicic acid, a nonpolar molecule, is a more realistic representation of the silica surface than silanol, which is a polar molecule. Due to the possibility of adsorption on impurities such as alumina (about 3%, Hammel at el., 1989) on the silica surface, H_2AlOH was chosen.

Full geometry optimizations of the adsorbates, surface models, and complexes were done at the Restricted Hartree-Fock (RHF) level using Gaussian 92 (Frisch et al., 1992) and Turbomole (Ahlrichs et al, 1989). For the calculation of correlation energy, Moller-Plesset perturbation theory, truncated at second order (MP2) was used. In all cases the core electrons were frozen in the MP2 level of theory. The basis set superposition error (BSSE) using the counterpoise correction method (Boys and Bernardi, 1970) was estimated.

All frequency calculations have been carried out at MP2/6-31G* level of theory and the heat of adsorption of the surface models with each molecule has been evaluated.

To calculate heat of adsorption of a gas molecule on a surface model using ab initio theory, the structures of the surface model, the gas molecule, and the complex (combination of the surface model with the gas molecule) were optimized and the energy of each were computed. Optimization were done at both RHF and MP2 levels of theory. Basis sets used for the calculations were 3-21G* (during search for the stable structure), 6-31G* and

6-31+G**. Diffuse functions were used in an attempt to minimize the basis set superposition error (BSSE). Frequency calculations were done at MP2/6-31G* for each molecule and the complexes and thermal (combination of vibrational, rotational, and translational) energies were obtained. Finally, heat of adsorption of the gas molecules with surface models at MP2/6-31G* and MP2/6-31+G** levels of theory were calculated using equations below:

$$\Delta E^{o} = E^{o}_{complex} - \left[E^{o}_{surf.model} + E^{o}_{gas}\right] \quad (1)$$

$$\Delta E^{thermal} = E^{thermal}_{complex} - \left[E^{thermal}_{surf.model} + E^{thermal}_{gas}\right] \quad (2)$$

$$\Delta H^{adsorption} = \Delta E^{o} + \Delta E^{thermal} - RT \quad (3)$$

The calculations were performed using VAX 9000 computer at Oregon State University and an IBM RS/6000 model 580 workstation at the Colorado School of Mines .

5.3 Results and Discussions

In order to locate the stable equilibrium structure, the potential energy surface of all adsorbate-silanol is extensively explored at low level of theory (MP2/3-21G*). The structures of two minima found during the search for N_2-Silanol and CO_2-Silanol are presented in Figure 5.1. It was also found that structure I (for both complexes) is more stable due to higher interaction energy than structure II. As a result, only structure I is considered for the rest of the calculations.

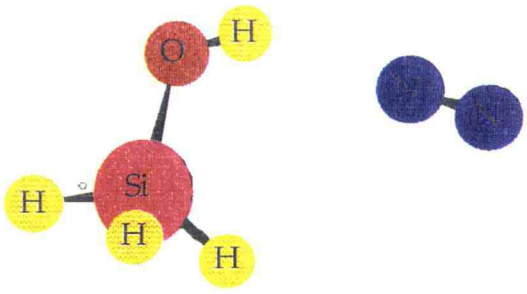

Structure I (N_2-Silanol)

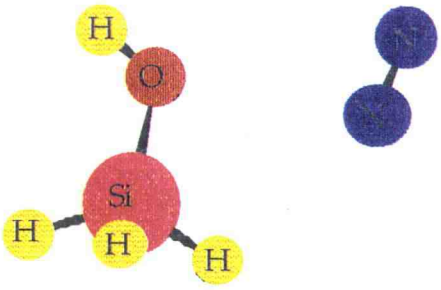

Structure II (N_2-Silanol)

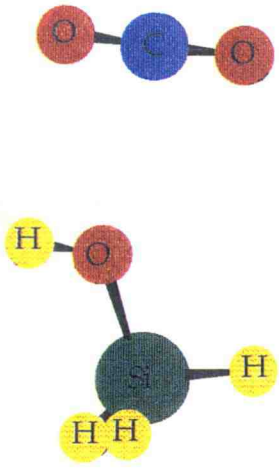

Structure I (CO_2-Silanol)

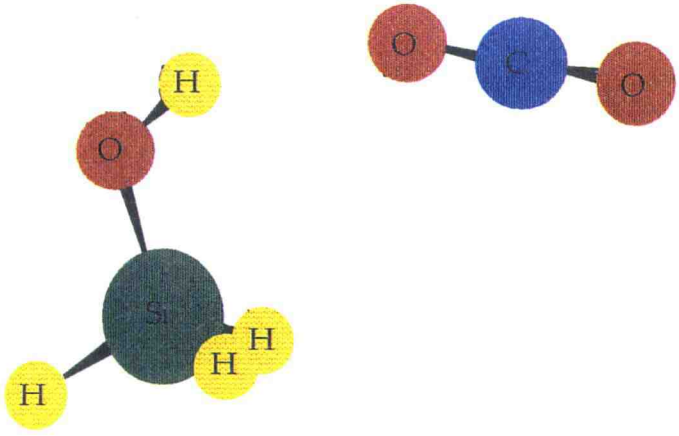

Structure II (CO_2-Silanol)

Figure 5.1 Stable structures of N_2-Silanol and CO_2-Silanol complexes, structure I is more stable than structure II for both molecules.

The sensitivity of the structures and energetics of molecules containing Si-O bonds to the flexibility of the basis set have been reported (Nicholas et al., 1992). It was concluded that Si-O bonding was very sensitive to the size of the basis set and the inclusion of electron correlation. The fact that total energies go down with the increase in the size of the basis set is well known and does not need to be discussed. Therefore, 6-31G* basis set is used and structures and energies at both RHF and MP2 levels of theory were calculated. Then, larger basis set (6-31+G**) is used to verify results.

The effect of correlation on internal coordinates for N_2, silanol, and N_2-Silanol molecules is presented in Table 5.1. Some internal coordinates are affected significantly by the inclusion of the electronic correlation term. In particular, the distance between nitrogen and the hydrogen of an OH group is much smaller ($\approx$0.2 Å) in the case with the addition of correlation, showing stronger interaction or a higher hydrogen bonding effect. O-H bond lengths are slightly larger, whereas, the $\angle$Si-O-H and $\angle$O-H-N angles are smaller with correlation than at the RHF level of theory. Note that N-N, Si-O bond lengths for the complex are shorter when they are compared to the same bond lengths for a nitrogen or silanol molecule, whereas, the O-H bond length for the complex is larger than that of the same bond length in a silanol molecule. The $\angle$Si-O-H angle is smaller in the complex when it is compared to the same angle in a silanol molecule.

The effect of electron correlation on interaction energy is presented in Table 5.2. The trends in the interaction energies are the same at RHF and MP2 levels of theory, however, the binding energies are about twice as strong with inclusion of the correlation. Thus, there is a significant contribution from the dispersion energy due to the inclusion of electron correlation which is essential for obtaining accurate energy values.

Table 5.1 i) Geometry and Energy for N_2

	RHF/6-31G*	MP2/6-31G*	MP2/6-31+G**
N-N (Å)	1.0784	1.1307	1.1307
Energy (H)	-108.9439495	-109.2552776	-109.26192910

ii) Geometry and Energy for Silanol

	RHF/6-31G*	MP2/6-31G*	MP2/6-31+G**
Si-O (Å)	1.6471	1.6718	1.6792
O-H (Å)	0.9461	0.9689	0.9625
∠Si-O-H	118.9405	116.3911	118.5254
Energy (H)	-366.1303957	-366.3904650	-366.4374967

iii) Geometry and Energy of N_2-Silanol Complex

	RHF/6-31G*	MP2/6-31G*	MP2/6-31+G**
Si-O (Å)	1.6453	1.6694	1.6771
O-H (Å)	0.9464	0.9694	0.9633
H-N (Å)	2.5064	2.3547	2.5024
N-N (Å)	1.0779	1.1302	1.1304
∠Si-O-H	118.6499	115.0179	116.8824
∠O-H-N	166.8131	150.8818	142.1148
Energy (H)	-475.0760910	-475.6494178	-475.7026306

Table 5.2 Effect of Electron Correlation on Total Interaction Energy (Before BSSE Correction), All Values are in kcal/mole

Compound	ΔE (RHF/6-31G*)	ΔE (MP2/6-31G*)	ΔE (MP2/6-31+G**)
N_2-Silanol	-1.10	-2.40	-2.01
N_2-$Si(OH)_4$	-1.20	-2.83	-2.57
N_2-H_2AlOH	-0.89	-2.06	-1.85

Table 5.3 shows the effect of polarization and the diffuse function on the interaction energy. Addition of polarization to heavy atoms and the hydrogen atoms (columns 3 and 4 respectively) make the interaction energy values for each molecule more negative, indicating that the molecule is more stable. Addition of the diffuse function (column 5) has a similar effect. The energy decreases with addition of polarization and the diffuse function. The total energy decreases by about 15% with the addition of polarization on heavy atoms. There is little change (about 3%) with the addition of the second polarization on hydrogen atoms. The decrease in energy is about 10% with the inclusion of the diffuse function. Note that the values of MP2/6-31G* and MP2/6-31G** for a nitrogen molecule are the same as expected because all the atoms present in a nitrogen molecule are considered to be heavy atoms (no hydrogen atom).

Table 5.3 Effect of Polarization and Diffuse Function on Energies, ΔE Values are Before BSSE Correction

Compound	MP2/6-31G	MP2/6-31G*	MP2/6-31G**	MP2/6-31+G**
N_2 (H)	-109.1110991	-109.2552776	-109.2552776	-109.2619291
Silanol (H)	-366.2254385	-366.3904650	-366.4267738	-366.4374967
N_2-Silanol (H)	-475.3408359	-475.6494178	-475.6856045	-475.7026306
ΔE (kcal/mole)	-2.70	-2.31	-2.23	-2.01

The fourth order correlation (MP4) contribution is small (the difference between MP2/6-31G* and MP4/6-31G* is less than 3%), as shown in Table 5.4. Small effects of third and fourth order correlations have also been reported (Del Bene et al., 1988 and Frisch et al., 1985). Because of the small contribution of the third and fourth terms of the correlation and the high computational costs involved with these calculations, only second order correlation (MP2) is being considered.

Table 5.4 Effect of Order of Correlation on the Energy of the System

Compound	MP2/6-31G*	MP4/6-31G*
N_2 (H)	-109.2552776	-109.2729965
Silanol (H)	-366.3904650	-366.4171875
N_2-Silanol (H)	-475.6494178	-475.6937773
ΔE (kcal/mole)	-2.31	-2.25

The total interaction energy (before and after BSSE correction), total thermal energy, and heat of adsorption for all three different systems at both MP2/6-31G* and MP2/6-31+G** levels of theory are presented in Table 5.5. BSSE is about 50% of the total binding energies. Since the calculations have been carried out at a relatively large basis sets (MP2/6-31G* and MP2/6-31+G**), BSSE correction values are unexpectedly high.

From Table 5.5, the interaction energy of nitrogen with $Si(OH)_4$ is the highest, followed by H_3SiOH and H_2AlOH for both levels of theory.

Thermal (vibrational, rotational, and translational) energies obtained from frequency calculations of a nitrogen molecule, surface models, and their complexes at MP2/6-31G* level of theory are reported in Table 5.6, and the thermal energy changes are presented in Table 5.5. The thermal energies of N_2-H_3SiOH and N_2-$Si(OH)_4$ are the same and are about 10% higher than that

Table 5.5 Interaction Energies, Thermal Energies, and Heat of Adsorption at MP2/6-31G* and MP2/6-31+G** Levels of Theory, All Values are in kcal/mole, the Values of Thermal Energies and Heat of Adsorption are Calculated at 77 K and 1.0 atm.

	N_2-Silanol	N_2-$Si(OH)_4$	N_2-H_2AlOH
ΔE^a(MP2/6-31G*)	-2.40	-2.85	-2.06
ΔE^b(MP2/6-31G*)	-1.15	-1.23	-1.00
ΔE^a(MP2/6-31+G**)	-2.01	-2.57	-1.85
ΔE^b(MP2/6-31+G**)	-1.03	-1.34	-0.99
$\Delta E^{thermal}$ (MP2/6-31G*)	0.714	0.714	0.659
ΔH^{adsorb}(MP2/6-31G*)	-0.59	-0.67	-0.49
ΔH^{adsorb}(MP2/6-31+G**)	-0.47	-0.79	-0.48
$\frac{\Delta H^{Theory}}{\Delta H^{Expt.}}$ (MP2/6-31+G**)	0.49	0.83	0.50

a Before BSSE correction
b After BSSE correction

Table 5.6 Thermal Energy at MP2/6-31G* Level of Theory, 77 K and 1.0 atm.

Compound	$E^{thermal}$ (kcal/mole)
N_2	3.491
Silanol	25.286
$Si(OH)_4$	37.037
H_2AlOH	17.455
N_2-Silanol	29.491
N_2-$Si(OH)_4$	41.242
N_2-H_2AlOH	21.605

of N_2-H_2AlOH. The heat of adsorption values of nitrogen on the surface models were calculated using equations 1 to 3 and are presented in Table 5.5. Heat of adsorption of nitrogen on silica hollow fiber membranes was calculated to be -0.955 kcal/mole at 77 K using the BET equation and experimental adsorption data (Thoen et al., 1994). The calculated heat of adsorption at the MP2/6-31G* (-0.59 kcal/mole) and MP2/6-31+G** (-0.47 kcal/mole) levels of theory is about 40% and 50% lower than the experimental value respectively when silanol is used to model the silica

surface. Other more realistic surface models predict the experimental heat of adsorption better. The calculated heat of adsorption using $Si(OH)_4$, as the surface model, is about 20% lower than that of the experimental value. This is fairly close considering the complexity of the silica surface. The interaction energy of N_2 with the H_2AlOH model is the smallest compared with other surface models.

The effect of electronic correlation and the diffuse function on the thermal energy of a silanol molecule is shown is Table 5.7. Although the addition of the diffuse function only changes the thermal energy by about 2% at the RHF level of theory, the addition of the correlation increases the thermal energy by about 20%. As a result of these findings, all thermal energy calculations have been carried out at MP2/6-31G* level of theory.

Table 5.7 Effect of Electron Correlation on Thermal Energy at 6-31G* and 6-31+G** Levels of Theory, All Values are in kcal/mole

Compound	RHF/6-31G*[a]	RHF/6-31+G**[a]	MP2/6-31G*
N_2	3.903	3.896	3.491
Silanol	23.632	23.519	25.286
N_2-Silanol	28.120	27.988	29.491
$\Delta E^{thermal}$	0.585	0.573	0.714

a The scale factor of 0.893 was used.

Heat of adsorption of other gaseous species (CO_2, CH_4, and CO) on silanol were also calculated and the results are presented in Table 5.8. The interaction energy and heat of adsorption of CO and CO_2 are higher than those of N_2 and CH_4 respectively. Although, these values are much lower than the experimental values obtained using the BET equation and the adsorbate adsorption isotherms, the same trend was observed experimentally (Thoen et al., 1994). The reason for the differences between the calculated heat of adsorptions with the experimental results is that the surface model (silanol) does not adequately describe silica surface, as shown above. Other surface models such as $Si(OH)_4$ need to be used to get more accurate heat of adsorption values (see Table 5.5).

An example of Gaussian 92 input file with the summary of the output file is presented in Appendix E.

5.4 Conclusions

The effect of the electron correlation, polarization, and the diffuse function on the interaction energy were found to be important for obtaining accurate results. BSSE correction was found to be about 50% of the total interaction energies. The effect of the electron correlation was found to be important on the thermal energy calculations, whereas, the thermal energy changed little with the addition of the diffuse function. The order of electron correlation had little effect on energy calculations. Thus, MP2/6-31+G** level of theory was needed for accurate energy calculation, whereas, MP2/6-31G* would introduce little error for thermal energy calculations.

Table 5.8 Interaction Energies, Thermal Energies, and Heat of Adsorption Values for Nitrogen, Carbon Monoxide, Carbon Dioxide, and Methane on Silanol at MP2/6-31+G** Level of Theory

Compound	ΔE^a	ΔE^b	$\Delta E^{thermal}$[c]	ΔH^{adsorb}	ΔH^{adsorb}[d] (Expt.)
N_2-Silanol	-2.01	-1.03	+0.71 @ 77 K	-0.47 @ 77 K	-0.955 @ 77K
CO-Silanol	-2.71	-1.89	+0.94 @ 87.5 K	-1.12 @ 87.5 K	-
CO_2-Silanol	-4.03	-2.34	+0.81 @ 273 K	-2.07 @ 273 K	-4.17 @ 273 K
CH_4-Silanol	-1.04	-0.34	+0.64 @ 157 K	-0.01 @ 157 K	-2.92 @ 156 K

a before BSSE correction
b after BSSE correction
c MP2/6-31G* level of theory are used
d Theon et al., 1994

Based on the results obtained from ab initio calculations, it was found that CO and CO_2 interact more strongly with the silica surface than those of N_2 and CH_4 respectively. The experimental observation shows the same trend.

It was found that $Si(OH)_4$ best represented the silica surface. The heat of adsorption of nitrogen on the silica surface obtained experimentally agreed well with the theoretical value calculated when $Si(OH)_4$ was used as the surface model. The predictions of the heat of adsorption using silanol as the surface model were much lower than the experimental values, however, trend was the same.

Chapter 6

Conclusions and Recommendations

6.1 Conclusions

The following conclusions are drawn from this work:

(1) The pore size of the microporous silica membrane was found to be 6.2 Å and 8.9 Å using H-K and S-F potential functions respectively. The pore geometry of the silica hollow fibers is tortuous and neither model describes the actual physical situation. However, the pore size of the silica hollow fiber membranes should be between the geometrical extremes of two flat parallel plates and a right cylinder.

(2) The permeances of gases with kinetic diameters ranging from 2.6 Å to 3.9 Å through silica hollow fiber membranes were inversely proportional to the kinetic diameter of the penetrant.

(3) The permeance values ranged from 10 to $2.3 \bullet 10^5$ Barrer/cm.

(4) The temperature dependencies of all gases on permeance were found to be exponential. Apparent activation energies for diffusion through the membranes were calculated from the slopes of Arrhenius plots of the permeation data.

(5) Apparent activation energies ranged from 4.61 to 14.0 kcal/mole and correlated well with kinetic diameter of the penetrants.

(6) The permeance of CO_2 and He were found to decrease with decreasing differential pressure driving force at $\Delta P < 5$ bar. No pressure dependency was found at $\Delta P \geq 5$ bar.

(7) No relationship between molecular weight of the penetrants and their permeance values were found.

From (4), (6), and (7), it can be concluded that Knudsen diffusion is not the transport mechanism through the microporous silica hollow fiber membranes.

(8) High selectivities were obtained for O_2/N_2 and CO_2/CH_4 mixtures.

(9) The O_2/N_2 mixed gas selectivities decreased from 11.3 at 298 K to 4.8 at 423 K and were up to 20% larger than the values calculated from pure gas permeances at temperatures below 373 K.

(10) The CO_2/CH_4 separation factor increased by 40% and the CO_2 permeance more than doubled after the membrane had been heated to above 398 K and then cooled in flowing He at 298 K. The CO_2/CH_4 mixed gas selectivities were higher than the values calculated from pure gas permeances at temperatures below 373 K. Based on FT-IR results, this behavior is attributed to the removal of physically adsorbed water from the membrane surface.

(11) The differences between the mixture and ideal separation factors is attributed to a competitive adsorption effect in which the more strongly interacting gases saturate the surface and impede the transport of the weakly interacting gases.

(12) Based on the results obtained from ab initio calculations and experimental observations, it was found that CO and CO_2 interact more strongly with the silica surface than those of N_2 and CH_4 respectively.

(13) Among the surface models studied, it was found that $Si(OH)_4$ best represented the silica surface.

(14) The experimental heat of adsorption of nitrogen on silica surface agreed well with the theoretical value calculated when $Si(OH)_4$ was used as the surface model.

(15) For ab initio calculations, it was important to include electron correlation, polarization, and diffuse function to obtain accurate interaction energy values. An example of a large basis set with electron correlation, polarization, and diffuse function would be MP2/6-31+G**.

6.2 Recommendations

The following recommendations are made for future research in the area of gas separation in selective microporous hollow fiber silica membranes:

(1) Since there are some inconsistencies among the reported values of the parameters used for the pore size calculation, it is recommended that the optimum values of the parameters could be obtained by measuring low pressure argon adsorption data for several samples with a known pore size. The pore size could be calculated using adsorption data and both H-K and S-F potentials with different values of parameters, then compared with the actual pore size of samples.

(2) The effect of "degas" temperature on the average pore size and pore size distribution could be studied. This could be achieved by degassing the silica sample at different temperatures (from 298 to 623 K), then obtaining the adsorption data, and finally calculating the pore size of the sample. The pore size should change, if there is any structural changes of the silica membrane upon heating.

(3) From the results obtained before, it was found that the flow rate of gases with large kinetic diameters such as C_2H_4 and CH_4 were very low

at low temperatures. To reduce the error caused by measuring low flow rates, the test system could be constructed such that each test tube could hold few silica membranes (10 fibers). This could also reduce the error caused by the small presence of air in the system when the flow rates of nitrogen and oxygen are being measured at low temperatures.

(4) To better understand the mechanisms of gases through microporous silica membranes, the pure gas permeabilities of gases that have little interaction with silica surface such as He, Ne, Ar, Kr, and Xe could be measured. The pure gas permeabilities of gases that have the same kinetic diameters (Kr, N_2, SO_2) but expected to have very different interactions with silica surface could also be measured. In addition, the permeabilities could be obtained from 250 K to 500 K for both pure and mixed gases. It is possible that even higher separation factors could be observed for lower temperatures. The transition from activated diffusion to surface and Knudsen diffusion might be observed with increasing temperature.

(5) High pressure adsorption isotherms for pure components and heat of adsorption of the gaseous species could be obtained to better understand the interaction of the penetrants with the silica surface..

(6) The surface structure of silica membranes could be changed from polar to non-polar using chemical treatments and similar measurements as explained above could be conducted to study the transport mechanisms.

(7) A combination of two silanol groups $(H_2SiOH)_2$ as a model for the silica surface could be used. In addition, $H_2Si\text{-}O\text{-}SiH_2$ could be used to model a dehydroxylated silica surface. The interaction energy of the

penetrants with both of surface models could be calculated using the ab initio theory.

(8) The internal coordinates and force constants obtained from ab initio calculations could be used to parametrize classical mechanical force fields for porous silica simulations. Then, these molecular dynamic simulations could be used to obtain diffusion coefficients of the penetrants passing through silica membranes.

Bibliography

Ahlrichs R., Bar M., Haser M., Horn H., Kolmel C., "Electronic Structure Calculations on Workstation Computers: The Program System Turbomole", *Chem. Phys. Lett.*, 162, 165-169 (1989).

Ash R., Barrer R. M., and Lowson R. T., "Transport of Single Gases and of Binary Gas Mixtures in a Microporous Carbon Membrane", *J. Chem. Soc. Faraday Trans.*, 1(69), 2166-2178 (1973).

Baker R., Cussler E. L., Eykamp W., Koros W. J., Riley R., and Strathmann H., "Research Needs in Membrane Separation Systems", Vol. 1 final report for DOE Contract No. DE-AC01-88ER30133 (1990).

Barrer R. M., "Migration in Crystal Lattices",*Trans. Faraday Soc.*, 37, 590-599 (1941).

Barrer R. M., "Diffusion in and Through Solids", Cambridge University Press: Cambridge, England (1951).

Barrer R. M., "Zeolites and Clay Materials as Sorbents and Molecular Sieves", Academic Press: London, England (1978).

Bhankarkar M., Shelekhin A. B., Dixon A. G., and Ma Y. H., "Adsorption, Permeation, and Diffusion of Gases in Microporous Membranes. I. Adsorption of Gases on Microporous Glass Membranes", *J. Mem. Sci.*, 75, 221-231 (1992).

Bhave R. , "Inorganic Membranes", Van Nostran Reinhold: New York, New York (1991)

Boys S. F. and Bernardi F.," The Calculation of Small Molecular Interactions by the Differences of Separate Total Energies. Some Procedures with Reduced Errors", *Mol. Phys.*, 19, 553 (1970).

Breck D. W., "Zeolite Molecular Sieves: Structure, Chemistry, and Use", Wiley: New York, NY (1974).

Brinker C. J., Ward T. L., Sehgal R., Raman N. K., Hietala S. L., Smith D. M., Hua D. W., and Headley T. J., "Ultramicroporous Silica-Based Supported Inorganic Membranes", *J. Mem. Sci.*, 77, 165-179 (1993).

De Almeida W. B., and O'Malley P.,"An Ab Initio Investigation of the Molecular Structure and Vibrational Spectrum of the Silanol-Hydrogen Molecular Complex", *J Chem. Soc. Faraday Trans.*, 89(7), 983-989 (1993).

Del Bene J. E., "Ab Initio Molecular Orbital Study of the Structures and Energies of Neutral and Charged Bimolecular Complexes of H_2O with Hydrides AH_n (A=N, O, F, P, S, and Cl)", *J. Phys. Chem.*, 92, 2874 (1988).

Everett D. H. and Powl J. C., "Adsorption in Slit-Like Cylindrical Micropores in the Henry's Law Region", *J. Chem. Soc., Faraday Trans. I*, 72, 619 (1976).

Fleming H. L., in "1986 Membrane Technology/Planning Conference Proceedings", Business Communications Co.: Cambridge, MA (1986).

Foresman J. B. and Frisch Æ., "Exploring Chemistry with Electronic Structure Methods: A Guide to Using Gaussian", Gaussian, Inc.: Pittsburgh, PA (1993).

Frankiewicz T. C. and Donnelly R. G., "Methane/Nitrogen Gas Separation Over the Zeolite Clinoptilolite by the Selective Adsorption of Nitrogen", in: T. E. White, C. M. Yon and E. H. Wagener (Eds.) ACS Symposium Series No. 223, American Chemical Society: Washington D. C., 213-233 (1983).

Frisch M. J., Foresman J. B., and Frisch Æ, *Gaussian 92 User's Guide*, Gaussian: Pittsburgh, PA (1992).

Frisch M. J., Pople J. A., and Del Bene J. E., "Molecular Orbital Study of the Dimers $(AH_n)_2$ Formed from NH_3, OH_2, FH, PH_3, SH_2, and ClH", *J. Phys. Chem.*, 89, 3664 (1985).

Garofalini S. H. , "Molecular Dynamics Computer Simulations of Silica Surface Structure and Adsorption of Water Molecules", *J. Non-Crystalline Solids*, 120, 1-12 (1990).

Garrone E., Kazansky V. B., Kustov L. M., Sauer J., Senchenya I. N., and Ugliengo P., "Spectroscopic and Ab Initio of the Interaction of Molecular Hydrogen with the Isolated Silica Hydroxyls and Related Systems", *J Phys. Chem.*, 96, 1040-1045 (1992).

Gilliland E. R., Baddour R. F., Perkinson G. P., and Sladek K. J., "Diffusion on Surfaces: I. Effect of Concentration on the Diffusivity of Physically Adsorbed Gases"' *Ind. Eng. Chem., Fundam.*, 13, 95 (1974).

Gregg S. J. and Sing K. S., "Adsorption, Surface Area, and Porosity", Second Edition Academic Press: New York (1982).

Hammel J. J., U.S. Patent 4,853,001, August 1, (1989).

Hammel J. J., Robertson W. J., Marshall W. P., Barch H. W., Das B., Smoot M. A., and Beaver R. P., U.S. Patent 4,842620, June 27, (1989).

Haser M., Ahlrichs R., "Improvements on the Direct SCF Method", *J. Comp. Chem.*, 10, 104-111 (1989).

Hassan M. H., Way J. D., Thoen P. M., and Dillon A. C., "Single Component and Mixed Gas Transport in a Silica Hollow Fiber Membrane", submitted to *J. Mem. Sci.* (1994).

Horvath G., and Kawazoe K., "Method for Calculation of Effective Pore Size Distribution in Molecular Sieve Carbon", *J. Chem. Eng. Japan*, 16, 470 (1983).

Hsieh H. P., "Inorganic Membranes," in Membrane Materials, and processes, *AIChE Symp. Series*, No. 261, Vol. 84, 1-18 (1988).

Hwang S. T., and Kammermeyer K., "Membrane in Separation", Krieger: Malabar, Florida (1984).

Iler R. K., "The Chemistry of Silica", Chapter 6, John Wiley & Sons: New York (1979).

Karger J. and Ruthven D. M., "Diffusion in Zeolites and Other Microporous Solids", Wiley: New York, (1992).

Knozinger H., "The Hydrogen Bond", Chapter 27, North-Holland Publishing Company (1976).

Koresh J. E., Kim T. H., and Koros W. J., "Study of Ultramicroporous Carbons by High-Pressure Sorption", *J. Chem. Soc., Faraday Trans. I*, 85(7), 1537-1544 (1989).

Koresh J. E., and Sofer A., "Molecular Sieve Carbon Permselective Membrane, Part I. Presentation of a New Device for Gas Mixture Separation", *Sepn. Sci. Tech.*, 18, 723-734 (1983).

Koresh J. E., and Sofer A., "Mechanism of Permeation through Molecular-Sieve Carbon Membrane", *J. Chem. Soc. Faraday Trans. I.* 82, 2057-2063 (1986).

Lasaga A. C., "Ab Initio Methods in Mineral Surface Reactions", *Reviews of Geophysics*, 30(3), 269-303 (1992).

Lin Y. S., and Burggraf A. J., "CVD of Solid Oxides in Porous Substrates for Ceramic Membrane Modification", *AICHE J.*, 38, 445-454 (1992).

Muruganandam N., and Paul D. R., "Evaluation of Substituted Polycarbonates and a Blend with Polystyrene as Gas Separation Membranes", *J. Mem. Sci.*, 34, 185-198 (1987).

Myers A. L. and Prausnitz J. M., "Thermodynamics of Mixed Gas Adsorption", *AICHE J.*, 11, 121-127 (1965).

Nicholas J. B., Winans R. E., Harrison R. J., Iton L. E., Curtiss L. A., and Hopfinger A. J., "Ab Initio Molecular Orbital Study of the Effects of Basis Set on the Calculated Structure and Acidity of Hydroxyl Groups in Framework Molecular Sieve", *J. Phys. Chem.*, 96, 10247-10257 (1992).

Okubo T., and Inoue H., "Improvement of Surface Transport Property by Surface Modification", *AIChE J.*, 34, 1031-1033 (1988).

Okubo T., and Inoue H., "Introduction of Specific Gas Selectivity to Porous Glass Membranes by Treatment with Tetraethoxysilane", *J. Mem. Sci.*, 42, 109-117 (1989).

Pan C. Y., "Gas Separation by High-Flux, Asymmetric Hollow-Fiber Membrane", *AIChE J.*, 32(12), 2020-2027 (1986).

Rabo J. A., "(Ed.) Zeolite Chemistry and Catalysis", ACS Monograph #171, American Chemical Society: Washington, D. C., New York (1976).

Rao M. B. and Sircar S., "Nanoporous Carbon Membrane for Separation of Gas Mixtures by Selective Surface Flow", *J. Mem. Sci.*, 85, 253-264 (1993).

Reid R. C. and Sherwood T. K., "The Properties of Gases and Liquids", McGraw-Hill Series in Chemical Engineering: New York, NY, 646 (1966).

Riekert L., "Sorption, Diffusion, and Catalytic Reaction in Zeolites", *Adv. Catal.*, 21, 281-321 (1970).

Ross and Olivier J. P., "On Physical Adsorption", J. Wiley and Sons: New York (1964).

Saito A. and Foley C., "Curvature and Parametric Sensitivity in Models for Adsorption in Microporoes", *AICHE J.*, 37(3), 429-436 (1991).

Shelekhin A. B., Dixon A. G., and Ma Y. H., "Adsorption, Permeation, and Diffusion of Gases in Microporous Membranes II. Permeation of Gases in Microporous Glass Membranes", *J. Mem. Sci.*, 75, 233-244 (1992).

Shelekhin A. B., Dixon A. G., and Ma Y. H., "Adsorption, Permeation, and Diffusion of Gases in Microporous Membranes. III. Application of Percolation Theory to Interpretation of Porosity, Tortuosity, and Surface Area in Microporous Glass Membranes", *J. Mem. Sci.*, 83, 181-198 (1993).

Shelekhin A. B., Grosgogeat E. J., and Hwang S. T., "Gas Separation of a New Polymer/Inorganic Composite Membrane", *J. Mem. Sci.*, 66, 129-141 (1991).

Sircar S., Rao M. B., and Golden T. C., "Gas Separation by Adsorbent Membranes", U.S. Patent 5, 104, 425 (1992).

Spillman R., "Economics of Gas Separation Membrane", *Chemical Engineering Progress*, 41-62 (1989).

Thoen P. M., Hassan M. H., Dillon A. C., McCarley K., and Way J. D., "Pore Sizes and Adsorption Properties of Silica Hollow Fiber Membranes", to be submitted to I&EC Research.

Ugliengo, P., Saunders, V. R., and Garrone, E., "Silanol as a Model for the Free Hydroxyl of Amorphous Silica: Quantum Mechanical Calculation of the Interaction with CO", *J. Phys. Chem.*, 93, 5210-5215 (1989).

Ugliengo P., Saunders V. R., and Garrone E., "Silanol as a Model for the Free Hydroxyl of Amorphous Silica: Ab Initio Calculation of the Interaction with Water", *J. Phys. Chem.*, 94, 2260-2267 (1990).

Ugliengo P., Saunders V. R., and Garrone E., "Silanol as a Model for the Free Hydroxyl of Amorphous Silica: Ab Initio Calculation of the Interaction with Formaldehyde", *Chemical Physics Letters*, 169(6), 501-508, (1990).

Uhlhorn R. J. R., Keizer K., and Burggraf A. J., "Gas and Surface Diffusion in Modified γ-alumina Systems", *J. Mem. Sci.*, 46, 225-241 (1989).

Unger "Porous Silica", Elsevier/North-Holland Inc.: New York, New York (1979).

Van Vuren R. J., Keizer K., and Burggraf A. J., "Gas Separation with Modified Ceramic Alumina Membranes," Paper Number 9-P02, International Congress on Membranes, Tokyo, Japan, June 8-12 (1987).

Wagner B., De Almeida, and O'Malley P. J., "An Ab Initio Investigation of the Molecular Structure and Vibrational Spectrum of the Silanol-Hydrogen Molecular Complex", *J. Chem. Soc. Faraday Trans.*, 89(7), 983-989 (1993).

Way D. J., and Roberts D. L, "Hollow Fiber Inorganic Membranes for Gas Separations", *Sepn. Sci. Tech.*, 27, 29-41 (1992).

Xiao J. and Wei J., "Diffusion Mechanism of Hydrocarbons in Zeolites I. Theory", *Chem. Eng. Sci.*, 47, 1123-1141 (1992a).

Xiao J. and Wei J., "Diffusion Mechanism of Hydrocarbons in Zeolites II. Analysis of Experimental Observations", *Chem. Eng. Sci.*, 47, 1143-1159 (1992b).

Zolandz R. R. and Fleming G. K., "Definitions, in: W. S. Winston Ho and K. K. Sirkar (Ed.) Membrane Handbook", Van Nostrand Reinhold: New York, NY (1992).

Appendices

Appendix A

Ideal Adsorbed Solution (IAS) Theory

This section is a brief discussion of the approximation of the multicomponent isotherms from pure component data using the ideal adsorbed solution theory (Myers and Prausnitz, 1965). In other words, to obtain an analytical expression for $\frac{\partial C_i}{\partial P_j}$ in terms of pure component isotherms and the known partial pressures of all species in the gas phase. Ideal adsorbed solution theory establishes the equality of all of the surface pressures of each individual species at a fictional "saturation partial pressure" of the pure component, $P_i^o(\pi)$. In the derivation of equations in the ideal adsorbed solution theory, it is assumed that both the adsorbed and gas phases behave ideally. When the gas and adsorbed phases are in equilibrium, the IAS equations are:

$$y_i P_T = x_i P_i^o \tag{A-1}$$

$$\psi_1^o(P_i^o) = \psi_2^o(P_2^o) = \ldots = \psi_N^o(P_N^o) \tag{A-2}$$

$$\sum_{i=1}^{N} x_i = 1 \tag{A-3}$$

There are 2N unknowns $\{P_i^o, x_i\}$ and 2N equations (A-1, A-2, and A-3). After the above equations are solved, the total amount adsorbed, C_t, is given by:

$$\frac{1}{C_t} = \sum_{i=1}^{N} \frac{x_i}{C_i^o} \tag{A-4}$$

The amount of ith component adsorbed is given by:

$$C_i = x_i C_t \tag{A-5}$$

Equation A-4, after combining with equation A-5 and replacing the amount adsorbed of species i by the partial pressure of ith component, can be written as:

$$C_i = \left(\frac{P_i}{P_i^o}\right)\left\{\sum_{k=1}^{N} \frac{P_k}{P_k^o C_k^o}\right\}^{-1} \tag{A-6}$$

Taking the derivative of equation A-6 with respect to P_j leads to:

$$\frac{\partial C_i}{\partial P_j} = \frac{C_t}{P_i^o}\frac{\partial P_i}{\partial P_j} - \frac{P_i C_t}{(P_i^o)^2}\frac{\partial P_i^o}{\partial P_j} - \frac{P_i C_t^2}{P_i^o}\frac{\partial}{\partial P_j}\left(\sum_{k=1}^{N} \frac{P_k}{C_k^o P_k^o}\right) \tag{A-7}$$

The partial derivative of the last term can be simplified as:

$$\frac{\partial}{\partial P_j}\left(\sum_{k=1}^{N} \frac{P_k}{C_k^o P_k^o}\right) = \sum_{k=1}^{N}\left(\frac{1}{C_k^o P_k^o}\frac{\partial P_k}{\partial P_j} - \frac{P_k}{C_k^o (P_k^o)^2}\frac{\partial P_k^o}{\partial P_j} - \frac{P_k}{(C_k^o)^2 P_k^o}\frac{\partial C_k^o}{\partial P_j}\right) \tag{A-8}$$

where:

$$\frac{\partial P_i}{\partial P_j} = \delta_{ij} \tag{A-9}$$

$$\frac{\partial P_k}{\partial P_j} = \delta_{kj} \tag{A-10}$$

$$\frac{\partial C_k^o}{\partial P_j} = \frac{\partial C_k^o}{\partial P_k^o}\frac{\partial P_k^o}{\partial P_j} \tag{A-11}$$

Combining equations A-7 through A-11 and simplifying, the cross terms for multicomponent can be written as:

$$\frac{\partial C_i}{\partial P_j} = \frac{C_t}{P_i^o}\delta_{ij} - \frac{P_i C_t}{(P_i^o)^2}\frac{\partial P_i^o}{\partial P_j} - \frac{P_i C_t^2}{P_i^o P_j^o C_j^o} + \frac{P_i C_t^2}{P_i^o}\left\{\sum_{k=1}^{N}\left(\frac{1}{P_k^o} + \frac{1}{C_k^o}\frac{\partial C_k^o}{\partial P_k^o}\right)\frac{P_k}{C_k^o P_k^o}\frac{\partial P_k^o}{\partial P_j}\right\} \tag{A-12}$$

where P_1^o can be obtained from equations A-1 through A-3 and C_t can be obtained from equation A-4. The terms C_k^o and $\frac{\partial C_k^o}{\partial P_k^o}$ can be obtained from the adsorption isotherms of pure component. The terms $\frac{\partial P_i^o}{\partial P_j}$ can be obtain:

$$(X) = (A)^{-1}(B) \tag{A-13}$$

where:

$$(A) = \begin{pmatrix} \frac{C_1^o}{P_1^o} & -\frac{C_2^o}{P_2^o} & . & . & . & 0 \\ \frac{C_1^o}{P_1^o} & 0 & -\frac{C_3^o}{P_3^o} & . & . & 0 \\ . & . & . & . & . & . \\ . & . & . & . & . & . \\ \frac{C_1^o}{P_1^o} & 0 & 0 & 0 & 0 & -\frac{C_N^o}{P_N^o} \\ \frac{P_1}{(P_1^o)^2} & \frac{P_2}{(P_2^o)^2} & . & . & . & \frac{P_N}{(P_N^o)^2} \end{pmatrix} \qquad \text{(A-14)}$$

$$(B) = \begin{pmatrix} 0 & . & . & . & . & 0 \\ . & . & . & . & . & . \\ . & . & . & . & . & . \\ . & . & . & . & . & . \\ 0 & . & . & . & . & 0 \\ \frac{1}{P_1^o} & \frac{1}{P_2^o} & . & . & . & \frac{1}{P_N^o} \end{pmatrix} \qquad \text{(A-15)}$$

$$(X) = \begin{pmatrix} \frac{\partial P_1^o}{\partial P_1} & \frac{\partial P_1^o}{\partial P_2} & . & . & . & \frac{\partial P_1^o}{\partial P_N} \\ . & . & . & . & . & . \\ . & . & . & . & . & . \\ . & . & . & . & . & . \\ \frac{\partial P_N^o}{\partial P_1} & \frac{\partial P_N^o}{\partial P_2} & . & . & . & \frac{\partial P_N^o}{\partial P_N} \end{pmatrix} \qquad \text{(A-16)}$$

Appendix B

Gaussian Functions

As an example, for s, p_y, and d_{xy} orbitals, the Gaussian functions would be:

$$g_s = \left(\frac{2\alpha}{\pi}\right)^{\frac{3}{4}} e^{-\alpha r^2} \tag{B-1}$$

$$g_y = \left(\frac{128\alpha^5}{\pi^3}\right)^{\frac{1}{4}} y e^{-\alpha r^2} \tag{B-2}$$

$$g_{d_{xy}} = \left(\frac{2048\alpha^7}{\pi^3}\right)^{\frac{1}{4}} xy e^{-\alpha r^2} \tag{B-3}$$

where r is the distance to the nucleus, and the coefficient α is chosen to provide a best representation of a hydrogen-type function or to provide the best agreement with numerical Hartree-Fock calculations for atomic functions on individual atoms. The size of α in the Gaussian determines the size of the function or how close the electron charge is to the nucleus.

Appendix C

Data Reduction for Gases with High Flow Rates

C.1 Theory

A silica hollow fiber membrane can be considered as a long tube (ratio of its length to inside diameter is greater than 10^3). Inside and outside diameters of the membrane are 35 μm and 45 μm. The length of the membrane is measured to be 14.0 centimeters. One end of the membrane is sealed off by the torch flame, and the other end is kept open to the atmosphere. The gas diffuses from the outside of the fiber where the pressure, P_{out}, is kept constant, into the inside of the fiber and then flows out to the atmosphere, P_1.

The resistance to flow is very high, since the diameter is small, as a result, there is a large pressure drop. The gas flow through the membrane is considered to be a compressible flow.

Mass flow rate , W along the tube can be obtained by using mass balance at steady state, in one-direction (z-direction), and is given as:

$$\frac{dW}{dZ} = -2\pi r_i f_i \qquad \text{(C-1)}$$

where f_i is the mass flux through the tube wall at the inside radius.

Momentum balance for this system (isothermal, long tube, z-direction) can be reduced to:

$$\frac{d(\rho v_Z^2)}{dZ} = -\frac{2\pi r_i \tau_w}{\pi r_i^2} - \frac{dP_T}{dZ} \qquad \text{(C-2)}$$

where ρ is the density of gas flowing through the tube, v_z velocity of the gas in z-direction, τ_w is the wall shear stress, P_T is the total pressure along the tube, and r_i is the inside radius of the tube.

In equation C-2 ρ, v_z, P_T, and τ_w all vary along the tube.

Density can be obtained using an equation of state, v_z is related to W by definition, and τ_w is a function of density, ρ, velocity, v_z, and friction factor, λ, as shown by equations below:

$$\rho = \frac{P_T M}{RT} \qquad \text{for ideal gas} \tag{C-3}$$

$$W = \pi r_i^2 \rho v_Z = \frac{\pi r_i^2 P_T M v_Z}{RT} \tag{C-4}$$

$$\tau_w = \frac{\lambda \rho v_Z}{2} \tag{C-5}$$

If the friction factor for laminar flow in a microporous tube is the same as in a nonporous one, then λ is given as:

$$\lambda = \frac{16}{Re} = \frac{8\pi r_i \mu}{W} \tag{C-6}$$

Assuming that the permeability coefficient, Q, does not depend on pressure in the microporous membrane , then the mass flux, f_i , can be defined as:

$$f_i = -\frac{Q_i M (P_T - P_1)}{r_i \ln\left(\frac{r_o}{r_i}\right)} \tag{C-7}$$

where P_1 and M are the pressure at the outlet and molecular weight respectively.

The resultant equations, after combining equations C-1 through C-7, are:

$$\frac{dW}{dZ} = 2\pi\left(\frac{Q_i M(P_T - P_1)}{\ln\left(\frac{r_o}{r_i}\right)}\right) \qquad \text{(C-8)}$$

$$\frac{dP_T}{dZ} = \frac{-4\pi r_i f_i - 8\pi\mu}{\left(\frac{\pi^2 r_i^4 M P_T}{RTW} - \frac{W}{P_T}\right)} \qquad \text{(C-9)}$$

The boundary conditions for equations C-8 and C-9 are:

$$W = 0.0 \qquad @\ Z=L_f$$

$$P_T = P_1 \qquad @\ Z = 0.0$$

Where: μ can be calculated using Whalley correlations (Reid and Sherwood, 1966) as explained by Shelekhin et at. (1992).

For nonpolar gases:

$$\mu\xi = 3.4\text{x}10^{-4} T_r^{0.94} \qquad \text{if } T_r \langle 1.5$$

$$\mu\xi = 1.778\text{x}10^{-4}(4.58T_r - 1.67)^{\frac{5}{8}} \qquad \text{if } T_r \rangle 1.5$$

For polar gases (hydrogen-bonding types):

$$\mu\xi = (7.55T_r - 0.55)x10^{-5}z_c^{-\frac{5}{4}} \qquad \text{if } Tr<2$$

$$\xi = \frac{T_c^{1/6}}{M^{1/2}P_c^{2/3}}$$

Both the equations C-8 and C-9 with the boundary conditions can be solved simultaneously to get both the mass flow rate, W, and pressure, P_T, along the length of the fiber. These two equations were solved using a variable order, variable step size finite difference method with deferred corrections, developed by Lentini and Pereyra and implemented in the IMSL Inc. mathematical software library.

C.2 FORTRAN Program for Pressure Drop Calculation

A listing of the FORTRAN code for the calculation of the pressure drop along a microporous silica hollow fiber membrane is presented on this section. Figure C.1 shows the pressure drop along the length of the tube for He at 423 K and 827 (permeability) Barrer.

```
C     ***************************************************
C     ***** This program calculates the permeability of a      *****
C     ***** gas passing through a silica hollow fiber          *****
C     ***** membrane. For a high permeate flow rate, the      *****
C     ***** pressure drop along silica membrane needs to be   *****
C     *****              accounted for.                      *****
C     ***** Steps for running this program are as follow:     *****
C     ***** 1) Guess permeability at a given temperature      *****
C     ***** 2) The program calculates the pressure drop       *****
C     *****    drop along the tube.                          *****
```

```
C     ***** 3) The program calculates the volumetric flow      *****
C     *****    rate at the exit of the tube.                   *****
C     ***** 4) Check the calculated volumetric from rate       *****
C     *****    (from step 3) with the value measured           *****
C     *****    experimentally. If the values are close         *****
C     *****    enough, stop, if not, go to step 1.             *****
C     *****                                                    *****
C     ***** Equations C-8 and C-9 with the boundary            *****
C     ***** conditions are normalized and then solved          *****
C     ***** simultaneously using a variable order, variable    *****
C     ***** step size finite difference method with deferred   *****
C     ***** corrections implemented in the IMSL Inc.           *****
C     ***** mathematical software library.                     *****
C     ************************************************************
C     *****                                                    *****
C     *****          By: Mohammed H. Hassan                    *****
C     *****                                                    *****
C     ************************************************************

C     *****          Defining variables and parameters         *****

C     ***** ALPHA     Conversion factor                        *****
C     ***** P3        Outside pressure of the membrane         *****
C     ***** RI        Inside radius of the membrane            *****
C     ***** RO        Outside radius of the membrane           *****
C     ***** R         Gas constant                             *****
C     ***** XL        Total length of the membrane             *****
C     ***** PO        Pressure at the exit of the membrane     *****
C     ***** T         Temperature                              *****
C     ***** Troom     Room temperature                         *****
C     ***** PERM      Permeability                             *****
C     ***** XMW       Molecular weight of a gas passing        *****
C     *****           through the membrane                     *****
C     ***** TC        Critical temperature of a gas passing    *****
C     *****           through the membrane                     *****
C     ***** TR        Reduced temperature of a gas passing     *****
C     *****           through the membrane                     *****
C     ***** PC        Critical pressure of a gas passing       *****
C     *****           through the membrane                     *****
C     ***** XMU       Viscosity of a gas passing through the   *****
C     *****           membrane                                 *****
C     ***** volrate   Volumetric flow rate                     *****


      Character*10 fname
      INTEGER LDYFIN,LDYINI,MXGRID,NEQNS,NINIT
```

```
      PARAMETER (MXGRID=45,NEQNS=2,NINIT=45,LDYFIN=NEQNS,
     &          LDYINI=NEQNS)
C
      INTEGER I,J,NCUPBC,NFINAL,NLEFT,NOUT
      REAL CONST,ERREST(NEQNS),FCNBC,FCNEQN,FCNJAC,FLOAT,
     &     PISTEP,TOL,XFINAL(MXGRID),XINIT(NINIT),XLEFT,
     &     XRIGHT,YFINAL(LDYFIN,MXGRID),YINIT(LDYINI,NINIT)

      REAL ALPHA,P3,RI,RO,R,XL,PO,T,PERM,XMW,TC,PC,FF,PI,Troom,
     &     ZITA,TR,XMU,AA,BB,CC,DD,EE,FI,FIP,SORAT,SORATT,XRAJ

      COMMON XMU,FI,RI,RO,R,T,XMW,ALPHA,SORAT,XRAJ,AA,BB,CC,DD,
     & EE,XL,P3,PO,PERM,SORATT,FIP,TC,PC,TR,ZITA,FF,PI,Troom
C
      LOGICAL LINEAR,PRINT
      INTRINSIC FLOAT

      EXTERNAL BVPFD,CONST,FCNBC,FCNEQN,FCNJAC,UMACH
C
      NLEFT = 1
      NCUPBC = 0
      TOL = 0.000001
      XLEFT = 0.0
      XRIGHT = 1.0
      PISTEP = 0.0
      PRINT = .FALSE.
      LINEAR = .FALSE.
C
      DO 10 I=1,NINIT
        XINIT(I) = XLEFT+(I-1)*(XRIGHT-XLEFT)/FLOAT(NINIT-1)
       YINIT(1,I) = 1.0e-9
        YINIT(2,I) = (0.8*xinit(i) + 0.1)*.7622e-8
10    CONTINUE

C
C     *****                    Input                    *****
C
      write(*,*) 'Enter Temperature (oC)?'
      read(*,*) T
      write(*,*) 'Enter Permeability (Barrer)?'
      read(*,*) PERM
      T =  T + 273.15
C
      CALL
BVPFD(FCNEQN,FCNJAC,FCNBC,FCNEQN,FCNBC,NEQNS,NLEFT,
```

```
     &        NCUPBC,XLEFT,XRIGHT,PISTEP,TOL,NINIT,XINIT,
     &         YINIT,LDYINI,LINEAR,PRINT,MXGRID,NFINAL,XFINAL,
     &        YFINAL,LDYFIN,ERREST)

      DO 15 I=1,NFINAL
      YFINAL(2,I) = YFINAL(2,I)/BB
   15  CONTINUE

C
C     *****                    Output                    *****
C
     CALL UMACH(2,NOUT)
      write(*,*) 'Enter name of the result file ?'
     read(*,12) fname
   12  format(A)
      open(2,file=fname,status='unknown')

     WRITE(NOUT,997)
     WRITE(NOUT,998)(I,XFINAL(I),(YFINAL(J,I),J=1,NEQNS),I=1,
    &          NFINAL)
      WRITE(NOUT,999)(ERREST(J),J=1,NEQNS)
  997  FORMAT(4X, 'I', 7X, 'X',14X, 'WR', 13X, 'PR')
  998  FORMAT(I5, 1P3E15.6)
  999  FORMAT(\' Error Estimates', 4X, 1P2E15.6)

        volrate=yfinal(1,nfinal)*60.0*R*Troom*1.0e9/(xmw*po)
       write(*,996) volrate,perm
  996  format(\\2x,'Volumetric Flow Rate =',e15.5,2x,
     &       'Permeability =',e15.5)
     WRITE(2,995)
     WRITE(2,994)(I,XFINAL(I),(YFINAL(J,I),J=1,NEQNS),I=1,
    &          NFINAL)
     WRITE(2,993)(ERREST(J),J=1,NEQNS)
  995 FORMAT(4X, 'I', 7X, 'X',14X, 'WR', 13X, 'PR')
  994 FORMAT(I5, 1P3E15.6)
  993 FORMAT(\' Error Estimates', 4X, 1P2E15.6)

        volrate=yfinal(1,nfinal)*60.0*R*Troom*1.0e9/(xmw*po)
       write(2,992) volrate,perm
  992  format(\\2x,'Volumetric Flow Rate =',e15.5,2x,
     &       'Permeability =',e15.5)

     END
C
C     *****                  Input equations             *****
C
```

```
      SUBROUTINE FCNEQN(NEQNS,X,Y,P,DYDX)
      INTEGER NEQNS
      REAL    X,Y(NEQNS),P,DYDX(NEQNS)

      REAL ALPHA,P3,RI,RO,R,XL,PO,T,PERM,XMW,TC,PC,FF,PI,Troom,
     &     ZITA,TR,XMU,AA,BB,CC,DD,EE,FI,FIP,SORAT,SORATT,XRAJ

      COMMON XMU,FI,RI,RO,R,T,XMW,ALPHA,SORAT,XRAJ,AA,BB,CC,DD,
     &     EE,XL,P3,PO,PERM,SORATT,FIP,TC,PC,TR,ZITA,FF,PI,Troom
C
      REAL ALOG
      INTRINSIC ALOG
C
C     *****                List of constants                *****
C
      ALPHA = 3.3466E-16
      P3 = 300.0*1.0135E5/14.7
      RI = 17.5E-6
      Ro = 22.5E-6
      R =  8.314
      XL = 14.0E-2
      Po = 1.0135E5
      Troom = 21. + 273.15


      XMW = 4.E-3
      TC = 5.25
      PC = 22.6
      ZITA = TC**(1./6.)/((XMW*1000.)**(1./2.)*PC**(2./3.))

      TR = T/TC
      IF(TR .LE. 1.5) THEN
        XMU = 3.4E-4*TR**(.94)/ZITA
      ELSE
        XMU = 1.778E-4*(4.58*TR - 1.67)**(5./8.)/ZITA
      ENDIF
      PI = 3.141592654
C
C     *****              Input equations                *****
C
      AA = -2.*PI*ALPHA*PERM*XMW/ALOG(RO/RI)
      EE = XMW*PI**2*RI**4/(R*T)
      FF = 8.0*PI*XMU/1000.0
      DD = PO-P3
      BB = XL*AA*DD
      CC = BB*XL/DD
```

```
      DYDX(1) = y(2)
       DYDX(2) = CC*(-2.*AA*DD*Y(2)/BB-ff)*y(1)*
     &        (DD*y(2)/BB+p3)/(ee*(DD*y(2)/BB+p3)**2-y(1)**2)

       RETURN
       END
C
C      *****                Derivatives of the equations                *****
C
       SUBROUTINE FCNJAC(NEQNS,X,Y,P,DYPDY)
       INTEGER NEQNS
       REAL X,Y(NEQNS),P,DYPDY(NEQNS,NEQNS)

       REAL ALPHA,P3,RI,RO,R,XL,PO,T,PERM,XMW,TC,PC,FF,PI,
     &     ZITA,TR,XMU,AA,BB,CC,DD,EE,FI,FIP,SORAT,SORATT,XRAJ

       COMMON XMU,FI,RI,RO,R,T,XMW,ALPHA,SORAT,XRAJ,AA,BB,CC,DD,
     &          EE,XL,P3,PO,PERM,SORATT,FIP,TC,PC,TR,ZITA,FF,PI
C
       sorat = CC*(-2.0*AA*DD*y(2)/BB-ff)*y(1)
     &       *(DD*y(2)/BB+p3)
       xraj = ee*(DD*y(2)/BB+p3)**2 - Y(1)**2
       dsoratw = sorat/y(1)
       dsoratp = CC*y(1)*(-4.*AA*DD**2*y(2)/BB**2 -
     &         (2.*AA*DD*P3/BB+FF*DD/BB))
       dxrajw = -2.*y(1)
       dxrajp = 2.*EE*DD*(DD*y(2)/BB+p3)/BB

       DYPDY(1,1) = 0.0
       DYPDY(1,2)= 1.0
       DYPDY(2,1) = (dsoratw*xraj-dxrajw*sorat)/xraj**2
       DYPDY(2,2) = (dsoratp*xraj-dxrajp*sorat)/xraj**2
       RETURN
       END
C
C      *****            Boundary conditions                             *****
C
       SUBROUTINE FCNBC(NEQNS,YLEFT,YRIGHT,P,F)
       INTEGER NEQNS
       REAL YLEFT(NEQNS),YRIGHT(NEQNS),P,F(NEQNS)

       REAL ALPHA,P3,RI,RO,R,XL,PO,T,PERM,XMW,TC,PC,FF,PI,
     &     ZITA,TR,XMU,AA,BB,CC,DD,EE,FI,FIP,SORAT,SORATT,XRAJ

       COMMON XMU,FI,RI,RO,R,T,XMW,ALPHA,SORAT,XRAJ,AA,BB,CC,DD,
```

```
     &          EE,XL,P3,PO,PERM,SORATT,FIP,TC,PC,TR,ZITA,FF,PI
C
      F(1) = YLEFT(1)
      F(2) = YRIGHT(2) - BB
       RETURN
      END
```

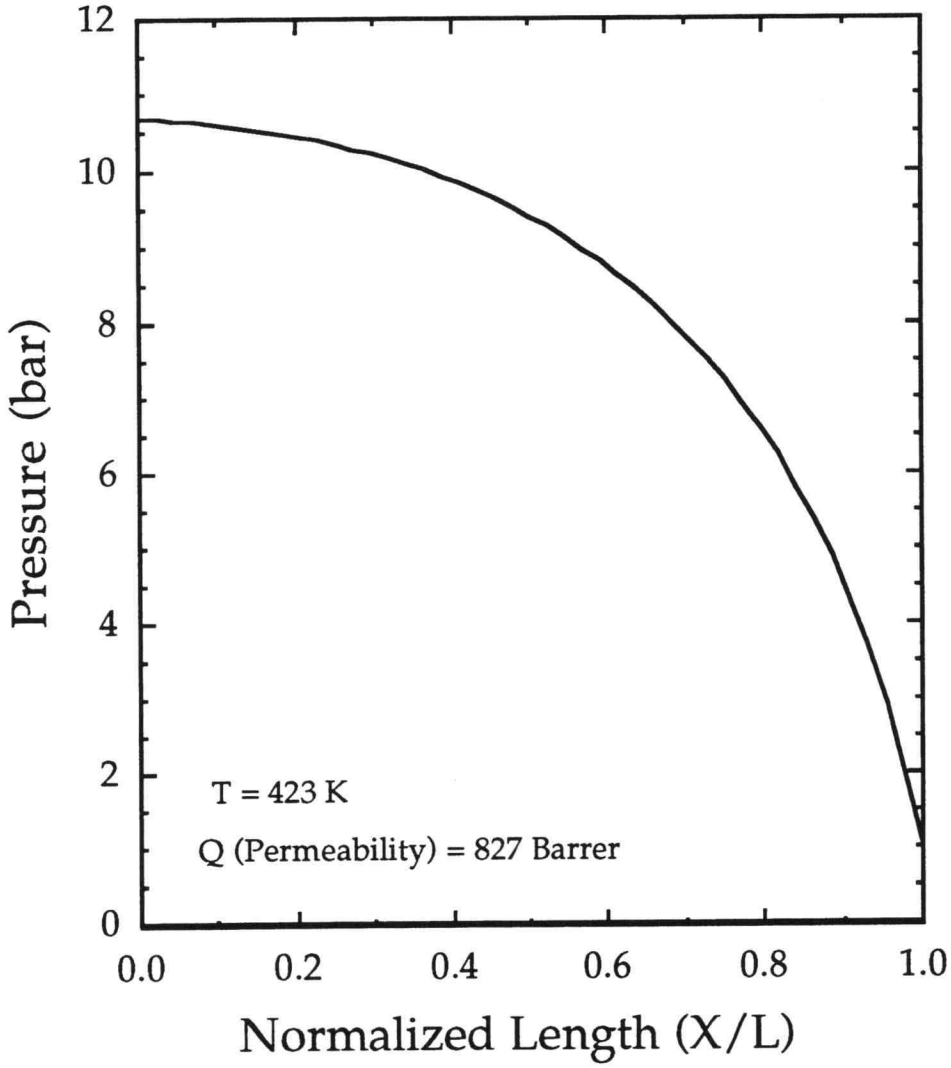

Figure C.1 Pressure drop along the length of microporous membrane for He at 423 K and 827 Barrer. The pressure outside the membrane is fixed at 20.4 bar.

Appendix D

Documentation for Pore Size Calculation

Documentation for pore size calculation (Chapter 3) is presented in this appendix. The physical parameters (kinetic diameters, magnetic susceptibilities, polarizabilities, and densities for both the adsorbate and adsorbent) and experimental adsorption data are needed for pore size calculations.

D.1 Procedures for Pore Size Calculation

Highly nonlinear equations (3-8 for H-K model and 3-13 for S-F model) can be solved using any nonlinear algorithm such as Newton or bisection method. An alternative, more efficient, approach for solution to equations 3-8 and 3-13 is as follows:

1) Guess pore size for both models
2) Use a MATLAB program (section D.2) to solve equations 3-8 and 3-13. The equations are in the form of P/P_o = f(pore size).
3) Obtain relationship between pore size and relative pressure [pore size = $f(P/P_o)$] using polynomial fit.
4) Use a FORTRAN program (section D.4) to calculate the pore size distribution.

An example of the polynomial obtained using physical parameters from Table 3.1 is presented on section D.3. The comparison of the results from step 2 and the polynomial is presented in Figure D.1. Finally, the pore size distribution result using argon adsorption data (run #1054) at 87.5 K is shown in Figure 3.4.

D.2 MATLAB Program

```
%  ******   This program calculates pore size                    ******
%  ******   distribution (pore size as a function                ******
%  ******   of relative pressure) using both H-K                 ******
%  ******   (slit) and S-F (cylinder) models.                    ******

%  ******   Guess Values for the pore size                       ******
%  ******   (both H-K and S-F Models)                            ******

L = [.8:0.01:1.9];
rp = [.53:0.01:.98];

%  ******              List of Constants                         ******

%  ******  Nav     Avogadro's number                             ******
%  ******  R       Gas Constant                                  ******
%  ******  T       Temperature                                   ******
%  ******  c       Speed of light                                ******
%  ******  M       Mass of an electron                           ******
%  ******  alphaa  Polarizability of the adsorbate               ******
%  ******  alphae  Polarizability of the adsorbent               ******
%  ******  kapaa   Magnetic susceptibility of                    ******
%  ******          the adsorbate                                 ******
%  ******  kapae   Magnetic susceptibility of                    ******
%  ******          the adsorbent                                 ******
%  ******  dena    Density of the adsorbate                      ******
%  ******  dene    Density of the adsorbent                      ******
%  ******  da      Diameter of the adsorbate                     ******
%  ******  de      Diameter of the adsorbent                     ******

Nav = 6.023e23;
R = 8.314;
T = 87.5.;
c = 3.e8;
M = 9.11e-31;
c2M = M*c^2
alphaa = 1.63e-24;
alphae = 0.85e-24;
kapaa = 3.22e-29;
kapae = 1.94e-29;
dena = 7.608e14;
dene = 3.75e15;
```

```
da = .340;
de = .304;

%  ******          Calculation of pore size distribution          ******

Aea = (6.*c2M*alphaa*alphae)/(alphae/kapae + alphaa/kapaa);
Aaa = 3.*c2M*alphaa*kapaa/2.0;

d = (da + de)/2.0;
do = d*1.e-7;
s = 0.858*d;
sigma1 = s*1.e-7;

c1 = Nav*(dena*Aaa + dene*Aea)/(R*T*sigma1^4)
c2 = - (s^4)/(3.*(d^3)) + (s^10)/(9.*(d^9))
c3 = (s^4)/3.
c4 = (s^10)/9.
c5 = (3.*pi*c1/4.)*(s/d)^4

%  ******                H-K (slit) Model                  ******

for i=1:110
P(i) = L(i) - d;
lnppo(i) = (c1/(L(i)-2.*d))*(c3/P(i)^3 - c4/P(i)^9 + c2);
ppo(i) = exp(lnppo(i));
pore(i) = L(i) - de;
psize(i) = pore(i)*10.0;
end

%  ******              S-F (cylinder) Model                ******

alpha(1) = 1.;
beta(1) = 1.;
for k=2:300
alpha(k) = alpha(k-1)*((-4.5-k)/k)^2;
beta(k) = beta(k-1)*((-1.5-k)/k)^2;
end
for i=1:45
porecyl(i) = 2.*rp(i) - de;
psizecyl(i) = porecyl(i)*10.0;
sum = (21./32.)*(d/rp(i))^10 - (d/rp(i))^4;
for k=1:299
c7(k)=(1./(k+1.))*(1.-d/rp(i))^(2.*k);
c8(k)=(21.*alpha(k+1)/32.)*(d/rp(i))^10 - beta(k+1)*(d/rp(i))^4;
c9(k) = c7(k)*c8(k);
sum = sum + c9(k);
```

```
end
lnppo2(i) = c5*sum;
ppo2(i) = exp(lnppo2(i));
end

%  ******          Polynomial fits and the outputs                    ******

disp(' Psizecyl      lnppocyl      ppocyl')

[psizecyl' lnppo2' ppo2']

disp(' Psize         lnppo              ppo')

[psize' lnppo' ppo']

pause
pos1=[50 400 400 300];
pos2=[500 400 400 300];
figure;
set(gcf,'position',[pos1]);
psizepoly=polyfit(lnppo,psize,7)
poly1 = poly2str(psizepoly,'X')
ypoly=polyval(psizepoly,lnppo);

psizecylpoly=polyfit(lnppo2,psizecyl,7)
poly3 = poly2str(psizecylpoly,'X')
ypoly1=polyval(psizecylpoly,lnppo2);
plot(lnppo,psize,'y-',lnppo,ypoly,'r+',lnppo2,psizecyl,'y-
',lnppo2,ypoly1,'ro'),grid
%figure;
%set(gcf,'position',[pos2]);
%plot(psizecyl,lnppo2,'y+',psizecyl,ypoly1,'ro'),grid
```

D.3 Results Obtained from MATLAB Program

Polynomial results obtained from both H-K and S-F models using physical parameters from Table 3.1 are presented below.

Pore size (H-K Model):

0.0001 0.0040 0.0742 0.7526 4.5750 17.0169 37.8410 49.0206

Polynomial (H-K Model):

0.00009184 X^7 + 0.004018 X^6 + 0.07418 X^5 + 0.7526 X^4 + 4.575 X^3 + 17.02 X^2 + 37.84 X + 49.02

Pore size (S-F Model):

0.0000 0.0016 0.0299 0.3135 1.9907 7.8713 19.4828 35.3608

Polynomial (S-F Model):

0.00003508 X^7 + 0.001572 X^6 + 0.02986 X^5 + 0.3135 X^4 + 1.991 X^3 + 7.871 X^2 + 19.48 X + 35.36

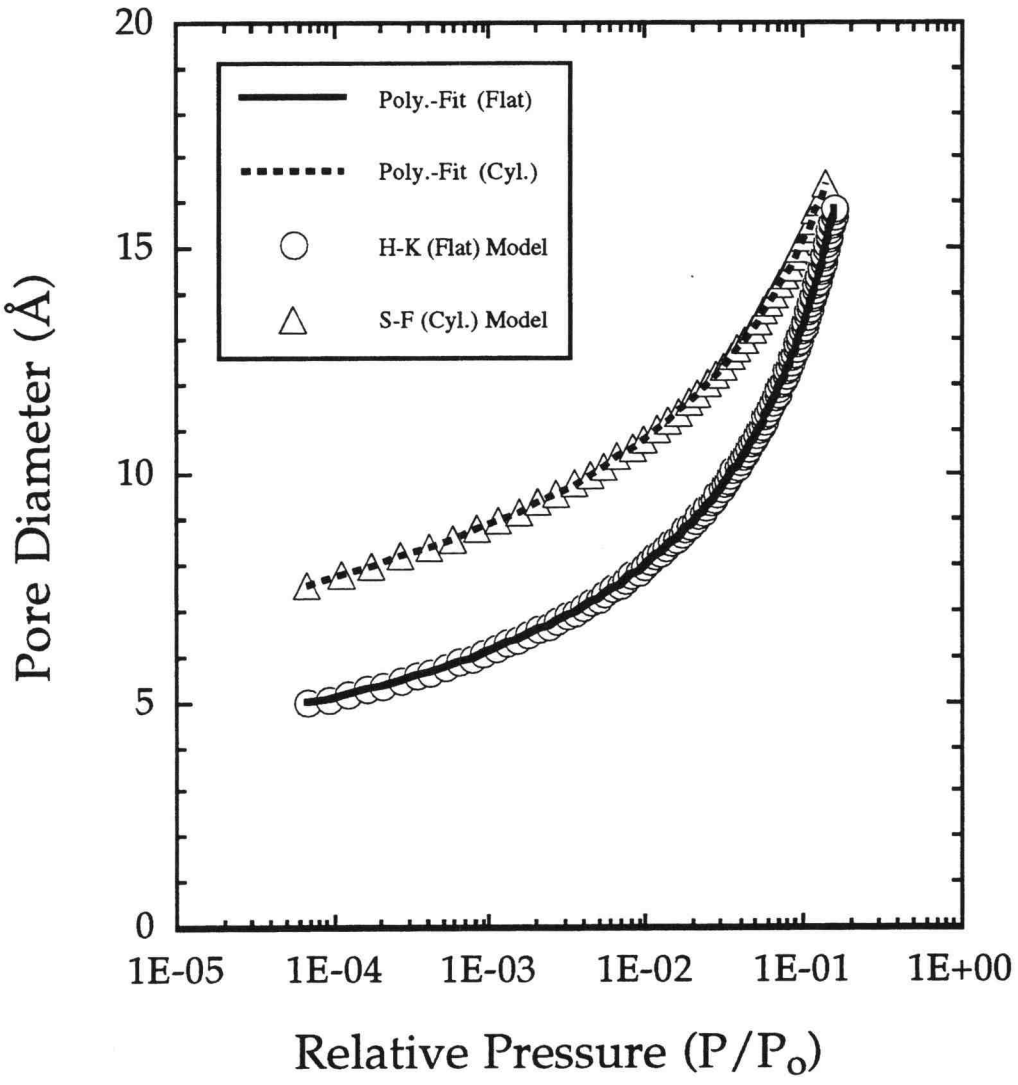

Figure D.1 Relationship between pore diameter and relative pressure. Physical parameters from Table 3.1 is used for pore size calculation.

D.4 FORTRAN Program for Pore Size Calculation

```
c     ************************************************************
c     ******      Pore Size Calculation in Slit and              *****
c     ******      Cylindrical Geometries (H-K and S-F            *****
c     ******                  models).                           *****
c     ******      The polynomial fit that is obtained            *****
c     ******      from the mathlab program and the               *****
c     ******      experimental adsorption isotherm               *****
c     ******      were used for the calculation of the           *****
c     ******      the pore size distribution.                    *****
c     ******                                                     *****
c     ******            BY: Mohammed H. Hassan                   *****
c     ************************************************************

c     ******            Defining variables and parameters        *****

c     ******      ppo   Relative pressure, P/Po                  *****
c     ******      w     Amount adsorbed                          *****
c     ******      wo    maximum amount adsorbed                  *****
c     ******      wwo   Normalized amount adsorbed               *****
c     ******      pflat Pore size using H-K model                *****
c     ******      pcyl  Pore size using S-F model                *****

      implicit real*8 (a-h,o-z)
      real*8 lnppo
      PARAMETER (NMAX=500)
       CHARACTER*10 FNAME1, FNAME2, FNAME3
      DIMENSION ppo(100),w(100),lnppo(100),wwo(100)
      dimension pflat(100),pcyl(100),dwwo(100),dpflat(100)
      dimension rflat(100),dpcyl(100),rcyl(100),dwdrflat(100)
      dimension dwdrcyl(100),a1(100),a2(100),a3(100),a4(100)

c     *****       Reading the experimetal adsorption             *****
c     *****                  data file.                          *****

       WRITE(*,*) 'Enter name of the original data file'
      READ(*,12)  FNAME1

c     *****       Name of the files that the results             *****
c     *****             would be stored in.                      *****

       WRITE(*,*) 'Enter name of the pore size results data file'
```

```
      READ(*,12)  FNAME2
       WRITE(*,*) 'Enter name of d(W/Wo)/dR results data file'
      READ(*,12) FNAME3
12     FORMAT(A)

       open(1,file=FNAME1,status='old')
       open(2,file=FNAME2,status='UNKNOWN')
       open(3,file=FNAME3,status='UNKNOWN')

      write(*,*) 'Enter type of calculations, 1 for "Coulter/VDW",',
     &           ' 2 for "Coulter/Kin", 3 for "Coulter/PLW",',
     &        ' 4 for "Micromeritics/VDW", 5 for "Micromeritics/Kin",',
     &           ' 6 for "Micromeritics/PLW", 7 for "S-F/VDW",',
     &        ' 8 for "S-F/Kin", and any other integer for "S-F/PLW" ?'
       read(*,*) M

      do 5 i=1,NMAX
       read(1,*, END=3) a1(i),a2(i),a3(i),a4(i),ppo(i),w(i)
5     continue
3     N = I-1
      wo = w(N)

       do 9 i=1,N
        lnppo(i) = log(ppo(i))
        wwo(i) = w(i)/wo
9      continue

c       ******  Polynomial fits obtained from mathlab program       *****

      if(M .eq. 1) then
       do 10 i=1,N
          pflat(i) = 0.00009145*lnppo(i)**7 + 0.004198*lnppo(i)**6
     &             + 0.08179*lnppo(i)**5 + 0.8816*lnppo(i)**4
     &             + 5.7370*lnppo(i)**3 + 23.0392*lnppo(i)**2
     &           + 55.7229*lnppo(i) + 76.9961

          pcyl(i) = 0.00007629*lnppo(i)**7 + 0.003317*lnppo(i)**6
     &             + 0.06086*lnppo(i)**5 + 0.6138*lnppo(i)**4
     &             + 3.7164*lnppo(i)**3 + 13.8635*lnppo(i)**2
     &           + 31.7327*lnppo(i) + 50.0803

10     continue
       else
        if(M .eq. 2) then
         do 11 i=1,N
            pflat(i) = 0.0001410*lnppo(i)**7 + 0.006096*lnppo(i)**6
```

```
     &              + 0.1113*lnppo(i)**5 + 1.1177*lnppo(i)**4
     &              + 6.7303*lnppo(i)**3 + 24.8203*lnppo(i)**2
     &             + 54.6934*lnppo(i) + 69.0024

            pcyl(i) = 0.00008903*lnppo(i)**7 + 0.003777*lnppo(i)**6
     &             + 0.06739*lnppo(i)**5 + 0.6585*lnppo(i)**4
     &             + 3.8457*lnppo(i)**3 + 13.7786*lnppo(i)**2
     &            + 30.2149*lnppo(i) + 46.4131

11         continue
           else
            if(M. eq. 3) then
             do 14 i=1,N
                pflat(i) = 0.0001346*lnppo(i)**7+0.005808*lnppo(i)**6
     &                + 0.1055*lnppo(i)**5 + 1.0481*lnppo(i)**4
     &                + 6.2128*lnppo(i)**3 + 22.4162*lnppo(i)**2
     &               + 48.0305*lnppo(i) + 59.3778

                pcyl(i) = 0.00005176*lnppo(i)**7+0.002329*lnppo(i)**6
     &                + 0.04402*lnppo(i)**5 + 0.4551*lnppo(i)**4
     &                + 2.8091*lnppo(i)**3 + 10.6301*lnppo(i)**2
     &               + 24.6823*lnppo(i) + 41.1348

14              continue
                else
                if(M .eq. 4) then
                 do 16 i=1,N
                  pflat(i) = 0.0001647*lnppo(i)**7 + 0.006898*
     &                     lnppo(i)**6 + 0.1219*lnppo(i)**5
     &                   + 1.1821*lnppo(i)**4 + 6.8656*
     &                     lnppo(i)**3 + 24.3731*lnppo(i)**2
     &                   + 51.6054*lnppo(i) + 62.2683

                  pcyl(i) = 0.00008667*lnppo(i)**7 + 0.003635*
     &                     lnppo(i)**6 + 0.06412*lnppo(i)**5
     &                   + 0.6196*lnppo(i)**4 + 3.5809*
     &                     lnppo(i)**3 + 12.7059*lnppo(i)**2
     &                   + 27.6566*lnppo(i) + 42.1498

16                continue
     else

     if(M .eq. 5) then
      do 18 i=1,N
         pflat(i) = 0.00009184*lnppo(i)**7 + 0.004018*lnppo(i)**6
     &            + 0.07418*lnppo(i)**5 + 0.7526*lnppo(i)**4
```

```
     &          + 4.5750*lnppo(i)**3 + 17.0169*lnppo(i)**2
     &         + 37.8410*lnppo(i) + 49.0206

          pcyl(i) = 0.00003508*lnppo(i)**7 + 0.001572*lnppo(i)**6
     &          + 0.02986*lnppo(i)**5 + 0.3135*lnppo(i)**4
     &          + 1.9907*lnppo(i)**3 + 7.8713*lnppo(i)**2
     &         + 19.4828*lnppo(i) + 35.3608

18     continue
       else
        if(M .eq. 6) then
         do 22 i=1,N
           pflat(i) = 0.00006360*lnppo(i)**7 + 0.002880*lnppo(i)**6
     &           + 0.05489*lnppo(i)**5 + 0.5730*lnppo(i)**4
     &           + 3.5705*lnppo(i)**3 + 13.5544*lnppo(i)**2
     &          + 30.6597*lnppo(i) + 41.0798

           pcyl(i) = 0.00001534*lnppo(i)**7 + 0.0007521*lnppo(i)**6
     &           + 0.01565*lnppo(i)**5 + 0.1802*lnppo(i)**4
     &           + 1.2577*lnppo(i)**3 + 5.4817*lnppo(i)**2
     &          + 15.0593*lnppo(i) + 31.1173

22       continue
         else
          if(M. eq. 7) then
           do 24 i=1,N
             pflat(i) = 0.00004425*lnppo(i)**7+0.002040*lnppo(i)**6
     &             + 0.03967*lnppo(i)**5 + 0.4233*lnppo(i)**4
     &             + 2.7017*lnppo(i)**3 + 10.5351*lnppo(i)**2
     &            + 24.5529*lnppo(i) + 33.7776

             pcyl(i) = 0.00003311*lnppo(i)**7+0.001471*lnppo(i)**6
     &             + 0.02758*lnppo(i)**5 + 0.2845*lnppo(i)**4
     &             + 1.7643*lnppo(i)**3 + 6.7721*lnppo(i)**2
     &            + 16.1883*lnppo(i) + 28.3229
24           continue
            else
            if(M .eq. 8) then
             do 26 i=1,N
              pflat(i) = 0.0001254*lnppo(i)**7 + 0.004753*
     &                 lnppo(i)**6 + 0.07649*lnppo(i)**5
     &               + 0.6814*lnppo(i)**4 + 3.6706*
     &                 lnppo(i)**3 + 12.2379*lnppo(i)**2
     &               + 24.7975*lnppo(i) + 30.8043

              pcyl(i) = 0.00004147*lnppo(i)**7 + 0.001776*
```

```
     &                lnppo(i)**6 + 0.03204*lnppo(i)**5
     &              + 0.3174*lnppo(i)**4 + 1.8873*
     &                lnppo(i)**3 + 6.9321*lnppo(i)**2
     &              + 15.8627*lnppo(i) + 26.9572

 26          continue

           else
           Do 28 i=1,N
             pflat(i) = 0.00007294*lnppo(i)**7 + 0.003182*
     &                lnppo(i)**6 + 0.05867*lnppo(i)**5
     &              + 0.5952*lnppo(i)**4 + 3.6236*
     &                lnppo(i)**3 + 13.5265*lnppo(i)**2
     &              + 30.2947*lnppo(i) + 40.5759

             pcyl(i) = 0.00002752*lnppo(i)**7 + 0.001245*
     &                lnppo(i)**6 + 0.02390*lnppo(i)**5
     &              + 0.2541*lnppo(i)**4 + 1.6371*
     &                lnppo(i)**3 + 6.5880*lnppo(i)**2
     &              + 16.6936*lnppo(i) + 31.8331
 28          continue

          endif
          endif
          endif
          endif
          endif
         endif
       endif
     endif

c    ******              Numerical Differentiation              *****

     Do 20 i=1,N-1
       dwwo(i) = wwo(i+1) - wwo(i)
       dpflat(i) = pflat(i+1) - pflat(i)
       rflat(i) = (pflat(i+1) + pflat(i)) / 2.
      dpcyl(i) = pcyl(i+1) - pcyl(i)
      rcyl(i) = (pcyl(i+1) + pcyl(i)) / 2.
      dwdrflat(i) = dwwo(i) / dpflat(i)
      dwdrcyl(i) = dwwo(i) / dpcyl(i)
 20   continue

c    ******                    Output                     *****

     write(2,99)
```

```
99      format(6x,'P/Po',10x,'W',10x,'W/Wo',6x,'Pore Flat',3x,
     &        'Pore CYL.')
        Do 30 i=1,N

        write(2,100) ppo(i),w(i),wwo(i),pflat(i),pcyl(i)
100     FORMAT(2X,E10.3,2X,E10.3,2X,E10.3,2x,e10.3,2x,e10.3)
 30     continue

        write(3,98)
98      format(2x,'d(W/Wo)/dR Flat',4x,'Pore flat',6x,'d(W/Wo)/dR
     &          CYL.',5x,'Pore CYL.')
        DO 40 i=1,N-1

        write(3,97) dwdrflat(i),rflat(i),dwdrcyl(i),rcyl(i)
97      format(2x,e12.6,5x,e12.6,5x,e12.6,5x,e12.6)
40      continue
      STOP
      END
```

Appendix E

Calculation of Interaction Energy Using Gaussian 92

E.1 Procedures to Generate Gaussian 92 Input File

Gaussian 92 input has the following sections (Foresman and Frisch, 1993):

Route Section: Specifies the job type and model chemistry (# method basis-set type-of-job [additional-keywords])

Title Section: Describes the job for the output

Molecular Specification: Gives the structure of the molecule to be studied

Variables Section: Specifies values for the variables used in the molecule specification

All the sections are separated by blank lines.

The route section contains:

Method: HF, UHF, RHF, ROHF, MP2, MP3, and other methods for calculation of electronic energies

Basis Set: STO-3G, 3-21G, 3-21G*, 4-31G, 6-31G, 6-31G*, 6-31G**, 6-31+G**, etc.

Type of Job: SP(calculation of single point energy), OPT (optimization of molecular geometry and calculation of energy), FREQ (computation of vibrational frequencies), etc.

Title section is a description of the calculation. This might contain the compound name, the symmetry, the electronic state and any other information. Title card appears in the output for purposes of identification and description.

Molecular Specification has the following format:

Molecular-Charge (overall charge of the system under investigation)
Spin-Multiplicity (1=singlet, 2=doublet, etc.)

Z-Matrix (internal coordinates of each atom in the molecule)

To better understand the input file for Guassian 92, lets use hydrogen peroxide as an example:

1) Invoke an editor and type the appropriate commands to set up the Gaussian 92 environment on the system.

2) Enter the route section:

#n HF/STO-3G OPT

This optimizes the geometry of hydrogen peroxide using HF/STO-3G model (HF = Hartree Fock, and STO-3G = minimal basis set). This line always begins with a pound sign, #.

3) Enter a blank line, followed by a one-line description of the calculation

Optimization of Hydrogen Peroxide at HF/STO-3G

4) Enter another blank line after the title section, followed by specification of the molecular geometry:

0 1	(charge and multiplicity)
O1	(Oxygen #1) {placing the first oxygen atom at the origin}
H1 O1 ROH	(Hydrogen #1, connected to oxygen #1 by a bond length of ROH Å)
O2 O1 ROO H1 AHOO	(Oxygen #2, connected to oxygen #1 by ROO Å, and making a angle (H1-O1-O2) of AHOO degrees)
H2 O2 ROH O1 AHOO H1 DAHOOH	(Hydrogen #2, connected to oxygen #2 by a bond length of ROH, making an angle (H2-O2-O1) of AHOO degrees, with a dihedral angle (H2-O2-O1-H1) of DAHOOH)

Note: RO1H1 = RO2H2 = ROH and $<$ H1-O1-O2 = $<$ H2-O2-O1 = AHOO

5) Enter another blank line, followed by the list of variables:

ROH	0.9
ROO	1.4
AHOO	105.0
DAHOOH	120.0

6) End the file with another blank line. The complete input file looks like this:

```
#n HF/STO-3G OPT

Optimization of Hydrogen Peroxide at HF/STO-3G

0 1
O1
H1 O1 ROH
O2 O1 ROO H1 AHOO
H2 O2 ROH O1 AHOO H1 DAHOOH

ROH       0.9
ROO       1.4
AHOO      105.0
DAHOOH    120.0
```

7) Save the file under the name: Name.com

8) Execute the job

9) The output file is saved under Name.log

E.2 Information Obtained From Gaussian 92 Output File

There are three different types of calculations that can be performed using Gaussian 92: single point energy calculation, geometry optimization, and frequency calculation.

The output file contains molecular orbitals (e.g. highest occupied molecular orbital, HOMO, and lowest unoccupied molecular orbital), orbital energies, charge distribution, dipole and multipole moments, polarizability, frequencies and intensities, and thermodynamic properties.

E.3 Example of an Input File with the Summary of the Results

E.3.1 Input File for Optimization of N_2-$Si(OH)_4$ Complex

```
$ set def students:[hassanm]
$ @assign_g92.com
$ run gauss_exedir:g92
%chk=n2sio4h4
#n MP2=(fc,direct)/6-31+g** opt scf=direct optcyc=200

Si(OH)4--N2  at mp2/6-31+g**

0 1
 si
 o2   1   rsio1
 o3   1   rsio1   2   aosio1
 o4   1   rsio1   2   aosio1   3   t1
 o5   1   rsio1   4   aosio1   2   -t1
 h6   2   roh1    1   ahosi1   5   t3
 h7   3   roh1    1   ahosi1   4   -t3
 h8   4   roh1    1   ahosi1   3   -t3
 h9   5   roh1    1   ahosi1   2   t3
 x10  6   1.0     2   90.0     1   180.0
 n11  6   rnh     10  anhx     2   t4
 x12 11   1.0     6   90.0     10  0.0
 n13 11   rnn     12  annx     6   t5

 rsio1          1.7023
 roh1           0.9711
 aosio1         105.7173
 ahosi1         123.7957
 t1             124.9327
 t3             85.8736
 rnh            2.2367
 anhx           119.791
 t4             167.2433
 rnn            1.1529
 annx           106.4002
 t5             170.6809
```

E.3.2 Summary of the Output File for Optimization of N_2-$Si(OH)_4$ Complex

1\1\GINC-D9000\POPT\RMP2-FC\6-31+G(D,P)\H4N2O4Si1\HASSANM\
23-JUN-1994\
1\\#N MP2=(FC,DIRECT)/6-31+G** OPT SCF=DIRECT OPTCYC=200\
\Si(OH)4--N2 at mp2/6-31+g**
\\0,1\Si\O,1,rsio1\O,1,rsio1,2,aosio1\O,1,rsio1,2,aosio
1,3,t1,0\O,1,rsio1,4,aosio1,2,-t1,0\H,2,roh1,1,ahosi1,5,t3,0\H,3,roh1,
1,ahosi1,4,-t3,0\H,4,roh1,1,ahosi1,3,-t3,0\H,5,roh1,1,ahosi1,2,t3,0\X,
6,1.,2,90.,1,180.,0\N,6,rnh,10,anhx,2,t4,0\X,11,1.,6,90.,10,0.,0\N,11,
rnn,12,annx,6,t5,0\\rsio1=1.65406\roh1=0.964305\aosio1=106.083511\ahos
i1=116.086636\t1=124.407706\t3=82.12471\rnh=2.324557\anhx=114.780715\t
4=175.224653\rnn=1.12958\annx=107.597784\t5=171.97174\\Version=VAX-
VMS-G90RevJ\HF=-699.8709368\MP2=-701.0360586\RMSD=0.651D8\
RMSF=0.133D-03\PG=C01 [X(H4N2O4Si1)]\\@

Time used:
IO time 0 days 5 hours 3 minutes 43.3 seconds.
CPU time 3 days 6 hours 34 minutes 34.7 seconds.
TOT time 3 days 11 hours 38 minutes 17.9 seconds.

HASSANM job terminated at 23-JUN-1994 16:22:34.72